Positioning of the Ducted Fan Propulsive Stabiliser

E. Adib

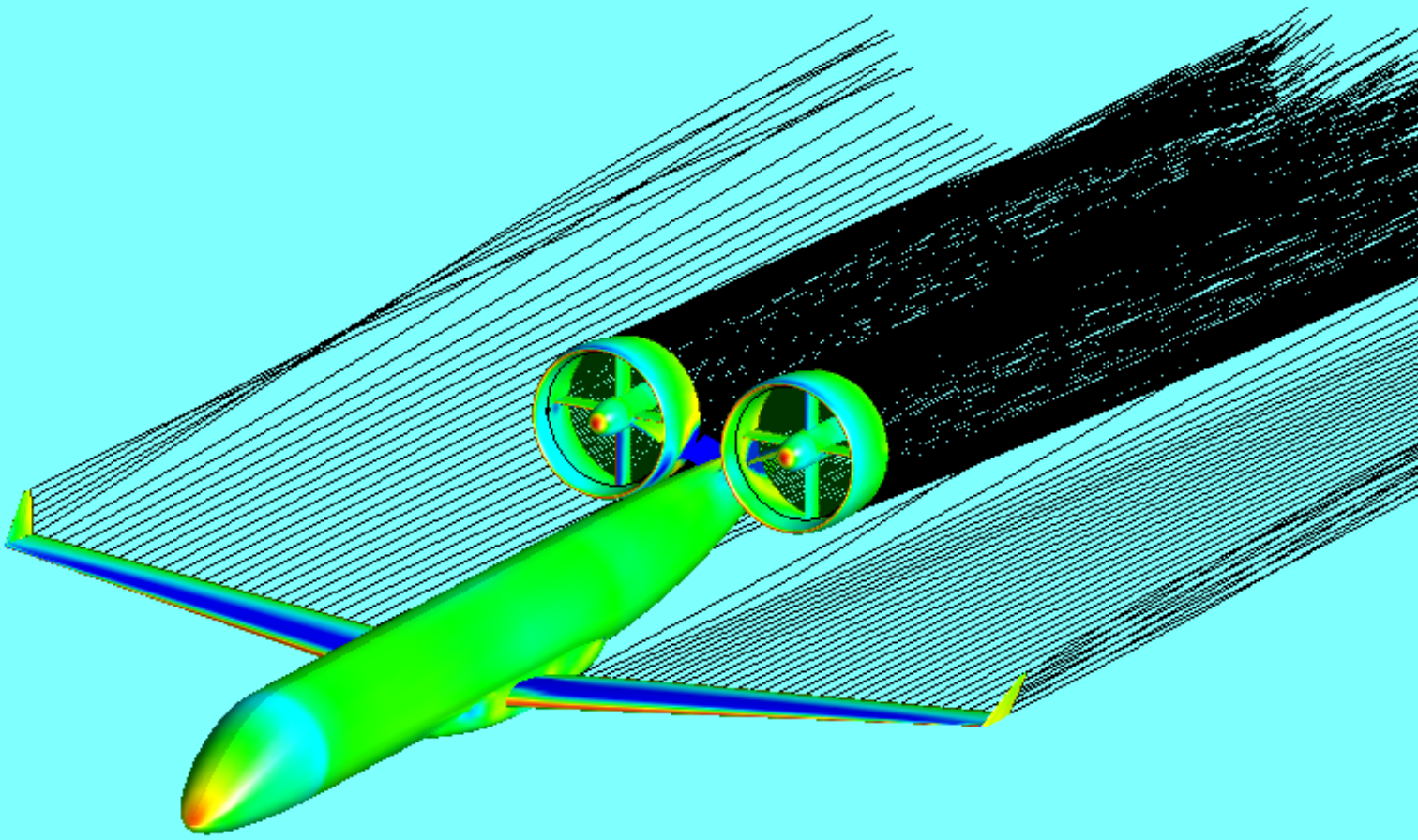

Technische Universiteit Delft

TU Delft

Positioning of the Ducted Fan Propulsive Stabiliser

by

E. Adib

to obtain the degree of Master of Science
at the Delft University of Technology,
to be defended publicly on Wednesday September 29, 2021 at 14:00.

Supervisor:	Dr. ir. M.F.M. Hoogreef	
Thesis committee:	Prof. dr. ir. L.L.M. Veldhuis,	TU Delft
	Dr. ir. M.F.M. Hoogreef,	TU Delft
	Ir. J. Sinke,	TU Delft

An electronic version of this thesis is available at `http://repository.tudelft.nl/`.

TU Delft

Preface

I would like to thank my supervisor Maurice Hoogreef and Leo Veldhuis for their continuous guidance and support throughout the year. At times, the Covid pandemic has not made it easy to work on the thesis, however with their support I was able to keep on track and keep moving forward. It has been a great but also challenging project to work on. A special thanks to Dr. Ahuja from Research in Flight for his support on FlightStream. I would also like to thank ir. J. Sinke for being part of grading this research.

I would like to dedicate my engineering degree and the fulfilment of this thesis to my parents. Without their unconditional support and love throughout my whole study I would not have made it to this place. During the study I have experienced a lot of ups and downs and my parents encouraged me to keep going through the times I felt the lowest. During my bachelor and master at TU Delft I have met great and incredibly smart people and have made amazing friends. I am happy to finish this chapter in life and start a new chapter. I feel proud and grateful to be at this position and will keep moving forward to keep fulfilling dreams.

E. Adib
Delft, September 2021

Summary

A new aircraft configuration, the Delft University Unconventional Configuration (DUUC), was recently invented by the Flight Performance and Propulsion group at TU Delft. As a solution to the concerns regarding the environmental and health impact due to increasing demand of air travel. The DUUC has a characteristic feature which consist of two ducted propellers at the empennage of the aircraft with vertical and horizontal vanes mounted downstream of the duct, spanning the whole diameter. With this newly integrated architecture the DUUC combines thrust with stability and control of the aircraft.

From previous research on the DUUC, where the propulsive stabiliser was in a fixed, aft-fuselage position with a fixed duct aspect ratio. It has been observed that the rear center of gravity (CG) position and a large shift in CG due to the propulsive stabiliser, poses a number of challenges. Research has to be done on the positioning of the propulsive stabiliser. Therefore, the objective of this research is to study the positioning of the ducted fan propulsive stabiliser, considering its impact on stability and control by development of a method to predict aerodynamic/stability & control derivatives for variable position and duct/fan size.

In order to study the positioning of the propulsive stabiliser. A new method is developed which combines an ESDU method, AVL and FlightStream and works on the basis of the moment balance of the aircraft. The ESDU method is used to determine the position of the aerodynamic center of the wing-fuselage combination. With the aerodynamic centre known, AVL is then used to calculate the lift, drag and moment of the wing-fuselage combination. Knowing the aircraft CG position, the lift required by the ducted propulsive stabiliser can be calculated and hence the required duct size can be determined. FlightStream is used to determine the aerodynamic characteristics of various sizes ducted propeller. Flightstream is a surface-vorticity solver which is more stable, more robust and has a lower sensitivity to surface perturbations, when compared to potential-flow solver which are pressure-based. Knowing the actual duct lift available and the lift required, an assessment is made on the feasible duct size and propulsive stabiliser position for take-off, descent and cruise conditions.

From FlightStream ducted propeller validation analysis it has been observed that the vorticity solver is able to produce accurate lift coefficient results in unpowered conditions, compared to analytical methods such as Weissinger and Maqsood. However, it is not able to predict stall. It should be noted that Weissinger and Maqsood do produce accurate results if the effects of the vanes and struts are added separately, with Weissinger producing the best results. FlightStream underpredicted the drag coefficient throughout the whole angle of attack range. In powered conditions the lift coefficient is also underpredicted, with a small difference in the vorticity and pressure model. The drag coefficient is also underpredicted in the powered conditions. From the analyses of various duct sizes it has been observed that the larger the duct size the higher the lift coefficient, using the wing area as the reference area. The opposite is true for the drag coefficient, where the drag is larger for smaller duct sizes at low angles of attack. At angle of attack above 10°, the larger duct sizes produce the most drag. Furthermore, a clear effect could be observed in the lift coefficient due to the wing and fuselage effects when comparing the installed and uninstalled duct.

Utilising the novel method combining an ESDU method, AVL and FlightStream, it has been observed that there are configuration of wing position, propulsive stabiliser position and duct size feasible, to guarantee a stable and controllable aircraft. However, this would mean that the duct installation angle has to be adjusted accordingly for cruise, take-off and descent. From these analyses it has been observed that for descent requirements it could be more beneficial to position the wing at 47.5% fuselage length. Furthermore, positioning the propulsive stabiliser more to the front results in less available combinations to satisfy the requirements. Lastly, from analysing 3 cases in cruise, a significant drag reduction is achieved by using a smaller duct at higher installation angle, compared to a larger duct at lower installation angle. Using the same duct size and installation angle, but positioning it more to the front resulted in minimal drag reduction.

Contents

List of Figures

Nomenclature

Acronym	Description
AVL	Athena Vortex Lattice
BWB	Blended Wing Body
CAD	Computer-Aided Design
CFD	Computational Fluid Dynamics
CFRP	Carbon Fiber Reinforced Polymer
CG	Center of Gravity
CR	Cruise
DE	Descent
DFDC	Ducted Fan Design Code
DUUC	Delft University Unconventional Concept
FMDP	Fuselage Mounted Ducted Propeller
MAC	Mean Aerodynamic Chord
MTOM	Maximum Take-off Mass
NP	Neutral point
OEM	Operation Empty Mass
PHALANX	Performance, Handling Qualities and Load Analysis Toolbox
RPM	Revolutions per minute
TF	Tail force
TMP	Tail Mounted Propeller
TO	Take-off
VTOL	Vertical Take-off and Landing
WMP	Wing Mounted Propeller

Symbol	Description	Unit
A	Area	[m^2]
AR	Aspect Ratio	[-]
b	Wing span	[m]
c	Chord length	[m]
C_D	Drag coefficient	[-]
C_{D_0}	Zero-lift drag coefficient	[-]
C_f	Friction coefficient	[-]
C_t	Thrust coefficient	[-]
C_p	Power coefficient	[-]
C_L	Lift coefficient	[-]
C_M	Moment coefficient	[-]
C_f	Skin friction coefficient	[-]
D	Diameter	[m]
D	Drag	[N]
e	Oswald efficiency factor	[-]
i	Installation angle	[deg]
J	Advance ratio	[-]
L	Lift	[N]
L_f	Fuselage length	[m]
l	Length	[m]
M	Mach number	[-]
M	Moment	[Nm]
m	mass flow	[kg/s]
n	Rotational speed	[rps]
P	Power	[W]
p	Pressure	[N/m^2]
p	Roll rate	[deg/s]
q	Pitch rate	[deg/s]
r	Yaw rate	[deg/s]
r	Radius	[m]
Re	Reynolds number	[-]
S	Surface area	[m^2]
T	Thrust	[N]
t	Thickness	[m]
u	Wake velocity	[m/s]
U_∞	Free-stream velocity	[m/s]
V	Velocity	[m/s]
V_h	Tail Volume Coefficient	[-]
W	Weight	[N]
x	Distance	[m]
α	Angle of atack	[deg]
β	Blade pitch angle	[deg]
ϵ	Downwash angle	[deg]
η	Efficiency	[-]
Λ	Wing sweep angle	[deg]
λ	Taper ratio	[-]
ξ_W	Weissinger lift reduction factor	[-]
ρ	Density	[kg/m^3]

1

Introduction

With the increasing demand of air travel and thereby increase in concerns of environmental and health impact, the need for the aviation industry to propose sustainable solutions with respect to noise per flight and fuel per passengers becomes more crucial[1]. In order to achieve these goals, engineers start to explore novel configurations. A new aircraft configuration, the Delft University Unconventional Configuration (DUUC), was recently invented by the Flight Performance and Propulsion group at TU Delft. The DUUC has a characteristic feature which consist of two ducted propellers at the empennage of the aircraft with vertical and horizontal vanes mounted downstream of the duct, spanning the whole diameter. With this newly integrated architecture, the DUUC combines thrust, stability and control of the aircraft, allowing clean wing aerodynamics[2]. The duct also functions as a shield against the propeller noise and debris and is able to generate a thrust force. Moreover, the duct reduces tip losses of the propeller, by eliminating reverse flow at the tips and thus increasing effective disk area, since the reverse flow at the tips restrict the amount of air able to flow through the propeller[3]. The DUUC aircraft with the propulsive stabiliser can be seen in Figure 1.1.

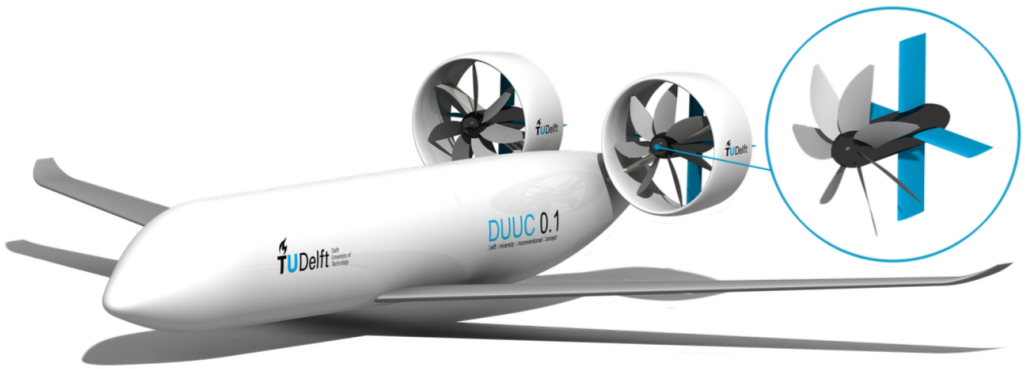

Figure 1.1: DUUC aircraft concept with detail of its propulsive empennage[2]

Previous studies have looked at this propulsive stabiliser in a fixed, aft-fuselage position with a fixed duct aspect ratio, studying the overall concept and weight of the system. However, the rearward center of gravity position due to the propulsive stabiliser poses a number of challenges. Therefore, research has to be done on the positioning of the propulsive stabiliser. In order to understand whether the aft center of gravity position of the aircraft could be resolved by changing the position of the propulsive stabiliser, while maintaining sufficient stability and control. Apart from providing sufficient stability and control, the concept also has to be able to prove that it is able to outperform the conventional aircraft.

Furthermore, from Figure 1.2 it can be seen that over the years with every new generation engine, the bypass ratio increases, in order to improve the fuel economy of the engine. Since an increase in bypass ratio results in an increase of the propulsive efficiency[4]. The trend between bypass ratio and thrust specific fuel con-

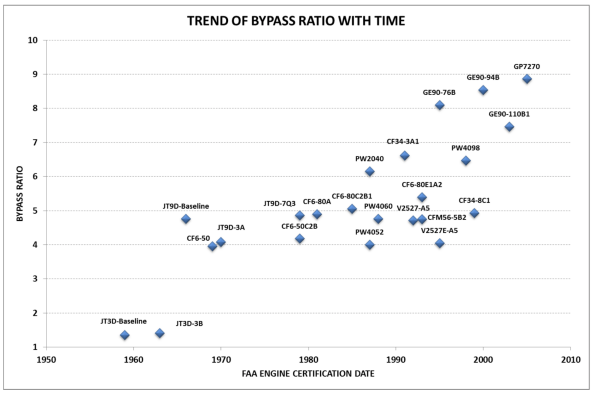

Figure 1.2: Trend in bypass ratios over the years[4]

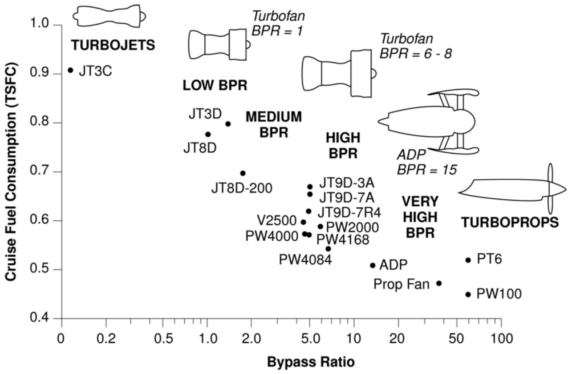

Figure 1.3: Bypass ratios vs thrust specific fuel consumption[5]

sumption is depicted in Figure 1.3. However, these increasingly larger bypass ratio engines will at a certain point not fit below the wings anymore. As an example, the size of the engine of the A320ceo is compared to the upgraded A320neo. The A320ceo uses CFM56 engines, with a bypass ratio of 5.5[6], while the next generation LEAP engines have a bypass ratio of 11[7]. The difference between the 2 engines below the wing can be seen in Figure 1.4. It can be seen that ground clearance starts to become an issue with increasing bypass ratio. Therefore, further highlighting the importance of this research than the study on the DUUC alone.

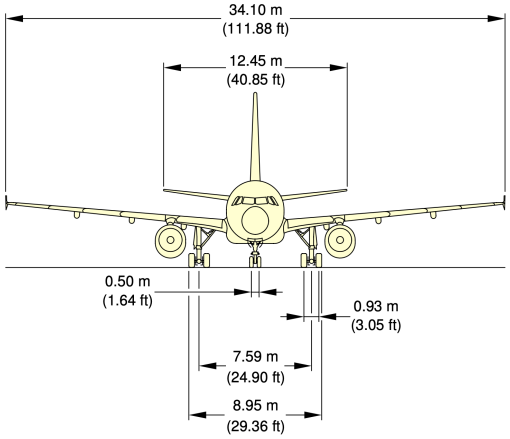

(a) A320ceo

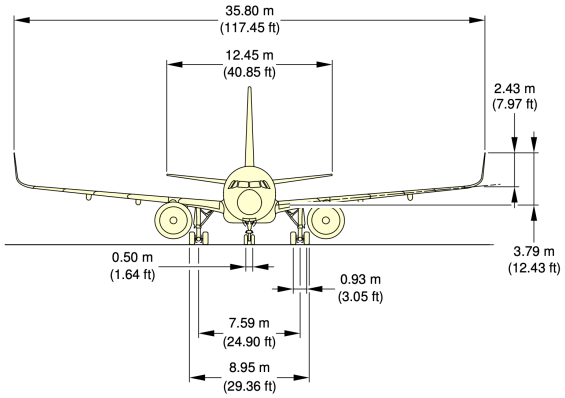

(b) A320neo

Figure 1.4: Comparison engine size A320ceo vs A320neo[8]

In this chapter the research question formulated with the corresponding sub-questions to answer the main question is presented in Section 1.1. The objective is presented in Section 1.2 as well as the necessary subgoals to achieve this. The complete report outline is given in Section 1.3.

1.1. Research question

From the literature review, it has been concluded that the aft center of gravity position of the DUUC, due to the propulsion system, leads to an unfavourable large CG shift. Allowing conventional wing-mounted propeller aircraft to outperform the DUUC. In these previous studies, the position of the propulsion system has been kept fixed. Hence the need to perform a research on the ducted propulsive stabiliser, where the location of the propulsive stabiliser is treated as a variable and the effect on stability and controllability is analysed. Furthermore, in the previous studies the effect of flight speed is also not taken into account, which will be done in this research.

Therefore, the main research question of this research is:

Where to position the ducted fan propulsive stabiliser for a longitudinal stable and controllable aircraft for high and low cruise speeds?

In order to answer this question, the problem has been divided into multiple sub-questions which will aid into solving the main question. The sub-question are formulated as follows:

1. How to determine the stability & control derivatives of an aircraft?
2. How to determine the aerodynamic coefficients of an aircraft?
3. How does the position of the propulsive stabiliser influence stability & control
4. How does the cruise speed influence stability & control of an aircraft?
5. What is the effect of duct size on stability and control?

1.2. Research objective

The main research objective of this thesis is:

> "To study the positioning of the propulsive stabiliser, considering its impact on stability and control (lateral, directional and longitudinal) by development of a method to predict aerodynamic/stability & control derivatives for variable position and duct/fan size.".

To achieve this objective, first some prior steps are required such as an aerodynamic analysis. The following sub-goals have been established that will aid into achieving the above mentioned research objective and research question. The DUUC will be used in this research as the case study, hence these sub-goals all apply to the DUUC.

- Generate a model in Flightstream.
- Perform analysis in Flightstream to obtain the aerodynamic coefficients.
- Create a model in Matlab and incorporate the results from the aerodynamic analysis.
- Study the control and stability characteristics in Matlab for different positions and sizes of the propulsive stabiliser.
- Analyse influence of flight condition on the control and stability characteristics.

1.3. Report outline

This report describes the thesis project with the objective to study the positioning of a ducted fan propulsive stabiliser, considering its impact on stability and control by development of a method to predict aerodynamic/stability & control derivatives for variable position and duct/fan size. An elaborate overview of the previous studies that have been performed on the DUUC are presented in Chapter 2 as well as the theory on propeller, annular wings and ducted fans aerodynamics. In Chapter 3, a detailed description of the methodology used is given. As part of this research, a validation study has also been performed and the results are presented in Chapter 4. The results of the analysis on the aerodynamic analysis as well as the results on the positioning of the propulsive stabiliser can be seen in Chapter 5. Finally, the conclusions are presented in Chapter 6.

2

Background

This chapter gives an overview on the various studies that have been performed on the Delft University Unconventional Configuration (DUUC) aircraft. In Section 2.1 a brief description of the concept will be given, after which the various analyses performed in the past on the DUUC will be elaborated upon in Section 2.2. The theory on propellers is given in Section 2.3, the concept of ring wings and ducted fans are further elaborated upon in Sections 2.4 and 2.5, respectively.

2.1. Concept description

The DUUC consist of a conventional fuselage and wing. However, instead of having a horizontal and vertical tail, the aircraft has this integrated with the propulsion system. Which consists of two ducted propellers at the empennage of the aircraft with vertical and horizontal vanes mounted downstream of the duct. These vanes provide the stability and control of the aircraft, by deflecting up and down or sideways. The airfoil used for both the duct and the pylon is the NACA 0012 airfoil. The control vanes use a NACA0016 airfoil[2]. The DUUC concept aircraft can be seen in Figure 2.1. The aircraft is designed for medium range, therefore the design should be compared to aircraft such as ATR72-600.

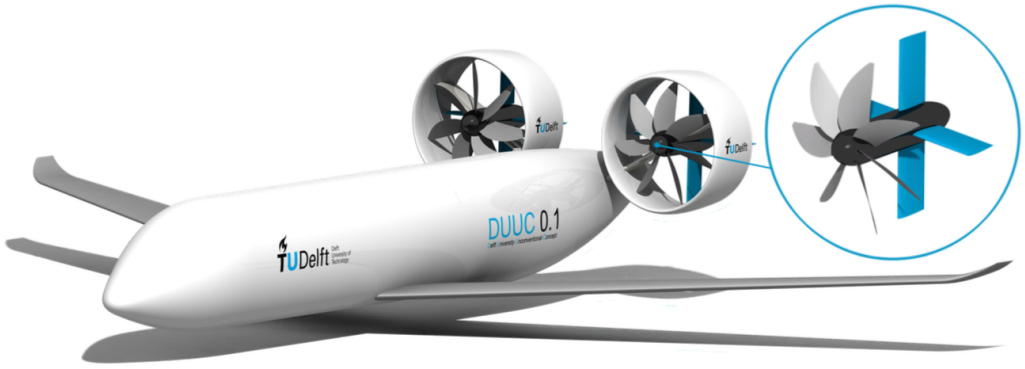

Figure 2.1: DUUC aircraft concept with detail of its propulsive empennage[2]

2.2. DUUC studies

This section elaborates on the research performed on the aerodynamic characteristics as well as stability and control analyses. After which a brief description of the weight analysis and performance analyses are presented. Please note that in the context of this research, the topics on aerodynamics and stability & control are treated more in detail compared to other topics.

2.2.1. Aerodynamic analysis

Various aerodynamic studies have been performed on the DUUC. As an analytical method to determine the lift characteristics of the duct, Weissingers[9] method has been used in the research of Harinarain[10]. First, the methods used by Harinarain will be explained, after which the results will be presented. With this analytical model, the lift curve slope is given by Equation 2.1. Where ξ_W is given by Equation (2.2) and $\lambda = 1/AR$. Furthermore, the aspect ratio (AR) of the duct is defined as $\frac{D_{duct}}{c_{duct}}$.

$$C_{L_\alpha,duct} = \frac{\pi}{2}\xi_W c_{l_\alpha} \tag{2.1}$$

$$\xi_W = \frac{1}{1+\lambda(\pi/2)+\lambda\arctan(1.2\lambda)} \tag{2.2}$$

Equation (2.1) is for the power-off conditions, so in order to include the propeller effects on the duct, Equation (2.3) has to be used. The factor k_{prop} can be determined using the centerbody thrust coefficient as can be seen in Equation (2.4).

$$C_{L_\alpha,duct,on} = (1+k_{prop})C_{L_\alpha,duct} \tag{2.3}$$

$$k_{prop} = 0.2\sqrt{T_{c_{propcb}}} \tag{2.4}$$

The drag of the duct can be determined as the sum of the zero-lift drag and the lift-induced drag. In the research of Harinarain the zero-lift drag of the duct is calculated using the method described by Sadraey[11] and can be seen in Equation (2.5). This consists of the minimum airfoil drag coefficient ($C_{D_{min}}$), the skin friction coefficient for flat plates (C_f) which is determined using Equation (2.6). Furthermore, the Mach correction which is expressed as $f_M = 1-0.08^{1.45}$, a factor which depends on the airfoil thickness ratio as can be seen in Equation (2.7) and lastly the wetted area which can be seen in Equation (2.8).

$$C_{D_0} = C_f f_{tc} f_M \frac{S_{wet}}{S}\left(\frac{C_{D_{min}}}{0.04}\right)^2 \tag{2.5}$$

$$C_f = \begin{cases} \frac{0.455}{(\log_{10}Re)^{2.58}} \; for turbulent flow \\ \frac{1.327}{\sqrt{Re}} \; for laminar flow \end{cases} \tag{2.6}$$

$$f_{tc} = 1 + 2.7\left(\frac{t}{c}\right)_{max} + 100\left(\frac{t}{c}\right)^4_{max} \tag{2.7}$$

$$S_{wet_{duct}} = 2\pi D_{duct} c_{duct} + 2\pi D_{duct} 0.5\left(\frac{t}{c}\right)_{max} c_{duct} \tag{2.8}$$

The induced drag of the duct can then be calculated using Equation (2.9), where the Oswald efficiency factor (e) is equal to 2.

$$C_{D_{i,duct}} = \frac{C_L^2}{\pi ARe} = \frac{C_L^2}{2\pi AR} \tag{2.9}$$

So, the total lift and drag coefficient of the duct is then given by Equation (2.10) and (2.11), respectively. Where for power off conditions V_{duct} is given by V_∞ and for power on conditions by u. U is defined as the velocity of the ultimate wake and can be calculated using Equation (2.12).

$$C_L' = C_L'\left(\frac{V_{duct}}{V_\infty}\right)^2 \tag{2.10}$$

$$C_D' = (C'_{D_{0,duct}} + C_{D_{i,duct}})\left(\frac{V_{duct}}{V_\infty}\right)^2 \tag{2.11}$$

$$u = \frac{1}{2}\left(V_{prop} + \sqrt{\frac{2}{\rho}\frac{T_{prop}}{S_{prop}} + V_{prop}^2}\right) \tag{2.12}$$

In the research performed by Harinarain[10], Ducted Fan Design Code (DFDC) is used to combine with the analytical method determine the aerodynamic characteristic in powered conditions. DFDC is an open source tool developed by Massachusetts Institute of Technology (MIT). This tool uses axisymmetric panel method for the duct and centerbody and lifting line representation of the rotor blades. This allows the user to model the interaction effects between propeller and duct and predict the lift, drag, side force and control surface effectiveness coefficients[12]. Using DFDC, the user is able to quickly assess new designs of ducted fans on their aerodynamic performance.

To use DFDC, certain parameters such as the freestream velocity, rotor RPM, atmospheric density, speed of sound and dynamic viscosity are specified as operating conditions. The geometry of the duct and centerbody are denoted as absolute x and y coordinates. The geometry of the rotor is specified by the amount of radial station, having a specific chord length and the distribution of blade angle. The rotor can be modelled either as blade elements, which then gives a number of airfoil sections with their properties along the span. Or as an actuator disk, with a specific loading.

To perform the analysis with DFDC, first certain parameters of the airfoil are necessary as input. These parameters are listed below and could be obtained with XFoil.

- α_0, the zero lift angle of attack
- $\frac{dC_L}{d\alpha}$, the lift curve slope of the linear part of the lift curve
- $C_{L_{max}}$, the maximum lift coefficient
- $C_{L_{min}}$, the minimum lift coefficient
- $(\frac{dCL}{d\alpha})_{stall}$, the lift curve slope at stall
- C_m, the moment coefficient
- M_{crit}, the critical Mach number
- C_L at $C_{D_{min}}$, the lift coefficient at minimum drag coefficient
- $\frac{dC_D}{dC_L^2}$, derivative of drag with respect to the lift squared
- Re_{ref}, the Reynolds number
- f, Reynolds number scaling component

Since there are no validation studies available for DFDC, Harinarain[10] performed a comparison with DFDC himself in his research. Data from a past experiment performed by Grunwald & Goodson[13] were obtained and recreated with DFDC. The result of the comparison study can be seen in Figure 2.2. From this, it can be seen that there is a large offset between the results obtained from the experiment by Grunwald & Goodson and from DFDC.

The large offset was investigated by modelling the duct and propeller separately, to understand the source of the problem. First, the pressure distribution on the duct was assessed. In order to do this, the thrust of the propeller was set manually to produce 0 thrust, such that the pressure distribution only due to the duct can be assessed. From this, it has been observed that the duct aerodynamics is modelled correctly. The propeller thrust was then assessed by comparing the results with XFoil. From this, it has been observed that DFDC does not model the thrust of the propeller correctly and hence explain the large offset when the propeller and duct are modelled together. Finally, to understand whether the effect of duct thrust due to the propeller is modelled correctly, the value of the propeller thrust is set manually to equal the propeller thrust of the experiment. This then resulted in the new values as can be seen in Figure 2.3. From this, it can be seen that the offset has reduced significantly, with a maximum offset of 12.68% now. However, it should be noted that

Outcomes	Experiment	DFDC	Offset [%]
T_{tot} $[N]$	90.1	65.4	-27.4
T_{propcb} $[N]$	64.1	52.2	-18.5
T_{duct} $[N]$	24.3	13.2	-45.7
Q $[Nm]$	4.55	3.23	-28.9
η $[-]$	0.71	0.73	2.7

Figure 2.2: Comparison of DFDC and experiment[10]

this result is obtained by manually altering the analysis in DFDC. So, more experiments are required to verify this reasoning.

Outcomes	Experiment	DFDC	Offset [%]
T_{tot} $[N]$	90.1	91.4	1.48
T_{prop} $[N]$	64.1	64.1	0
T_{duct} $[N]$	24.29	22.3	12.68
Q $[Nm]$	4.546	4.63	1.85
η $[N/W]$	0.71	0.71	0

Figure 2.3: Comparison of DFDC and experiment with new values[10]

Harinarain[10] also performed a wind tunnel test on a scaled model of the ducted fans in order to attempt to validate the results of DFDC with predefined thrust levels from the analytical model described earlier. The test is performed on a duct with a diameter of 0.25m, chord length of 0.125m and aspect ratio of 2. Furthermore, the airfoil used for the duct is a NACA0012 and the fan consists of 3 propellers. The horizontal and vertical exit vanes both have an aspect ratio of 2 and also use a NACA0012 airfoil. The test setup can be seen in Figure 2.4 and the schematic of the test setup can be seen in Figure 2.5.

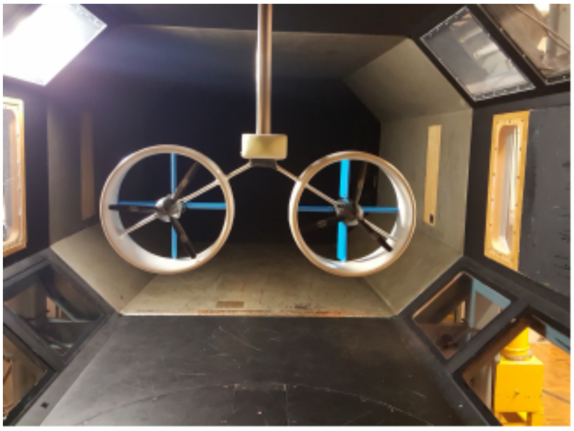

Figure 2.4: Test setup DUUC model[10]

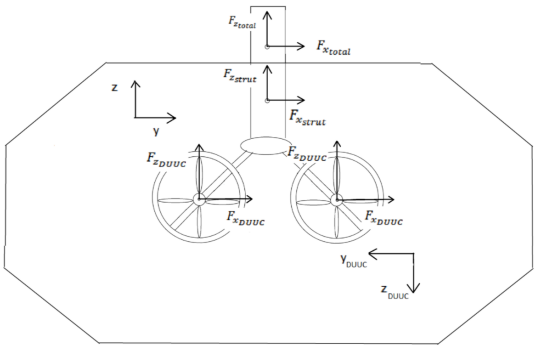

Figure 2.5: Schematic test setup of DUUC[10]

In the first part of the wind tunnel test, the DUUC is analysed in static conditions. Which means no air is blowing into the propeller. From the wind tunnel test, it has been observed that until 2000 RPM the static thrust is modelled correctly. However, after this the thrust is increasingly underestimated by the model, as can be seen in Figure 2.6. This difference is linked to either a drag estimate of the system which is too high or due to a incorrect Prandtl tip loss factor. For the elevator deflections, it has been observed that it is modelled correctly until an elevator deflection angle of 20°. After this point, the wind tunnel test shows a drop in lift which indicates the elevators have stalled. The same applies for the rudders, which are correctly modelled in

the region of attached flow. At approximately −30° and 30°, there is a loss in sideforce and incorrect prediction of the model which indicates stall.

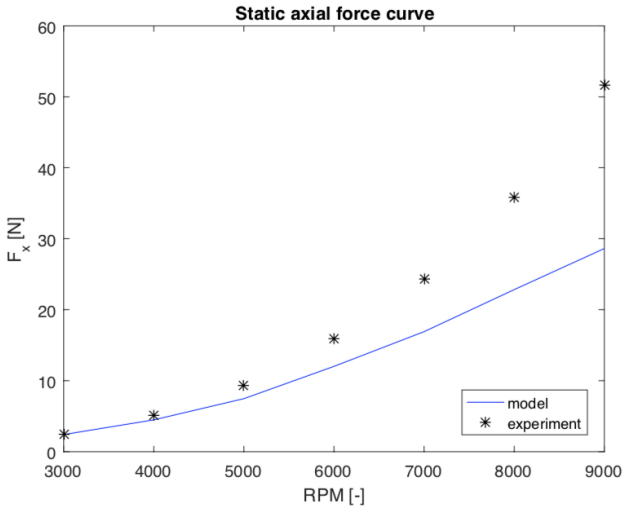

Figure 2.6: Static thrust - model vs experiment[10]

In the second part, power-off conditions were simulated. Hereby taping the propellers to the duct in order to prevent windmilling. From Figure 2.7, it can be seen that the lift curve slope is modelled correctly until angle of attack of approximately 15°. The drag is significantly underestimated, as can be seen in Figure 2.8. In the research, this is attributed to an underestimation of interference effects of the model. Which was thought to be due to the Reynolds number which is much lower in the wind tunnel, while the model for interference drag is defined for high Reynolds numbers.

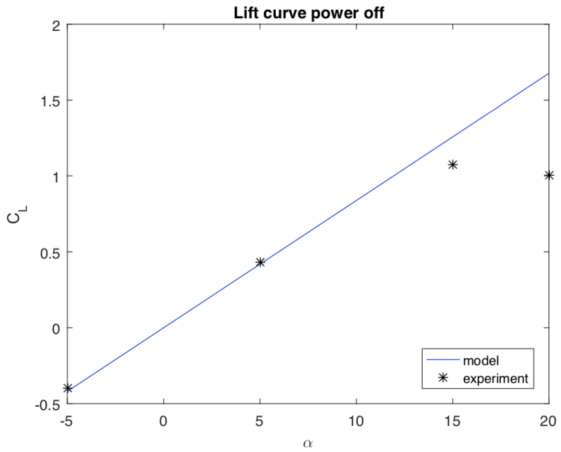

Figure 2.7: Lift curve power-off - model vs experiment[10]

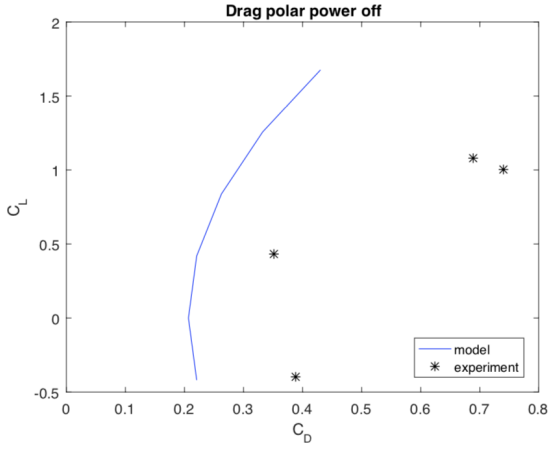

Figure 2.8: Drag polar power-off - model vs experiment[10]

In the third part of the test, the propeller is modelled as power on and tested for advance ratios of 0.28, 0.42 and 0.56. From this, it was observed that the lift is correctly modelled for an advance ratio of 0.42. The advance ratio of 0.28 shows a large deviation between model and experiment, where the experiment shows a steeper lift curve slope than the model. Lastly, the advance ratio of 0.56 showed an overestimation of the lift by the model. For the elevator effectiveness, it has been observed that for all the advance ratios, the unstalled region is from 0° till 10°. From Figure 2.9 and Figure 2.10, it can be seen that elevator effectiveness has been overestimated by the model. The rudder effectiveness for positive and negative deflection angles at various advance ratios can be seen in Figure 2.11. From this, it can be seen that the rudder effectiveness decreases with advance ratio.

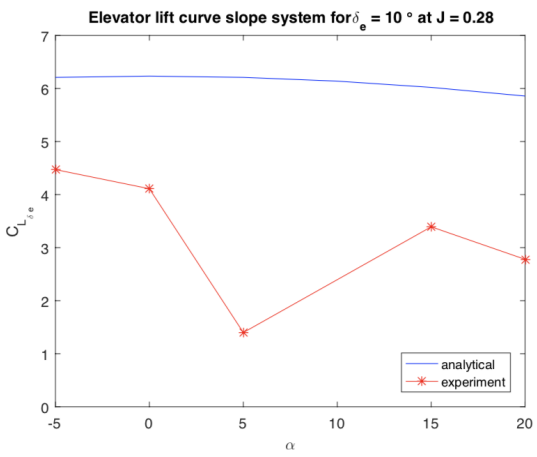

Figure 2.9: Elevator effectiveness for $\delta_e = 10°$ - model vs experiment[10]

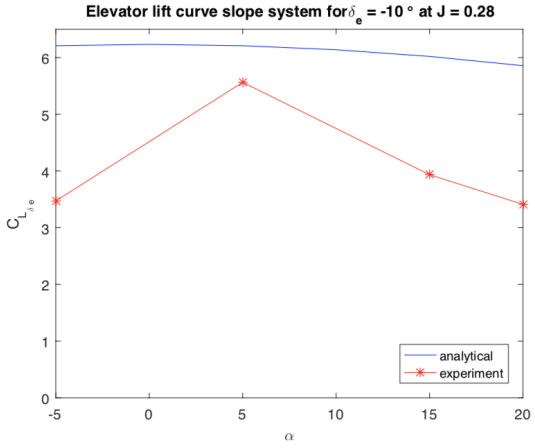

Figure 2.10: Elevator effectiveness for $\delta_e = -10°$ - model vs experiment[10]

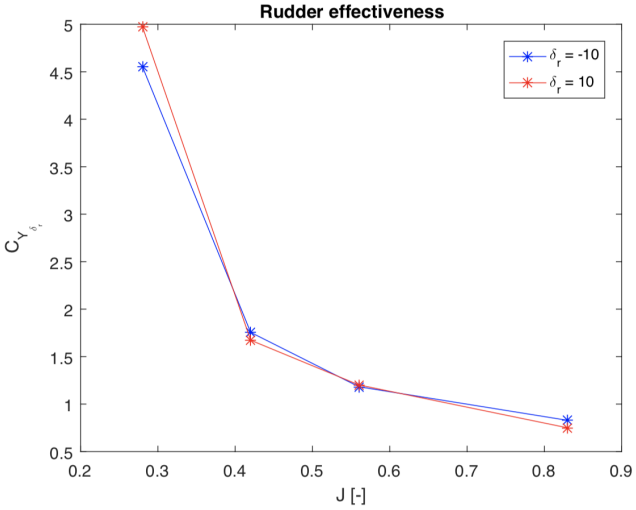

Figure 2.11: Rudder effectiveness for various advance ratios[10]

So to summarise, from this wind tunnel test it has been observed that over a range of operational conditions the thrust is modelled accurately. The lift and side forces are predicted within acceptable margins before stall, however the stall angle as well as the maximum lift are not correctly estimated by DFDC. The drag coefficient has been been observed to be underpredicted by DFDC, which is linked to the fact that the model lacks information on the complex interference effects between components and separation of the flow. This means that more experiments are required to verify these results, so a solid conclusion can be drawn on the aerodynamic characteristics.

2.2.2. Stability and Control Analysis

Stability and control can be divided into three requirements. First, the aircraft has to ensure equilibrium in steady flight. This is defined as the trim condition. Secondly, the aircraft has to ensure stability around this state of equilibrium, such that a disturbance is restored. Finally, forces have to be generated for manoeuvring, which is the control of the aircraft[14].

In aircraft design, the first estimate for stability and control is done through the tail volume coefficient method. This coefficient is based on statistical data of reference aircraft and gives a tail-wing area ratio, provided a tail arm and mean aerodynamic chord is know[15]. This can be seen in Equation (2.13). However, the tail volume coefficient is based on data of conventional aircraft and hence cannot be used as reference for a unconventional design. Furthermore, this method does not prove that an aircraft is stable.

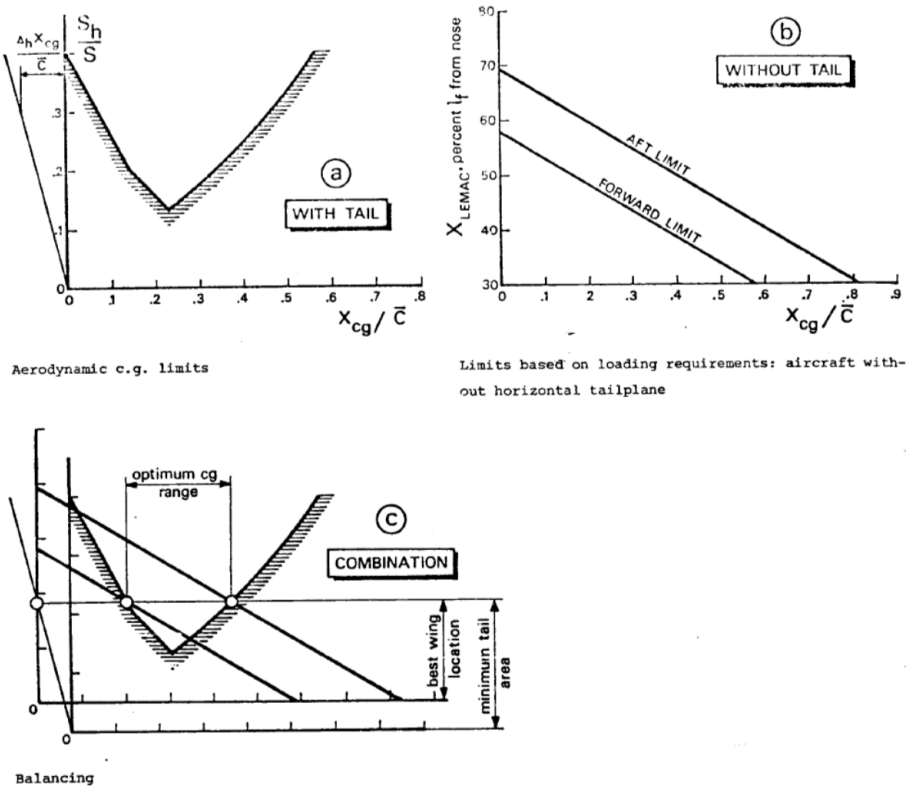

Figure 2.12: X-Plot method by Torenbeek[15]

$$\bar{V}_H = \frac{S_h l_h}{S_w \bar{c}} \tag{2.13}$$

A higher order method to determine the aircraft longitudinal stability and control is through Torenbeeks'[15] X-Plot method. This method of Torenbeek relies on the moment balance of the aircraft, which means that the tail of the aircraft should be a certain size such that it can create sufficient force to balance the aerodynamic moments of the aircraft without tail. Two plots are created and combined to determine the required tail-wing area ratio and the corresponding wing location, which guarantees a stable aircraft. This moment balance is carried out at various center of gravity (CG) positions while keeping the tail to wing area ratio as a variable. This is the first plot required for the X-Plot method and an example can be seen in the top left plot in Figure 2.12. The second plot presents the CG range for various wing positions and an example can be seen in the top right plot of Figure 2.12. These 2 plots are then combined and the intersection of these lines gives the minimum tail to wing area ratio and the location of the wing, this can be seen in the bottom plot of Figure 2.12.

The X-Plot method is analysed for the DUUC aircraft by Dungen[16]. However, Dungen modified the method of Torenbeek slightly since tail to wing area ratio cannot be treated as a variable for the DUUC after the aspect ratio of the duct is chosen. The X-Plot of the DUUC can be seen in Figure 2.13. The most aft position of the wing is at 50.8% of the fuselage to guarantee neutral stability with a 5% margin. The most forward location is constrained by control at take-off and stall. However, this design was also used in the research of Hameeteman[17] and resulted in a static margin of 40%. Hence, the scissor plot is not the best estimation method for the DUUC.

The loading diagram of the DUUC created by Dungen[16] can be seen in Figure 2.14. In his research he compared the loading diagram of the DUUC with the ATR72-600 aircraft. Due to the ducted fans at the rear of the aircraft, the OEM CG position is located at 0.65MAC while this is 0.35MAC for the ATR72. Furthermore, from the figure it can be seen that the CG excursion of the ATR72 is only 0.33MAC while the DUUC has a CG excursion of 0.49MAC. The large CG excursion poses the challenge to find the optimal wing position as well

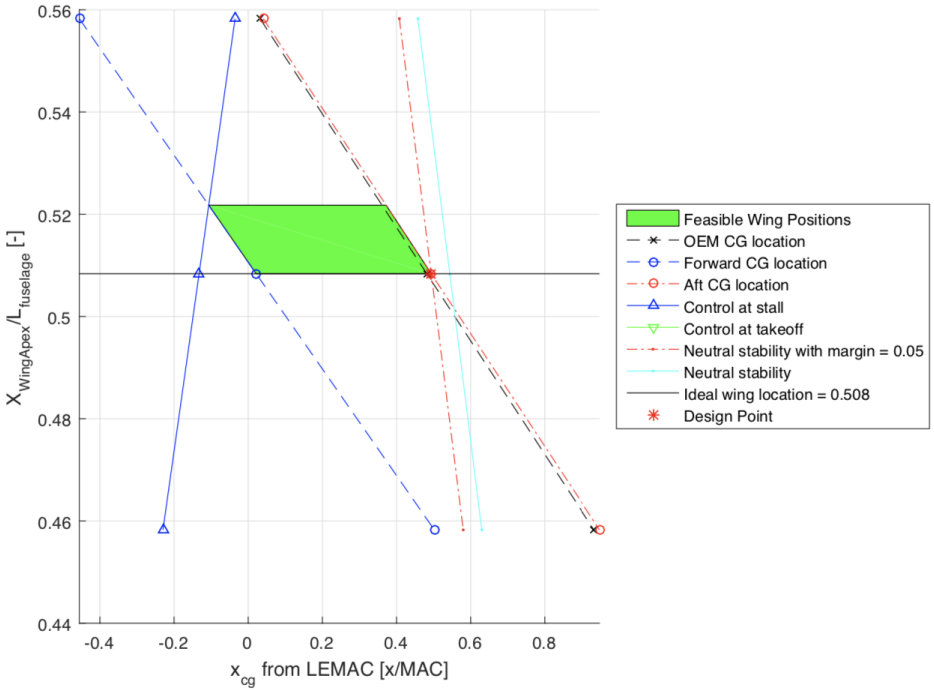

Figure 2.13: X-Plot DUUC aircraft[16]

as an efficient horizontal stabilising surface. Since an aft CG position of the DUUC, requires a large horizontal stabiliser downforce (C_{L_h} = -0.52 and $C_{L_{tail-off}}$ = 1.3) which induces a large trim drag.

Since the X-Plot method is still a preliminary method for the determination of aircraft control and stability. A more advanced method is necessary to understand the flight mechanics of the DUUC. This advanced method is carried out using PHALANX in the research of Hameeteman[17]. PHALANX is developed by TU Delft and is a flight dynamics simulation model. The program is written in Simulink and Matlab and utilises the Simscape package in order to model the physical system[18].

Since PHALANX is built in a modular fashion, it is easy to incorporate unconventional models like the DUUC. Hameeteman[17] started modelling the DUUC from an existing blended wingbody (BWB) model. This BWB is modelled in PHALANX as a body with a single reference frame which is located in its center of gravity. How-

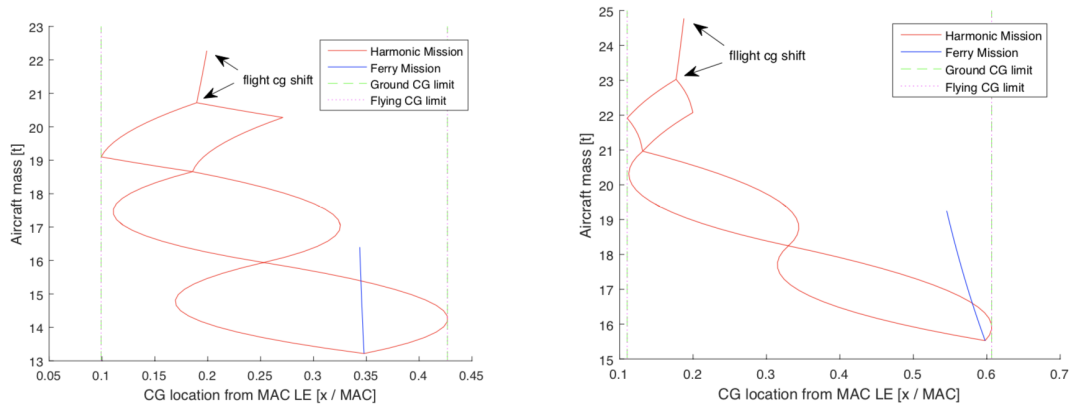

(a) ATR72-600 : $\frac{\Delta x_{cg}}{\bar{c}}\Big|_{max} = 0.33$, $\frac{\Delta x_{cg}}{\bar{c}}\Big|_{flight} = 0.0095 = 2.2\text{cm}$

(b) DUUC : $\frac{\Delta x_{cg}}{\bar{c}}\Big|_{max} = 0.49$, $\frac{\Delta x_{cg}}{\bar{c}}\Big|_{flight} = 0.0102 = 2.5\text{cm}$

Figure 2.14: Loading diagram DUUC and ATR72-600[16]

ever, a certain pitch rate simulated around the c.g. induces different local incidence angles on the nose and tail of the aircraft. Aerodynamic analysis has been performed to obtain the dynamic stability derivatives for the BWB to account for this. However, the DUUC does not have this data available, therefore Hameeteman implemented multiple reference frames in his model. These references are located at the quarter chord of the tail and wind and the midpoint of the fuselage. This is schematically depicted in Figure 2.15.

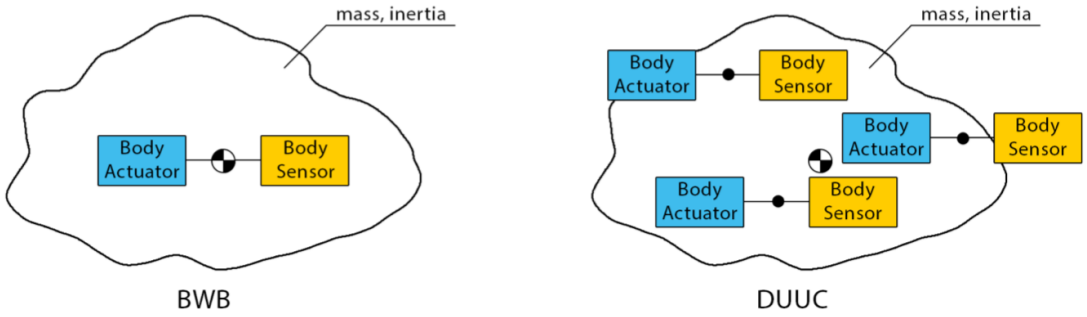

Figure 2.15: PHALANX body and reference frame schematically depicted[17]

In order to use PHALANX, the aerodynamic coefficients such as C_L, C_D and C_M of the DUUC needs to be known. Hameeteman[17] obtained these coefficients by performing a CFD analysis on the DUUC in his research. Since the Euler method used for the CFD analysis does not calculate the parasite drag, a drag correction has been implemented based on Raymer's form factor model. Finally, an estimation is made for the weight and moment of inertias of the DUUC, since these are necessary for the stability and control analysis.

Since no data was available on the inertia characteristics, an estimation based on statistical data was used. These estimations require the aircraft weight as input. However, since no weight data of the DUUC was available, the Boeing 737-700 data was used, since the scaled model of the DUUC was based on the Boeing 737-700. This results in the estimates of the inertias as can be seen in Figure 2.16.

Parameter	Description	Unit	Value
$MTOM$	Maximum take-off mass	kg	70,310
OEM	Operating empty mass	kg	38,150
FM	Fuel mass	kg	21,000
I_{xx}	Mass moment of inertia along the x-axis	kgm^2	635,923
I_{yy}	Mass moment of inertia along the y-axis	kgm^2	1,879,631
I_{zz}	Mass moment of inertia along the z-axis	kgm^2	2,414,932

Figure 2.16: Mass data used and inertia estimations of the DUUC[17]

The free body diagram used in the research of Hameeteman can be seen in Figure 2.17. From this figure, it can be seen that the aerodynamic forces are divided into three sections, wing, tail and fuselage. In order to achieve trim, the sum of these forces and moments should equal 0 and can be seen in Equations (2.14), (2.15) and (2.16). These forces and moments are a function of angle of attack, elevator deflection angle and throttle. So, PHALANX changes these parameters and a short simulation is performed to obtain the accelerations in X and Z direction and the pitch rate. This is then stopped when the accelerations, control surfaces or throttle reach a certain limit.

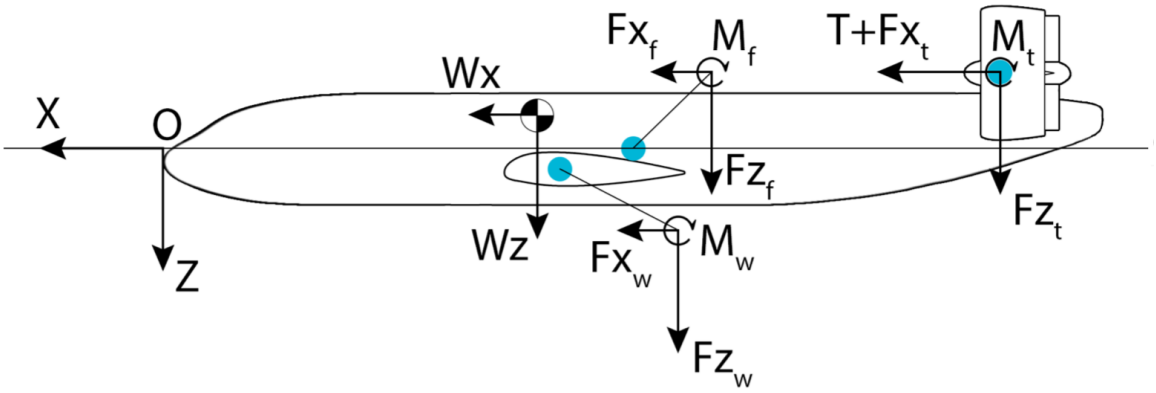

Figure 2.17: Reference coordinate system and free body diagram of DUUC used in PHALANX[17]

$$\sum F_X : F_{X_{wing}} + F_{X_{tail}} + F_{X_{fuselage}} + T - W\sin\theta = 0 \tag{2.14}$$

$$\sum F_Z : F_{Z_{wing}} + F_{Z_{tail}} + F_{Z_{fuselage}} + W\cos\theta = 0 \tag{2.15}$$

$$\begin{aligned}\sum M_Y : {} & M_{wing} + M_{tail} + M_{fuselage} \\ & + F_{Z_{wing}}(x_{cg} - x_w) + F_{Z_{tail}}(x_{cg} - x_t) + F_{Z_{fuselage}}(x_{cg} - x_f) \\ & + F_{X_{wing}}(z_w - z_{cg}) + (T + F_{X_{tail}})(z_t - z_{cg}) + F_{X_{fuselage}}(z_f - z_{cg}) = 0\end{aligned} \tag{2.16}$$

It should be noted that Hameeteman[17] performed the stability and control analysis with a static margin of 10% which was deemed more realistic, while the DUUC has a static margin of 40% due to the aft location of the engines. The short period was found to be stable while the phugoid was not. Furthermore, it was observed that it takes 2 seconds to return to trim after a disturbance of 1°. For controllability, a $6-8°/s^2$ pitch acceleration for large transport aircraft during take-off is recommended by Roskam[19]. This is achieved by the DUUC with a vane deflection of 10°. The longitudinal handling qualities have been assessed using the criteria specified in MIL-STD-1797A[20], and it is found that the short period and Control Anticipation Parameter (CAP) criteria are inside Level 2 region.

Finally, the effect of changing the centre of gravity as well as changing the mass on stability, has been analysed by Hameeteman[17]. It has been observed that the heavier aircraft responds slower to disturbances in both dynamic and static simulations. Furthermore, it has been observed that longitudinally the aircraft becomes less stable by moving the CG aft. In order to obtain a static margin of 10%, which is typical for this type of aircraft, the center of gravity should be positioned at 48% MAC.

2.2.3. Weight analysis

An extensive weight analysis has been performed in the research of Stavreva[21], since the previous studies used empirical relations for the weight analysis. Stavreva used the Class 2.5 weight estimation method where a simplified Finite Element Method was used to determine the static loadings. The three critical design conditions for the analysis of the duct were: take-off, cruise and dive. It has been observed that this analysis reduced the weight of the duct by half compared to the empirical relations. Furthermore, A mass reduction of over 70% can be achieved if CFRP is used as the material. The engine pylon has also been analysed using this method, an increase in pylon mass was obtained due to the high loading of the engine thrust. This can also be reduced to less than half of the original weight if CFRP is used.

A new performance analysis has been done in the research as well, with the improved weight estimation. This resulted in a reduction of the operational empty weight. Which means the freed weight could be used

to increase the range by increasing the fuel weight or increase the payload of the aircraft. However, when comparing the newly obtained performance characteristics with the performance of the ATR72-600, it has been observed that the DUUC is still not able to match the performance. The next section will elaborate on the performance characteristics of the DUUC, compared to other configurations.

2.2.4. Performance Analysis

Vos and Hoogreef[22] performed a system level assessment of three regional aircraft, with various propulsion-airframe configurations, of which one has ducted propellers at the rear of the fuselage. These three configuration can be seen in Figure 2.18 and are designed for a harmonic mission of 1530km and 7500kg payload. The goal in this study was to compare their aerodynamic and mission performance as well as their weight and balance.

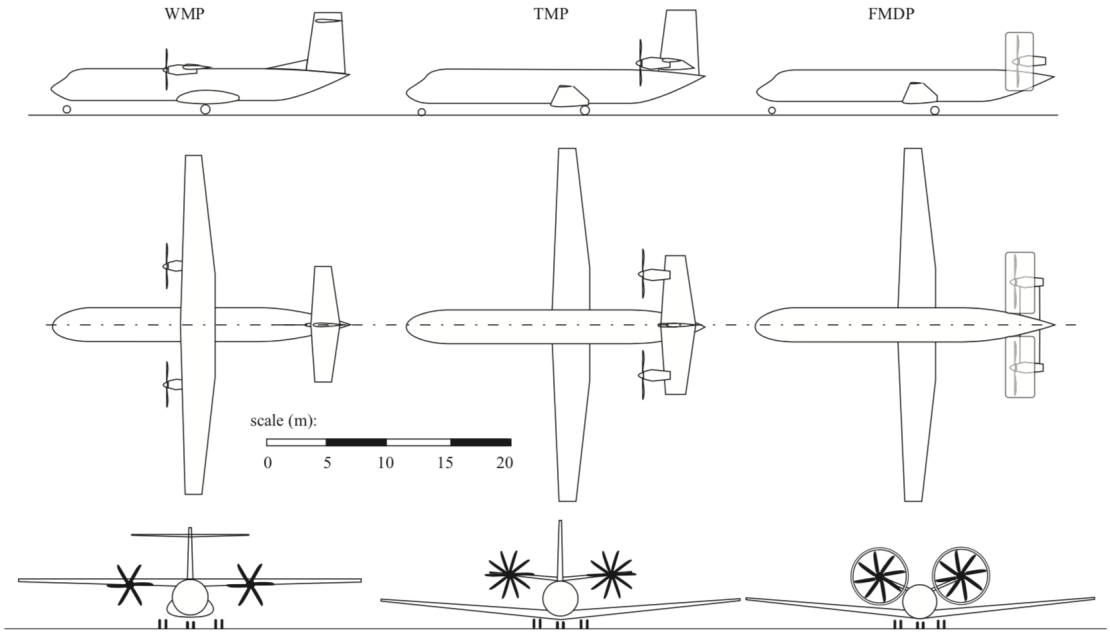

Figure 2.18: Three aircraft configurations for system level assessment[22]

Firstly, from the wing loading and power loading diagram, it has been observed that while the design point in terms of wing loading and power loading for the different configurations was the same. The fuselage-mounted ducted propellers (FMDP) configuration showed the lowest cruise excess power, while this was the highest for the wing-mounted propellers (WMP) configuration. Secondly, a loading diagram was created to understand the CG excursion of the three configurations and can be seen in Figure 2.19. The WMP configuration showed the most favourable CG excursion of 30% MAC, while the tail-mounted propeller (TMP) and FMDP have a CG excursion of 40% and 41% respectively. Furthermore, the WMP configuration is expected to have lower trim drag due the forward location of the CG as a result of the engine positioning, which results in a larger tail arm.

Thirdly, scissor plots were created to get a preliminary estimate for the tail size. The WMP showed the smallest tail-to-wing area ratio of 28%, while this was 37% and 31% for the TMP and FMDP, respectively. A comparison of the key performance indicators can be seen in Figure 2.21. It can be observed that the two aft-mounted engine configurations have a larger MTOW compared to the WMP. When comparing the harmonic profiles, it has been observed that the three configuration show an overall similarity except from climb. Where the aft-mounted engine configurations need more time to climb due to their lower excess power. Lastly, a comparison of the payload-range diagram can be seen in Figure 2.20. It can be observed that the WMP configuration has the highest off-design range, which is followed by the TMP and FMDP configuration. This is linked to the higher operating empty weight of the aft-mounted engine configurations as well as a higher friction drag. It

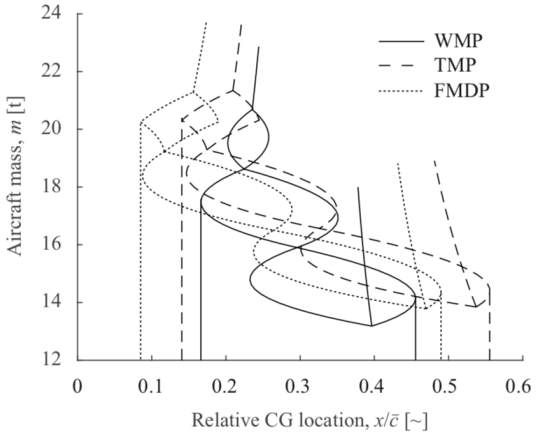

Figure 2.19: Comparison of the loading diagram of the three configurations[22]

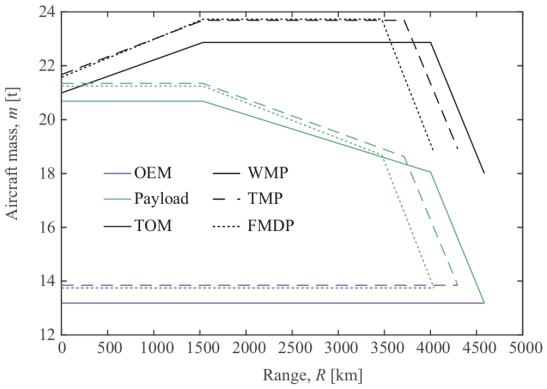

Figure 2.20: Comparison of the payload-range diagram for the three configurations[22]

should be noted that in this study the drag estimates of the FMDP were fairly conservative and the beneficial effect between fan and duct were not taken into account.

Parameter	Unit	WMP	TMP	FMDP
MTOM	t	22.9	23.7	23.7
OEM	t	13.2	13.8	13.7
Mission fuel	t	2.2	2.3	2.5
Power loading	N/kW	63.7	63.5	63.0
Wing loading	N/m^2	3330	3340	3350
$X_{\bar{c}/4}/L_{\text{fus}}$	-	0.47	0.49	0.52

Figure 2.21: Comparison of key performance indicators of the three configurations[22]

2.3. Propeller analysis theory

Since aerodynamic analysis will be performed on the propeller of the DUUC, the theory behind these analyses has to be understood. The propeller has been around for more than a century nowadays and it is known that the first propeller theory has been there before the first flight of the Wright brothers[23]. The main concept of the propeller is to convert engine torque into axial thrust, in order to provide the required force such that the aircraft can be propelled forwards. This displaces the volume of air rearwards, obeying Newton's third law. The measure of how well the propeller does this, is determined by the propeller efficiency. The propeller efficiency is influenced by a number of factors, these include for example: diameter, pitch, number of blades, blade angle, solidity, tip speed and chord variation along the blade. The lift and drag coefficients of the propeller also play a role, these are influenced by the angle of attack of the propeller blades[24]. There are various methods to determine the performance of the propeller. In the following subsection these methods will be elaborated upon.

Propeller charts

A method to determine the propeller efficiency can be done with the propeller charts. In these charts, the propeller performance is given in term of η_j(propulsive efficiency), J(advance ratio) and $\beta_{0.75}$, which is the blade pitch angle measured at 75% of the chord. The thrust coefficient (C_t) and power coefficient (C_p) are also plotted against the advance ratio, for certain blade pitch angles[25]. Examples of these propeller charts can be seen in Figure 2.22. However, these chart represent data from experimental results from not-representative propellers. Therefore, different methods have to be analysed.

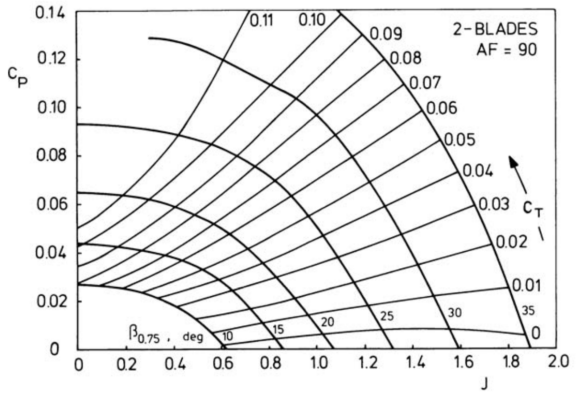

(a) Propeller chart

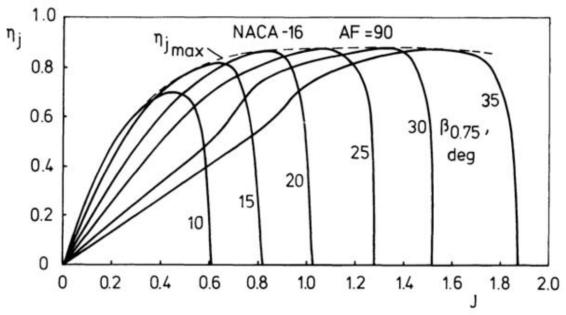

(b) Propulsive efficiency

Figure 2.22: Propeller performance of a NACA-16 2-bladed variable-pitch propeller[25]

Actuator disk theory

The most classic and efficient method for modelling the influence of a propeller is the actuator disk theory[26]. With this model, the flow around each propeller blade is not examined in detail, but is instead treated as a large amount of blades such that it can be replaced by an infinitely thin disc in its plane. This causes an uniform and instantaneous increase of velocity and pressure after the disc[27]. In Figure 2.23 the flow through the propeller modelled by actuator disk theory can be seen.

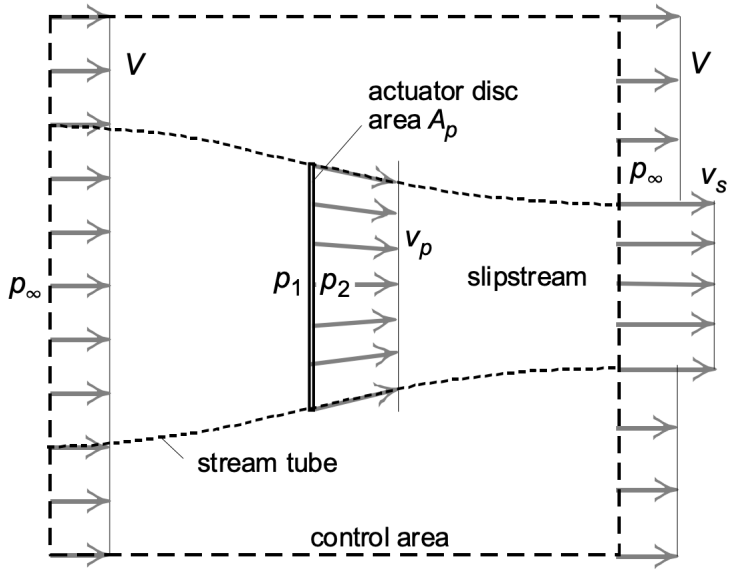

Figure 2.23: Actuator disk theory flow through propeller[27]

It can be assumed that the surrounding flow does not experience a change in momentum. This means that the surrounding flow and propeller do not exert a reaction force on each other. Therefore, the thrust is defined by the change in momentum slipstream and can be seen in Equation (2.17)

$$T = \dot{m}_a(v_s - V) \tag{2.17}$$

The thrust provided by the propeller is also given by Equation (2.18), which is the force exerted on the disc surface due to the jump in pressure. The pressures p_1 and p_2 are given by Equations (2.19) and (2.20), respectively.

$$T = (p_2 - p_1)A_p \tag{2.18}$$

$$p_1 = p_\infty + \frac{1}{2}\rho\left(V^2 - v_p^2\right) \tag{2.19}$$

$$p_2 = p_\infty + \frac{1}{2}\rho\left(v_s^2 - v_p^2\right) \tag{2.20}$$

Filling in the pressure difference into Equation (2.18) and equating this to Equation (2.17) results in Equation (2.21). With this equation, it can be observed that the velocity through the plane of the propeller is equal to the average value of the velocities far in front and far behind the propeller.

$$v_p = \frac{v_s + V}{2} \tag{2.21}$$

Using the power delivered from the slipstream velocity and propeller velocity, the propeller efficiency can then be determined. The power delivered is given by Equation (2.22). Knowing that the power available is given by $P_{av} = TV$, the difference in power delivered and power available the jet efficiency can be calculated using Equation (2.23).

$$P_j = \frac{1}{2}\dot{m}_a(v_s^2 - V^2) = \dot{m}_a(v_s - V)\frac{v_s + V}{2} = Tv_p \tag{2.22}$$

$$\eta_j = \frac{P_{av}}{P_j} = \frac{TV}{Tv_p} = \frac{V}{\frac{v_s+V}{2}} = \frac{2V}{v_s + V} = \frac{2}{1 + \frac{v_s}{V}} \tag{2.23}$$

Blade element theory

The actuator disk theory can be used for a good estimation of the change in momentum flow and the kinetic energy of the flow through the propeller. However, it does not give the thrust that is exerted on the propeller. This means that the actuator disk theory is not suitable for detailed analysis on the propeller, to improve the design in terms of performance[27]. This can be done with the blade-element theory, since the aerodynamic forces are calculated on a number of blade elements and these are then integrated along the propeller blade. This then results in the thrust of the propeller. It has a higher accuracy, since the blade-profile drag as well as slipstream swirl is taken into account. The forces on a blade element can be seen in Figure 2.24, this is from a distance r from the shaft.

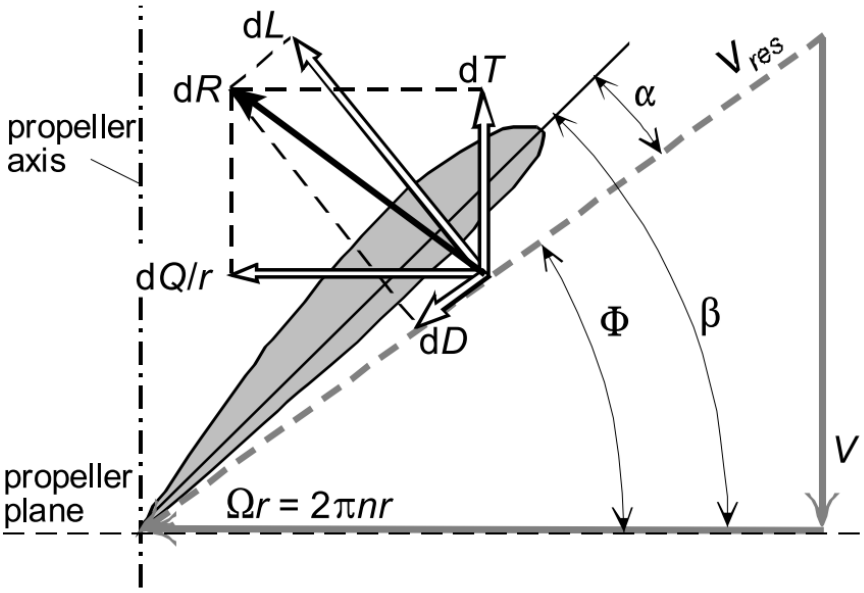

Figure 2.24: Forces on a propeller blade element[27]

In blade element theory, two dimensional flow assumption has been made. Hence, in the radial direction there is no flow. The resultant flow velocity is given by Equation 2.24, where the advance ratio (J) is given by Equation 2.25.

$$v_{res} = V\sqrt{1 + (\pi/J)^2(r/R_p)^2} \tag{2.24}$$

$$J = \frac{V}{2nR_p} \tag{2.25}$$

The resultant force dR can then be solved by taking the component perpendicular to the flow dL and the component in the direction of the flow dD, as can be seen in Equation (2.26) and (2.27), respectively.

$$dL = c_l \frac{1}{2}\rho v_{res}^2 c dr \tag{2.26}$$

$$dD = c_d \frac{1}{2}\rho v_{res}^2 c dr \tag{2.27}$$

As mentioned before, the blade thrust is then the integral over the blade elements along the radius. This is multiplied by the number of blades (B_p) to obtain the propeller thrust, as can be seen in Equation (2.28).

$$T = B_p \int_{R_h}^{R_p} (c_l cos(\phi) - c_d sin(\phi)) \frac{1}{2}\rho v_{res}^2 c dr \tag{2.28}$$

2.4. Annular wings

Annular wings have recently had an increased in popularity due to their application in ducted-fan UAVs. The static and dynamic thrust produced, are increased due to the annular shroud. However, in forward flight it can also act as a lifting surface when designed as an annular wing. The concept of ring wings on passenger aircraft have also been conceptualised. However, although work on ring wings can be traced back to 1947, the concept has not been fully studied and not received significant attention[28]. One of the more successful methods of determining lift of a ring wing has been derived by Weissinger[9], as has been used in the research of Harinarain[10].

The lift characteristics of the annular wing has been analytically derived by Ribner[29], where he concluded in his research that compared to a flatplate elliptical wing having the same aspect ratio, the lift curve slope of the annular wing is doubled. The aspect ratio is defined as $8R/\pi c$, with R as the radius of the ring and c the chord. This conclusion has also been confirmed in the research of Fletcher[30]. In his research, an experimental investigation was performed by varying the aspect ratios of the annular wings and using various theoretical models to compare the lift-curve slope. The aerodynamic characteristics of five annular wings were assessed, with the aspect ratios ranging from 0.33 to 3 and the Reynolds number ranging from 0.704-2.11 million (as the chord varied). In the research of Fletcher[30] and following researches treated in this section the aspect ratio is defined as the diameter of the ring wing divided by the chord.

Traub[31] furthered the investigation of Ribner[29] and performed the analysis on annular wings with aspect ratios of 1 and 2. This allowed him to modify the equations for lift curve slope of Ribner. Opposed to Ribner, the equations take into account aspect ratio, where first two different equations had to be used for low and high aspect ratios.

Maqsood and Go[28] introduced a further developed model, where the performance of the annular wing was estimated using the leading-edge suction analogy. With this concept, the total lift is calculated by taking the sum of the potential-flow lift as well as the lift associated with the leading edge and side egde vortices. This allows for a parameterization of the overall lift into pressure-induced contributions and vortex-induced contributions. Thus, allowing for a better insight into the factors contributing to aerodynamic performance.

Anderson et al[32] compared the models developed by Ribner, Traub and Maqsood with experimental data as well as AVL, as can be seen in Figure 2.25. From the figure it can be seen that there is no analytical model that predicts the lift curve slope the best for all aspect ratios. Traub's equation, particularly for aspect ratios of 2 and above, presents the best overall analytical prediction method. For the lower aspect ratios, the lift curve

slope is predicted very well by the methods Maqsood and Go and Lowry and Polhamus. AVL is identified to provide the best prediction method, however for correct utilisation this requires some skills on the user end.

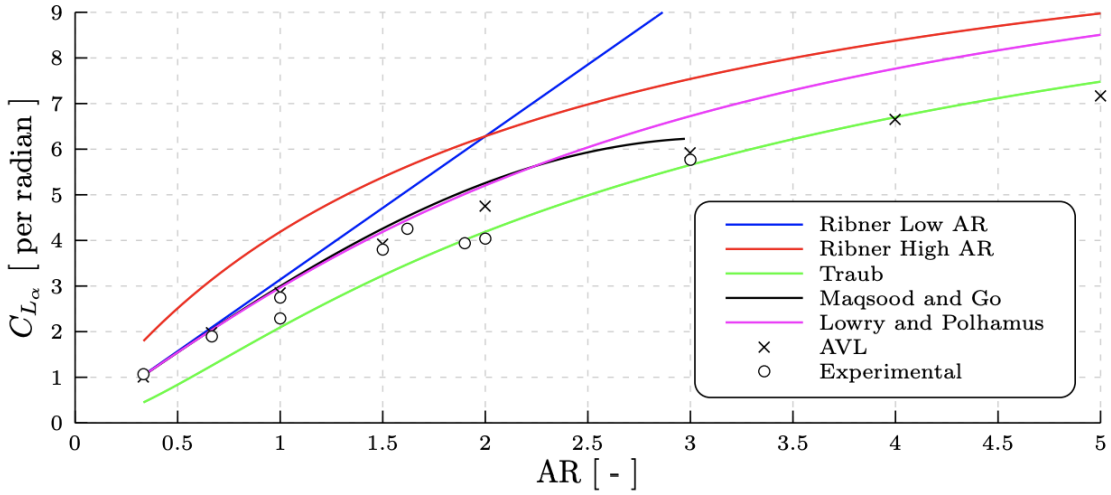

Figure 2.25: Comparison of theoretical models of annular wings with experimental data[32]

In a further research of Traub[33], the effect of stagger of the ring wing was investigated. From Figure 2.26, it can be seen that the research has been performed on 3 models: a ring wing with positive and negative stagger of 40°, as well as a flat wing. A NACA0012 profile was used for the models. From this research, the conclusion has been made that the annular wing with negative stagger reduces the minimum drag coefficient significantly, compared to the annular wing without stagger. The same applies for the sectional pressure drag variation with lift coefficient, which is also reduced. The reduction in drag due to stagger was observed to be due to the reduction of the laminar separation bubble as well as displacing it aft. Lastly, it has been observed that a strong nose-up pitching moments of the ring wing was generated with both positive and negative stagger. With negative stagger producing the best lift-to-drag performance.

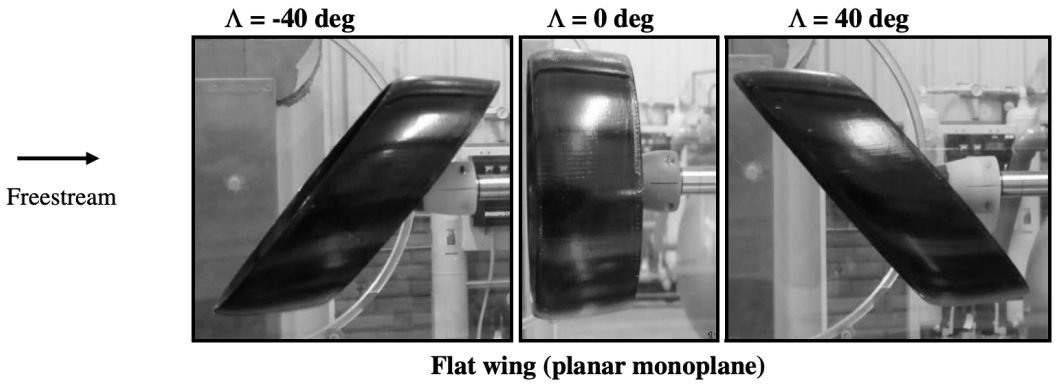

Figure 2.26: Geometry definition ring wing stagger[33]

2.5. Ducted fans

The advantages of ducted propellers have been proven experimentally already in 1931 by Stipa. The popularity of this concept grew with the development of VTOL and hover capable aircraft[34]. An extensive research on ducted propellers has been performed by Black et al[35]. In theory, the slipstream contraction is substantially reduced by the duct compared to a conventional propeller. This is schematically depicted in Figure 2.27. Due to the increased mass flow over the upstream surfaces of the duct, a suction pressure field is created. This results in a forwards thrust on the duct. The thrust produced by the propeller without the duct is larger than the propeller with duct. However, the combination of the thrust produced by duct and propeller

is larger than the propeller alone. When the duct exit area is equal to the propeller disk area, the theoretical thrust increase is 26% at static conditions. However, it has been observed that for increasing flight speeds these thrust benefits due the duct are diminished. Furthermore, when viscous effects are taken into account, the benefits are lost and the propeller without duct is performing better at high speeds.

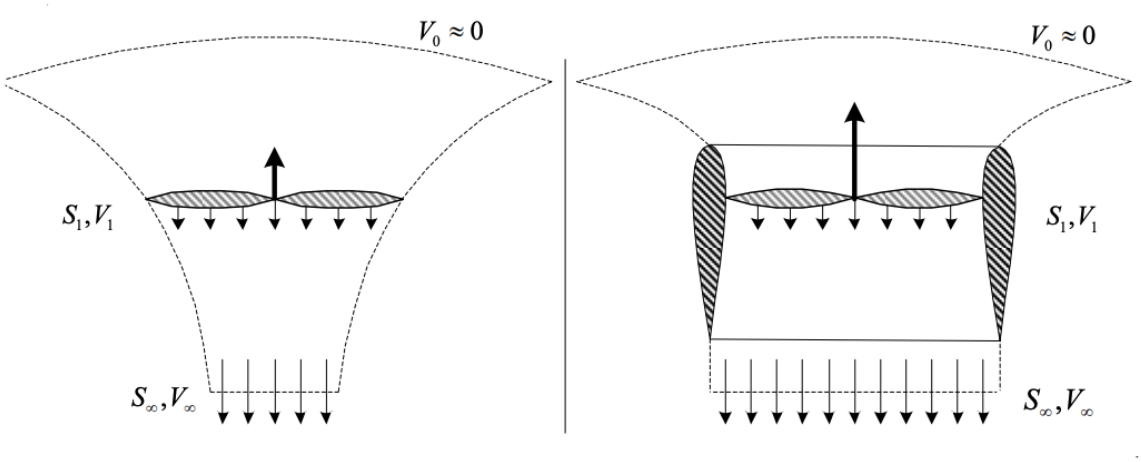

Figure 2.27: Free fan and ducted fan air stream contraction comparison[36]

The effects of the lip diameter, propeller rotation speed and Reynolds number has been studied by Parlett[37], and in his research it was found that the static thrust efficiency increases with increasing lip diameter. The effects of lip diameter has also been investigated by Graf et al[38]. In this research, it was concluded that a larger lip radius increased thrust in static conditions and the performance of a smaller lip radius was more favourable in crosswind conditions and forward flight.

The effect of duct shape on ducted propeller performance has been investigated by Yilmaz et al[39], for axial flight conditions and hover. The investigated duct shapes can be seen in Figure 2.28. From this research, it has been observed that the power coefficient of the propeller with duct is lower than without the duct, which means that the propeller with duct is more efficient. Furthermore, the thrust coefficient of the duct decreases with increasing advance ratio, until the advance ratio is larger than 0.35, after which it becomes negative for all duct geometries. The advance ratio is defined as $J = \frac{U_\infty}{nD}$, with U_∞ as the freestream velocity, n the revolutions per second and D the inner diameter of the duct. Overall, an increase of propulsive efficiency up to 10% was observed.

The effect of propeller location inside the duct has been analysed by Anderson et al[32]. In this research, a different approach is taken for the duct design, where it is treated as an annular wing. So, generating lift for high speed, cruise flight is the primary function of the duct. Furthermore, the effect on the duct performance at various angles of attack due the the thrust generated by the propeller was also analysed. It was observed that the difference in performance for different positions of the propeller inside the duct annular wing is small. Moreover, a delay in stall (increase in $C_{L_{max}}$ of the annular wing can be observed with the presence of the propeller at moderate power. However, performance of the duct is degraded with too much thrust, since a backward shift of the aerodynamic center of the ring wing is observed with increasing thrust. Also, a tractor configuration is preferable when stall is approaching, since it does not suffer from ingesting the detached flow of the ring wing like the pusher configuration. This can be seen in Figure 2.29. The effect of propeller location has also been analysed by Black et al[35]. Two propellers were tested, located at 25% and 40% of the leading edge from the duct. From the tests, it has been observed that the propeller located at 25% of the duct performed considerably better. At Mach 0.5, an average performance benefit of 13% was observed.

Research on the vane behind a ducted fan has been done by Yaggy et al[40]. The vane with a 25% chord flap configuration can be seen in Figure 2.30. Please note that this research has been performed for the Doak VZ-4DA aircraft. This prototype was meant as an Vertical Take-off and Landing (VTOL) aircraft and consisted of 2 ducted fans attached at the wingtips, as can be seen in Figure 2.31. These ducted fans were vertical for take-off and landing and would rotate to a horizontal position for flight. When rotating the ducts, an

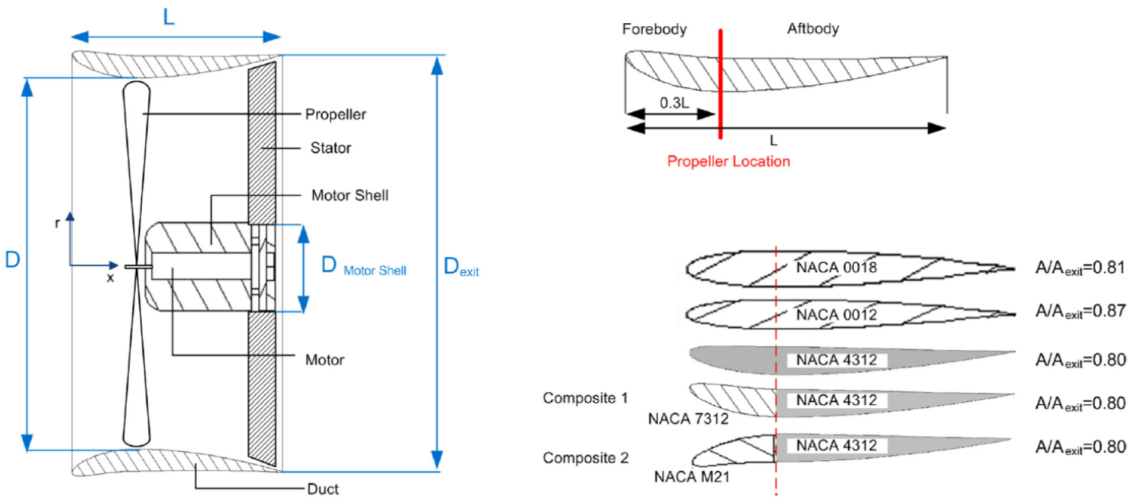

Figure 2.28: Duct shapes for experiment[39]

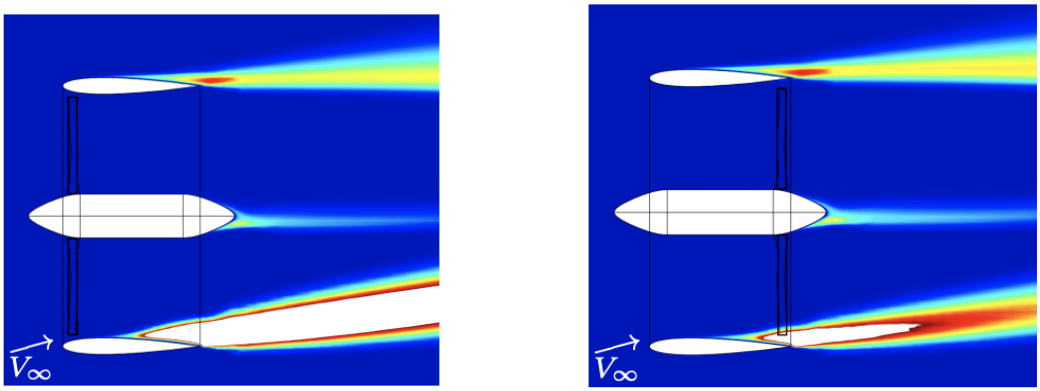

(a) Tractor configuration

(b) Pusher configuration

Figure 2.29: Comparison of stall characteristics[32]

unfavourable nose up pitching moment was observed, hence the need to perform the research to reduce the pitching moment with vanes. From the research, it has been observed that the vane was successful in reducing the pitching moment. From Figure 2.32, it can be seen that the vane was most successful with a deflection of 10° and a flap deflection of 20°.

The effect of duct length has been investigated by Black et al[35]. It is known that the duct must be sufficiently long to minimise the low speed slipstream contractions. In order to allow efficient diffusion as well as allowing low profile drag airfoils for cruise conditions. However, the propulsion system mass increases with long ducts as well as the friction drag. Therefore, 2 ducts with chord lengths of 50% and 66.7% of the propeller diameter were tested. From the tests, it has been observed that the 2 ducts showed similar performance characteristics until Mach 0.4. After this Mach number, the short duct adversely affects the performance. The reduction in thrust is almost 20% at Mach 0.5. It has been observed that at low power loadings, the degradation becomes more severe. The losses in performance at high Mach number are linked to the higher thickness ratio of the shorter duct.

Research on the side force produced by the vane at the exit of the duct has also been performed by Abrego and Bulaga[42]. It has been observed that although the vanes would partially block the downstream flow of the fan, they would also aid in aligning the swirl component of the flow black. Furthermore, these flapped vanes produces side forces, which could be used to produce control moments if the ducted fan is sufficiently

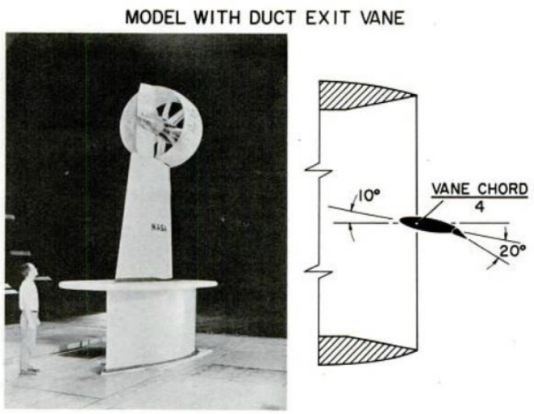

Figure 2.30: Ducted fan with vane full scale model for research[40]

Figure 2.31: Doak VZ-4DA prototype VTOL aircraft[41]

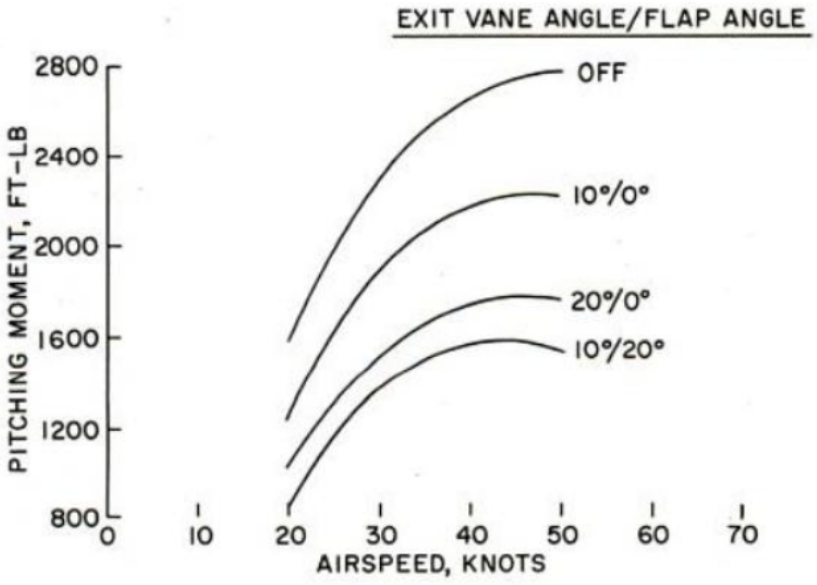

Figure 2.32: Reduction in pitching moment due to duct exit vane deflection[40]

located from the centre of gravity. The measurements were taken for 2 different exit vane flaps, a 3 inch vane with a 1 inch flap and a 3 inch vane with a 2.25 inch flap in axial flow conditions. From these measurements, it has been observed that the side force coefficients increased with increasing flap angle, as can be seen in Figure 2.33. Furthermore, a the 2.25 inch flap produced a slightly larger side force compared to the 1 inch flap.

An extensive research on the effect of exit vane deflection on a ducted fan has also been performed by Mort and Gamse[43]. In this research a 7 foot diameter ducted fan is analysed in the wind tunnel. The change in lift coefficient, drag coefficient, moment coefficient as well as power coefficient are measured for various exit vane deflections and thrust coefficients. It has been observed that for increasing thrust coefficients the gradient of the curves increases. Furthermore, the change in lift coefficient becomes less pronounced with increasing angle of attack. The opposite is true for the drag coefficient. Furthermore, the variation of moment coefficient due to the angle of attack is observed to be small. The same applies for the variation of power coefficient due the angle of attack.

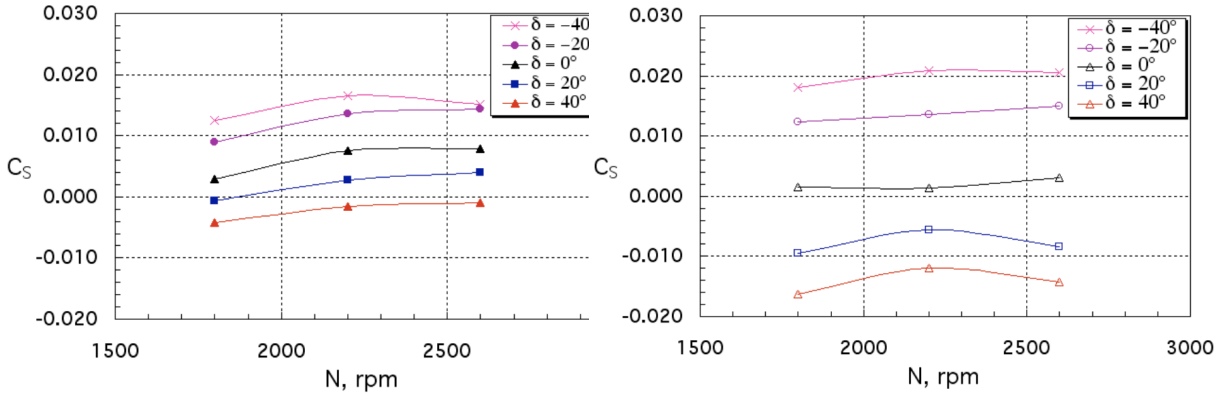

(a) 1 inch chord flap

(b) 2.25 inch chord flap

Figure 2.33: Side force coefficients for various flap angles[42]

2.6. Conclusion

This chapter described the various studies that have been performed on the DUUC as well the theory on propellers, ring wings and ducted fans. It has been observed that DFDC is able to predict the lift forces with an acceptable margin until stall, while the drag forces are underestimated. However, DFDC has to be tweaked manually to produce these results since the propeller thrust is not estimated correctly. The stability and control analysis showed that the DUUC has a very aft CG position as well as a large shift in CG due to the location of the ducted fans. Furthermore, from PHALANX the short period was found to be stable while the phugoid was not. However, this analysis has been performed with a static margin of 10% while the DUUC has a static margin of 40%. Furthermore, from a Class 2.5 weight analysis, a reduction of more than 50% of the duct weight is observed compared to the empirical relations. The performance analysis demonstrated that the aircraft with wing-mounted propellers has the lowest maximum take-off mass and burns the least amount of fuel. The two other configurations with the engines located at the rear of the fuselage have a slightly less performance, which is linked to the large CG excursion due to the aft-mounted propulsion system. An increase of 3% is predicted for the maximum take-off weight as well as a fuel burn increase between 5-10% for the innovative configurations. However, in this analysis the drag estimates for the ducted fan were conservative and the beneficial interaction between the duct and fan were not taken into account.

From the theory on propellers, it can be concluded that actuator disk theory is good for estimation of change in momentum flow and the kinetic energy of the flow through the propeller, however to calculate the thrust exerted on the propeller, blade element theory has to be used. It has been observed that the lift curve slope of an annular wing is doubled, compared to a flat wing with the same aspect ratio. From a comparison study of the different methods to calculate the lift on an annular wing, it has been concluded that there is no analytical model that predicts the lift curve slope the best for all aspect ratios. Furthermore, it has been observed that thrust produced by the duct and propeller is larger than the propeller only, due to the reduction of the slipstream contraction. This increases the mass flow upstream and creates a suction field. Furthermore, a larger lip radius increases the thrust in static conditions. A study on the exit vane of a ducted fan for controllability, showed the vane was most successful with a vane deflection of 10° and flap deflection of 20°. Lastly, a tractor configuration of the propeller was observed to be preferable when stall is approaching compared to a pusher configuration, while the difference is performance is small.

3

Methodology

As mentioned in the previous chapter stability and control can be divided into three requirements. First, the aircraft has to ensure equilibrium in steady flight. This is defined as the trim condition. Secondly, the aircraft has to ensure stability around this state of equilibrium, such that a disturbance is restored. Finally, forces have to be generated for manoeuvring, which is the control of the aircraft[14]. The method used to determine these forces is explained in Section 3.1. Section 3.2 elaborates on the method used to ensure stability. Section 3.3 gives details on the aerodynamic analysis tool used and in Section 3.4 the working of the program to determine the required duct size is described.

3.1. Sizing for controllability

To determine the force that has to be generated for manoeuvring, the free-body diagram has been created as can be seen in Figure 3.2. Where the subscript "WF" denotes wing-fuselage and "D" denotes duct. Writing out the sum of moments around the aircraft centre of gravity results in Equation (3.1). If one can determine all the variables except L_D, it is possible to calculate the required duct lift to provide sufficient control at a certain duct location. If the required lift is obtained, it is also possible to make a statement on the required duct size to provide the required lift. So, Equation (3.1) is rewritten to (3.2). Please note that equation is deliberately not transformed into coefficients, as is typically done. Since it is unclear what a correct reference surface area is for the duct. Overestimating the reference surface area will result in underestimating the lift coefficient and vice versa. However, in the later analyses to compare the various duct sizes, the aircraft wing area is used as reference area.

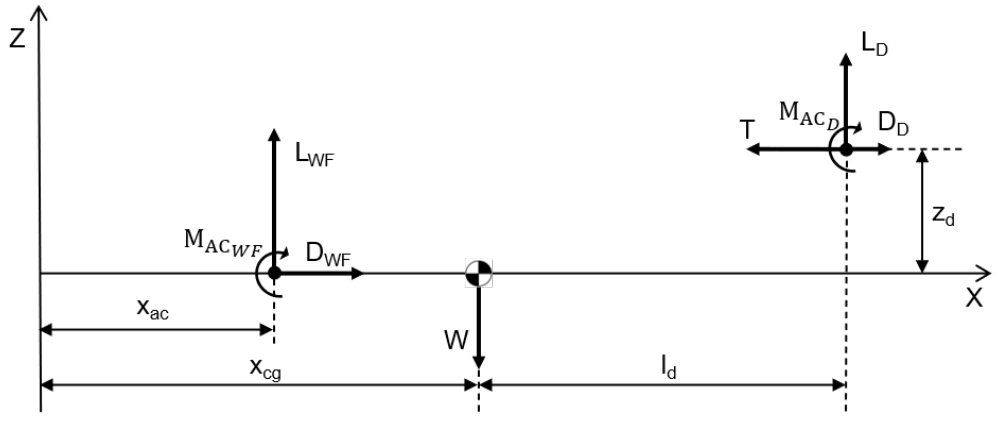

Figure 3.1: Forces and moments on DUUC aircraft during descent

$$\sum M_Y : M_{AC_{WF}} + M_{AC_D} + L_{WF}(x_{cg} - x_{ac}) - T \cdot z_d + D_D \cdot z_d - L_D \cdot l_d = 0 \tag{3.1}$$

$$L_D = \frac{M_{AC_{WF}} + M_{AC_D} + L_{WF}(x_{cg} - x_{ac}) - T \cdot z_d + D_d \cdot z_D}{l_d} \tag{3.2}$$

During flight, the aircraft rotates around the CG and the moments have to be taken around this point. However, during take-off roll the aircraft rotates around the main landing gear, hence the moments also have to be taken around this point to calculate whether the duct can provide sufficient force during take-off. The sum of moments around the main landing gear is described by Equation (3.3). The required lift that has to be generated by the duct during take-off roll, can then be calculated using Equation (3.4). So, for a specific duct location the duct lift required is assessed for both descent and take-off. This will make sure that the lift provided by the duct is sufficient for both descent and take-off.

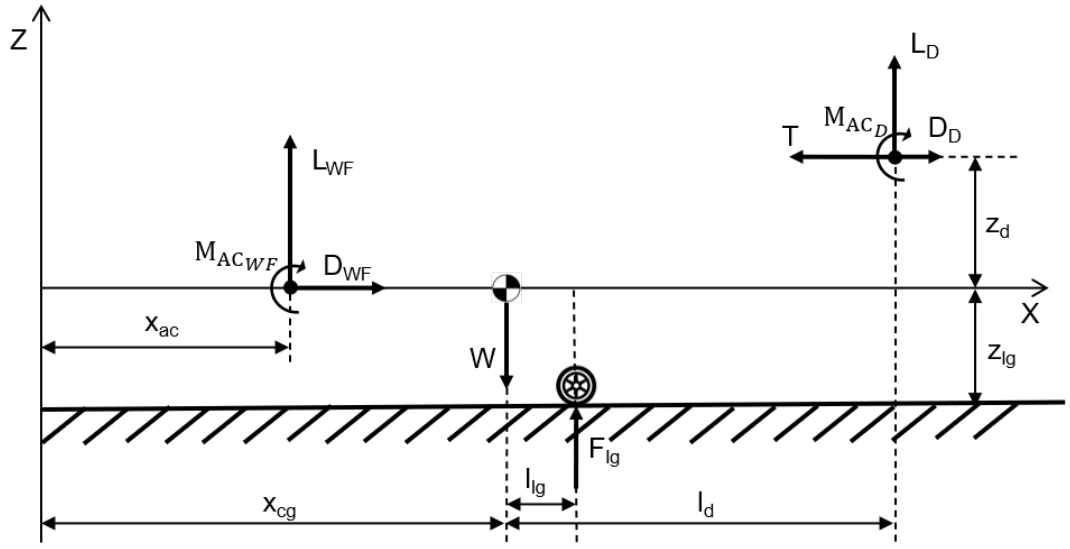

Figure 3.2: Forces and moments on DUUC aircraft during take-off

$$\sum M_Y : M_{AC_{WF}} + M_{AC_D} + L_{WF}(x_{cg} + l_{lg} - x_{ac}) + D_{WF} \cdot z_{lg} - W \cdot l_{lg} - T(z_d + z_{lg}) + D_D(z_d + z_{lg}) - L_D(l_d - l_{lg}) = 0 \tag{3.3}$$

$$L_D = \frac{M_{AC_{WF}} + M_{AC_D} + L_{WF}(x_{cg} + l_{lg} - x_{ac}) + D_{WF} \cdot z_{lg} - W \cdot l_{lg} - T(z_d + z_{lg}) + D_d(z_d + z_{lg})}{l_d - l_{lg}} \tag{3.4}$$

Please note that the starting point for this research is the final design of the DUUC obtained in the research of Stavreva[21]. This will be used as the baseline, so the aircraft dimension and weights have been determined using a class 2.5 weight estimation. Furthermore, the 2 critical points to size for control have been determined to be descent and take-off. Since high-lift devices are used and the velocities are the lowest, so the lift and moment are highest, which has to be counteracted by the duct. However cruise is also analysed. For take-off, the moments are taken around the point of rotation, which is the main landing gear. For descent and cruise the most aft CG position is used. Various combinations of propulsive stabiliser position, duct size and duct angle of attack are analysed, to understand which combinations are feasible.

The wing-fuselage moment and lift were determined using Athena Vortex Lattice (AVL) program created by Drela and Youngren[44]. AVL makes use of an extended vortex lattice model where the surfaces and the trailing wakes are modelled as vortex sheets, discretised into horseshoe vortex filaments. The fuselage is modelled via source+doublet filaments. The wing and fuselage is then modelled into AVL, with their respective flap setting and angle of attack for the conditions it is being tested on. This then results in a lift and moment of the wing-fuselage combination. The decision has been made to use AVL for its ease to combine with the Matlab program and ability to output results quickly.

In order to know where the lift and moment of the wing-fuselage combination acts upon, the aerodynamic centre (X_{ac}) has to be obtained. This is done using the method as described in ESDU 76015[45]. With this method, from the true wing planform an equivalent straight-tapered wing is created, as can be seen in Figure 3.3. This is then used to obtain the wing aerodynamic centre. A corrective term is then applied to take into account the effect of the fuselage.

It should be noted that this method is only valid for the area where the lift-curve slope is linear. Where the rate of change of pitching moment with lift is also linear. Hence, the method applies when the airflow over the wing-fuselage configuration is subsonic and fully attached. The method has been validated and showed a mean error of 0.013 Mean Aerodynamic Chord (MAC) for t/c of 0.06-0.10 and a mean error of 0.028MAC for t/c of 0.12[46], for the wing only aerodynamic centre. The fuselage correction factor is also validated and is able to predict within 0.03MAC[45]. There are however limitations on using the aircraft configuration that can be used with this method. These can be seen in Table 3.1.

A	6 to 12	d/b	0.08 to 0.14
$\Lambda_{1/2}$	0 to 45°	d/c_r	0.4 to 0.9
$Atan\Lambda_{1/2}$	0 to 7.5	m/c_r	1 to 3.5
λ	0.2 to 10	n/c_r	1.5 to 3

Table 3.1: Limitations on ESDU76015 method[45]

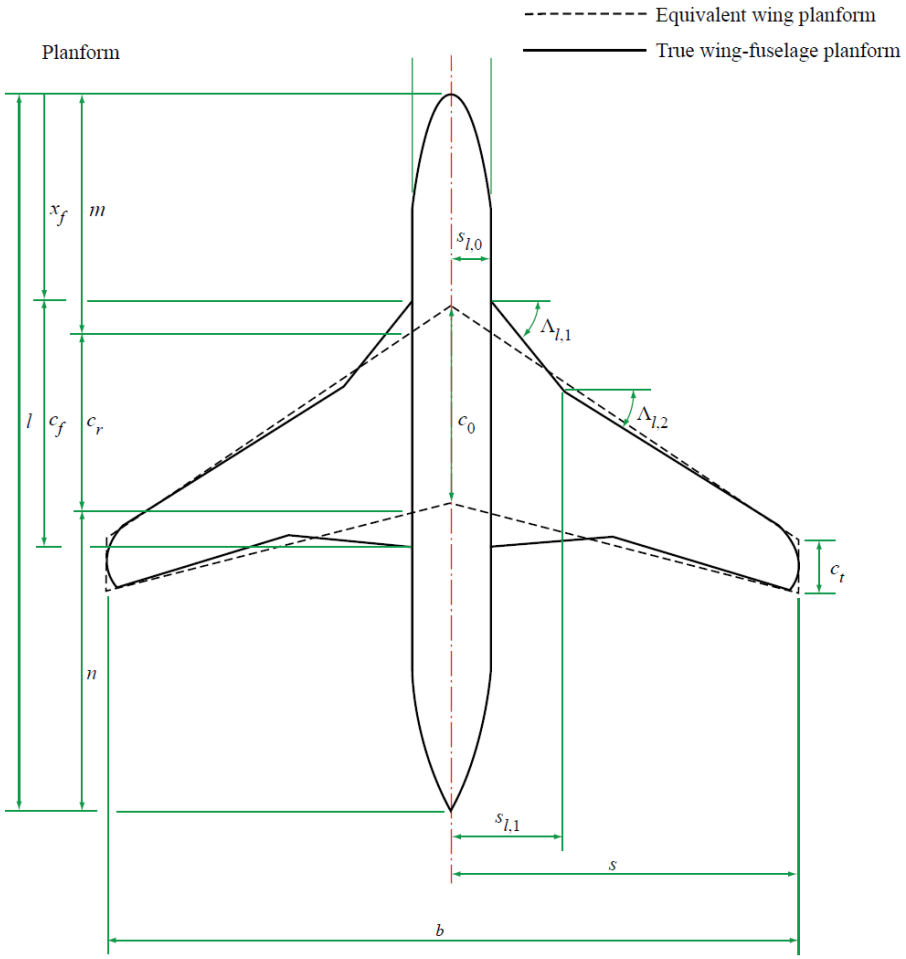

Figure 3.3: Equivalent wing planform[45]

With the position of the wing-fuselage aerodynamic centre determined, the next step would be to determine the location of the CG. Using the baseline configuration from Stavreva[21], the component weights and locations are already determined so the Operating Empty Weight (OEW) CG location can be calculated. However during operation this CG can move forward and aft, so to understand the maximum CG excursion a loading diagram has to be created. In a loading diagram the cg shift is shown when the aircraft is filled with passengers, front to back and back to front. The same applies for the cargo and fuel. An example of a 2-2 cabin configuration loading diagram can be seen in Figure 3.4. The most aft CG location can then be used to calculate the lift required from the duct.

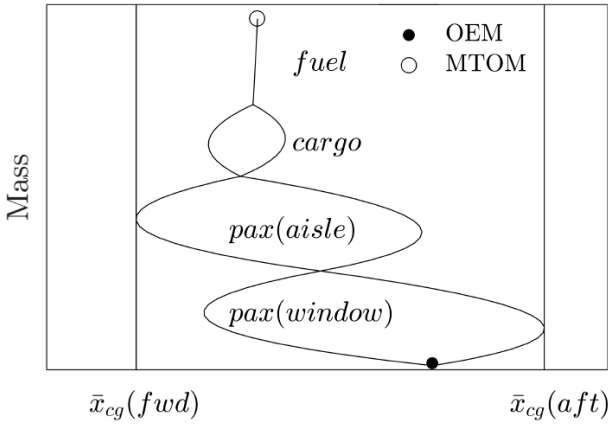

Figure 3.4: Typical loading diagram[47]

Before the duct lift can be calculated, it is also necessary to determine the thrust provided by the propeller and duct. Since the DUUC aircraft is expected to compete with the ATR72 aircraft, the same engine is used for the DUUC aircraft. Figure 3.5 presents the thrust per advance ratio for the F568 propeller, which is used on the ATR72 aircraft engine. From the research of Stavreva[21], it has been determined that for the take-off requirements a thrust of 8690N is required for each ducted propeller. Since the same design is used in this research, the same take-off thrust will be used. This is only possible at a certain advance ratio as can be seen from Figure 3.5, hence the propeller RPM will be adjusted to meet this advance ratio. The tip speed of this propeller RPM is calculated as well, to make sure it does not approach the speed of sound. Since this will result in high drag and noise. For descent, the thrust is assumed to be equal to 5% of the maximum thrust. The advance ratio is used again to determine the required propeller RPM. The aerodynamic analysis program used to calculate the loads on the propulsive stabiliser, models the propeller as an actuator disk and uses the thrust and RPM as input.

3.2. Sizing for stability

The previous section elaborated on the method used to obtain trim, so an equilibrium of forces during flight. However, this equilibrium also has to be maintained in case of a disturbance. Such as a gust of wind increasing the angle of attack of the aircraft and hence creating more lift on the wings. If the aircraft is statically unstable, the aircraft pitching moment will amplify this motion and further increase the aircraft nose, which is unwanted behaviour. If the aircraft is statically stable, the aircraft will have a restoring pitching moment, such that it returns to its equilibrium position without pilot input.

In order for the aircraft to restore the disturbance, the aircraft CG must be in front of the aircraft neutral point. The neutral point is the point through which the resultant change in lift acts when the angle of attack is changed. So, if the CG is in front of the neutral point, the resultant change in lift will create a nose down pitching moment and decrease the angle of attack. The free-body diagram depicting the effect of the disturbance and position of the neutral point can be seen in Figure 3.6.

The neutral point can be found by calculating the change in moment due to the change in angle of attack. At the neutral point the change in moment due to the change in angle of attack is equal to zero, since all the resulting forces acts on it. This moment balance is described by Equation (3.5). Rewriting this equation

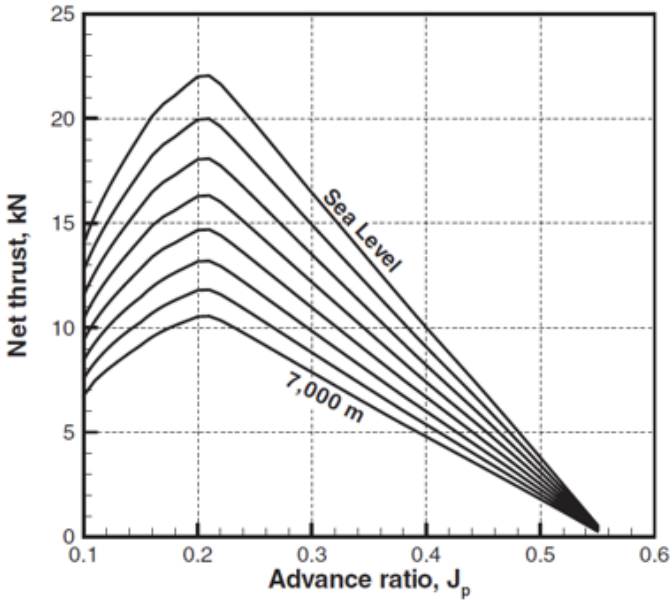

Figure 3.5: Thrust vs advance ratio F568-1 propeller[48]

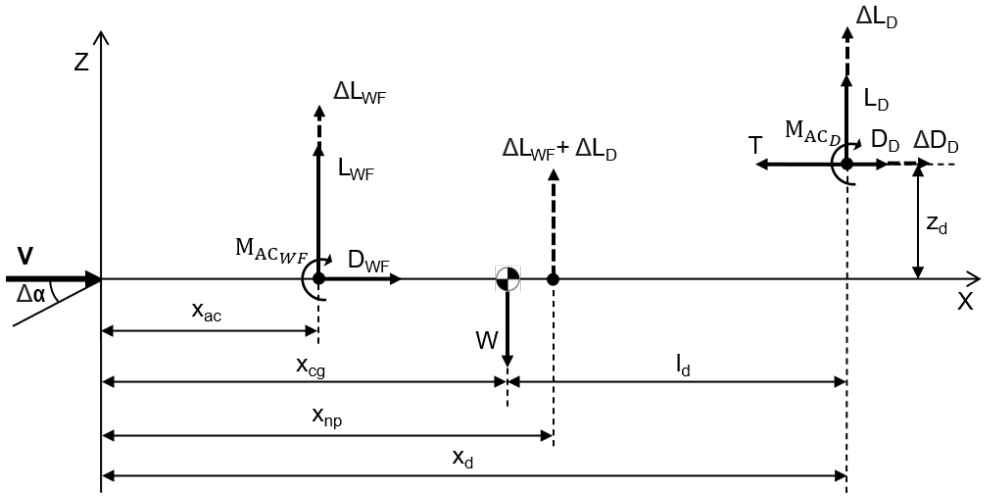

Figure 3.6: Forces and moments on DUUC aircraft due to disturbance

results in Equation (3.6), which gives the location of the neutral point. However, due to the flow of the wing, the propulsive stabiliser sees a different angle of attack than the wing. The relation of the duct angle of attack and wing angle of attack is given by $\alpha_D = \alpha - \varepsilon + i_D$. Where ε is the downwash caused by wing and i_D is the installation angle of the duct. So the change in duct angle of attack due to a change in aircraft angle of attack is given by Equation (3.7). This means that $\frac{dL_D}{d\alpha}$ as well as $\frac{dD_D}{d\alpha}$ has to be rewritten, as can be seen in Equation (3.8). Which results in Equation (3.9) to calculate the neutral point. This is the critical point at which the aircraft CG can be located. However, typically a 5% margin is used, called the static margin.

$$\frac{dL_{WF}}{d\alpha}(x_{np} - x_{ac}) - \frac{dL_D}{d\alpha}(x_d - x_{np}) + \frac{dD_D}{d\alpha} z_D = 0 \tag{3.5}$$

$$x_{np} = \frac{\frac{dL_{WF}}{d\alpha} x_{ac} + \frac{dL_D}{d\alpha} x_d - \frac{dD_D}{d\alpha} z_D}{\frac{dL_{WF}}{d\alpha} + \frac{dL_D}{d\alpha}} \tag{3.6}$$

$$\frac{d\alpha_D}{d\alpha} = \frac{d}{d\alpha}(\alpha - \varepsilon + i_D) = 1 - \frac{d\varepsilon}{d\alpha} \tag{3.7}$$

$$\frac{dL_D}{d\alpha} = \frac{dL_D}{d\alpha_D} \cdot \frac{d\alpha_D}{d\alpha} = \frac{dL_D}{d\alpha_D}\left(1 - \frac{d\varepsilon}{d\alpha}\right) \tag{3.8}$$

$$x_{np} = \frac{\frac{dL_{WF}}{d\alpha} x_{ac} + \frac{dL_D}{d\alpha_D}\left(1 - \frac{d\varepsilon}{d\alpha}\right) x_d - \frac{dD_D}{d\alpha_D}\left(1 - \frac{d\varepsilon}{d\alpha}\right) z_D}{\frac{dL_{WF}}{d\alpha} + \frac{dL_D}{d\alpha_D}\left(1 - \frac{d\varepsilon}{d\alpha}\right)} \tag{3.9}$$

3.3. Aerodynamic analysis

To calculate the forces the propulsive stabiliser can generate, the aerodynamic analysis tool FlightStream is used. Flightstream is a surface-vorticity solver which is more stable, more robust and has a lower sensitivity to surface perturbations, when compared to potential-flow solver which are pressure-based[49]. The potential flow approach as used in Flightstream is originally based on the formulation by Prandtl, called lifting line theory. The fundamental link between the circulation, which is geometry induced, and the lift and drag forces is defined by vortex-based theories. The theorem to provide this foundational connection is given by Kutta Joukowski, which for a defined geometry gives the net acceleration of the flow from the sum of forces acting on the stream[50][51]. Since Flightstream is surface-vorticity based, it allows the use of coarser meshes with an acceptable level of fidelity. To analyse the flow at higher speeds, a de-coupled, generalised, compressible flow-separation model has been incorporated into Flightstream[49]. In figure 3.7, the level of fidelity vs computational time of Flightstream compared to other solvers can be seen.

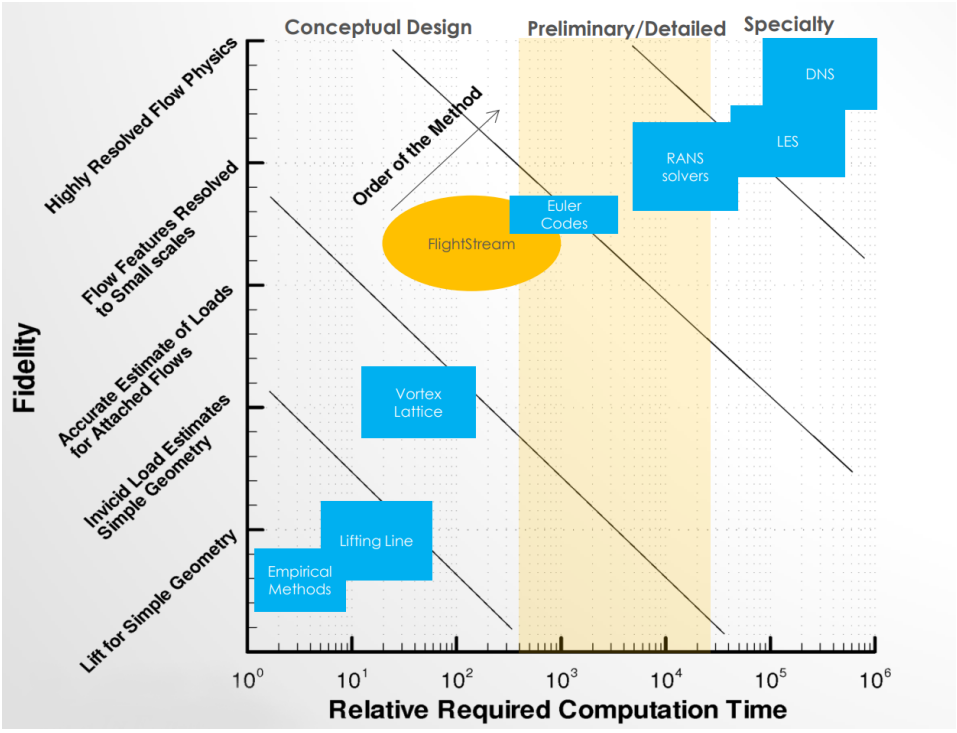

Figure 3.7: Comparison of methods[52]

The duct geometry is created in OpenVSP and initial meshing is done through the tessellation control in OpenVSP. Using the CompGeom tool, a single watertight surface is created with triangulated surface mesh. This can then be exported to FlightStream as a TRI file. Once imported into FlightStream, the trailling edges and wake termination nodes are selected through an automatised process. Where possible, FlightStream tries to convert the triangular mesh element into a quadrilateral mesh element which is parallel to the flow, in order to increase the performance of the solver. An actuator disk is used to model the propeller and the

thrust and RPM as defined in the previous section is put in. Flightstream then calculates the lift, drag and moment. For this analysis, the solver is run from an angles of attack range from −20° till 20°, with steps of 2°. This is done for 1.5m, 2m, 2.5m, 3m, 3.4m and 4m diameter duct sizes, to obtain a database with the forces a duct is able to generate.

3.4. Sizing program

With the method described in the previous sections, a Matlab program is written to perform the calculations. To run the program first some user input is required, these include for example the aircraft dimensions but also the weights of the various components. With the aircraft dimensions the program now runs the method of ESDU as described in Section 3.1 to obtain the location of the aerodynamic center. AVL will then run to obtained the wing-fuselage lift, drag and moment. After this point, the Matlab program starts a loop, where the propulsive stabiliser CG will shift from 95% fuselage length to 60%, with steps of 5%. With the propulsive stabiliser position at a certain position, the aircraft CG is calculated and hence the force required by the duct can be calculated. A stability check is performed to check whether the neutral point is behind the most aft CG position. The FlightStream datafiles, which contain values such as lift, drag and moment of the duct per angle of attack are now read by the program and checked whether the propulsive stabiliser can provide the amount of lift required. This step is repeated for the complete angle of attack range. Since it might not be able to provide sufficient lift at the take-off or landing angle of attack, but it can provide sufficient lift, if it is installed at a certain installation angle. The program repeats this for all the ducts sizes and positions, such that an overview is created which will indicate the combination of propulsive stabiliser position, duct size and angle of attack that will provide sufficient lift for a stable and controllable aircraft. This program is also visualised in a flowchart and can be seen in Figure 3.8.

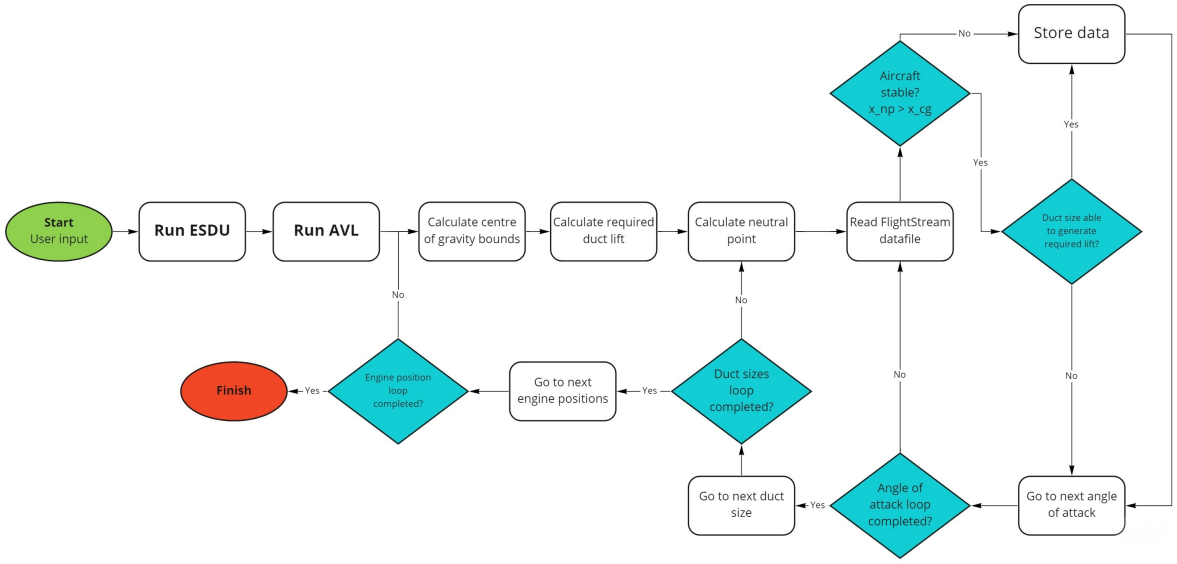

Figure 3.8: Matlab program flowchart

3.5. Conclusion

In order to study the positioning of the propulsive stabiliser. A new method is developed which utilises an ESDU method, AVL and FlightStream. The method of ESDU is used to determine the position of the aerodynamic center of the wing-fuselage combination. With AVL, the lift drag and moment of the wing-fuselage is obtained and FlightStream is used to determine the aerodynamic characteristics of the ducted propeller. Flightstream is a surface-vorticity solver which is more stable, more robust and has a lower sensitivity to surface perturbations, when compared to potential-flow solver which are pressure-based.

4

Validation

As part of this research, a validation study has been performed to understand how good FlightStream performs. In section 4.1 the setup of the wind-tunnel test is described. The results of the unpowered analyses are presented in Section 4.2, the results of the powered analyses can be seen in Section 4.3. These results have also been compared to analytical methods, which can be found in Section 4.4.

4.1. Wind-tunnel setup

In 1967 a wind-tunnel test has been performed on a 7 foot diameter ducted propeller by NASA[43]. During the wind-tunnel test the lift, drag and moment coefficient have been obtained for various propeller speeds and angles of attack. The ducted propeller inside the wind tunnel can be seen in Figure 4.1. The forces and moments were measured by the wind tunnel six-component balance. Furthermore, the wing fairing and support structure forces and moments were not transmitted to the balance and thus not measured. Therefore, only the duct with the struts and vane were modelled in FlightStream. Also, wind-tunnel wall effects are negligible[43]. The propeller was modelled as an actuator disk. FlightStream does have the option to model the propeller blade and apply the rotating fluid volume method, where the fluid volume encapsulating the propeller rotates, thereby imitating the propeller rotating through the air. However to use this, non-rotating components should not be included and hence the vane and struts could not be included. Therefore, the decision was made to model the propeller as an actuator disk.

The complete duct was created in OpenVSP and exported to FlightStream and can be seen in Figure 4.2. Through the advance ratio denoted in the wind-tunnel test report, the free-stream velocity was obtained. The solver settings which were used for this analysis can be seen in Table 4.1. FlightStream allows the user to select from two different model, the pressure model and vorticity model. The pressure model includes a vorticity-based separation model, which means it is able to predict stall, while the vorticity model does not[53]. The analysis has been performed with both the vorticity and pressure model for lift to assess the difference. The vorticity model is indicated as linear model and the pressure model as separation model in the graphs. Please note that the moment coefficient could not be assessed in this analysis since the moment reference point was not indicated in NASA wind-tunnel test report.

Solver settings	
Lift model	Vorticity & Pressure
Drag model	Vorticity
Moment model	Linear pressure
Boundary layer	Turbulent
Viscous model	Momentum integral
Flow seperation	True

Table 4.1: Solver settings FlightStream validation study

(a) Duct picture

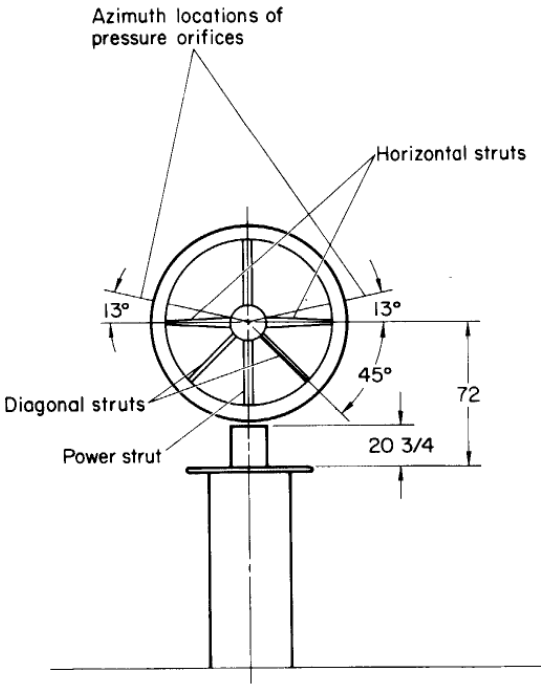

(b) Duct drawing

Figure 4.1: NASA wind tunnel experiment 7 foot diameter ducted propeller[43]

4.2. Unpowered analysis

The first analysis has been performed with the propeller excluded, in order to assess the validity of FlightStream without the effect of the propeller. The exit vane and struts are included, to fully replicate the NASA wind-tunnel test. The comparison between the lift curve slope of the NASA wind-tunnel test and FlightStream can be seen in Figure 4.4. From this figure, it can be seen that FlightStream is able to predict the lift coefficient accurately until stall is reached, which is not predicted by FlightStream. In theory the separation model should be able to predict stall, since it includes a vorticity-based separation model, however during the analysis stall occurred much later at an angle of attack of approximately 55 degrees. This means that there is a certain flow separation behaviour which FlightStream is not able to produce. Finally, it can be seen that the linear model follows the curve more accurate than the separation model at the higher angles of attack.

The comparison between drag coefficient of the wind-tunnel test and FlightStream, can be seen in Figure 4.5. In this figure there is only one FlightStream curve since there is no difference between the separation model and linear model. It can be observed that FlightStream underestimates the drag coefficient throughout the whole angle of attack range. This could be due to aspects in the geometry which increase drag, such as holes and protrusions which are not captured in the model created in OpenVSP. However, boundary layer effects and flow separation could also play a role, since these increase drag and are not captured by FlightStream.

4.3. Powered analysis

Figure 4.6 presents the comparison between lift curve slope of the wind-tunnel test and FlightStream, with the propeller included and exit vane at 0 degrees. The thrust coefficient is equal to 1.88, where thrust coefficient is defined $T_c = \frac{T}{\frac{1}{2}\rho V^2 S}$. In all the analyses, the surface area is defined as duct chord multiplied by duct exit diameter. From this figure it can be seen that the lift coefficient is predicted less accurately compared to the analysis without propeller. The lift coefficient is underpredicted by FlightStream, with the separation model and linear model producing similar results until an angle of attack of 40 degrees. This underprediction of lift coefficient could be due to propeller thrust effects on duct lift, which is not captured by FlightStream, since the duct lift coefficient without propeller is modelled correctly. This underprediction of lift coefficient

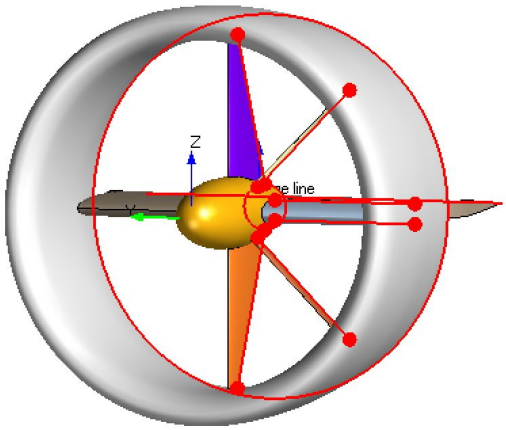

Figure 4.2: Duct modelled in FlightStream

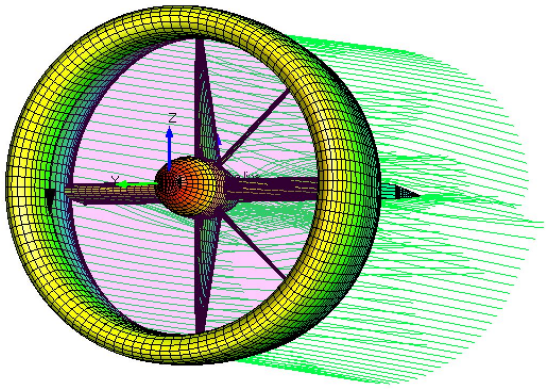

Figure 4.3: FlightStream analysis visualisation

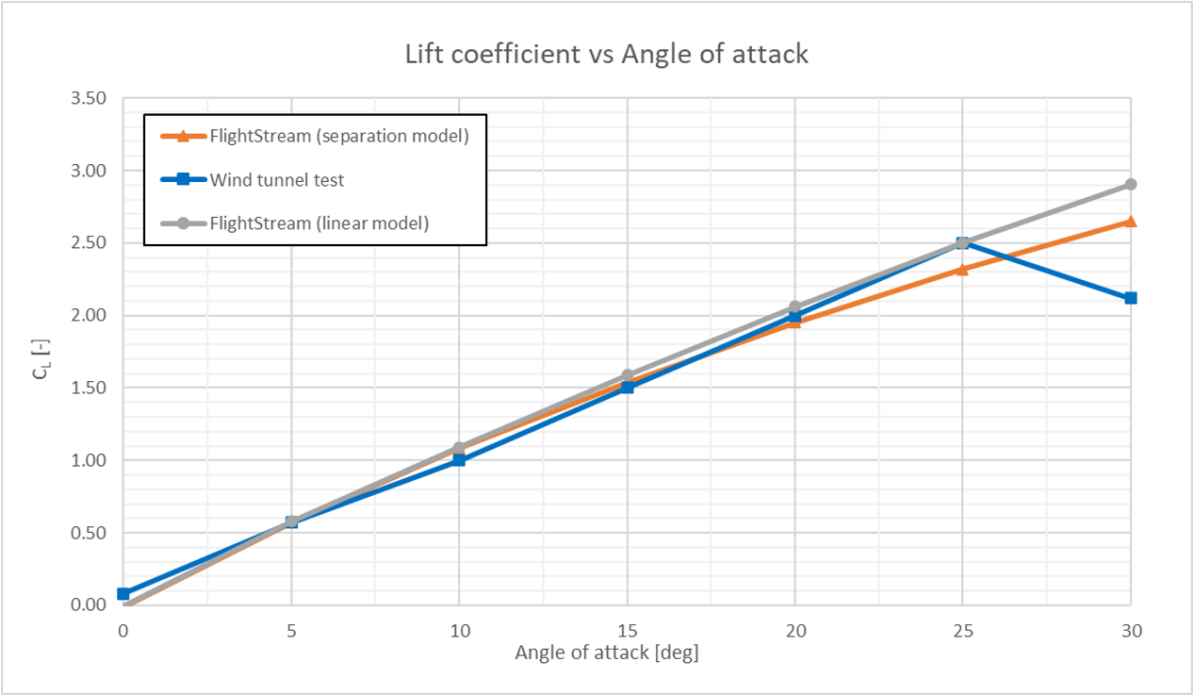

Figure 4.4: Comparison lift coefficient NASA wind tunnel test vs FlightStream, propeller excluded

is approximately 17%, which indicates that in the analyses to determine the required duct size, the duct sizes are overestimated.

The comparison between drag coefficient for this same analysis can be seen in Figure 4.7. Please note the negative drag coefficient until an angle of attack of approximately 35 degrees, which means that the thrust is more dominant in this region. Taking this in mind, it can be observed that FlightStream now overpredicts the drag coefficient until an angle of attack of 40 degrees, after which the drag coefficient is underpredicted. This could again be linked to the propeller which is modelled as an actuator disk in FlightStream.

The same has been done with the duct exit vane at -17 degrees, this showed similar results as the powered analysis with the duct exit vane at 0 degrees. However, the linear model was able to predict the lift coefficient better than the separation model. The comparison between the lift coefficient of the wind-tunnel test and

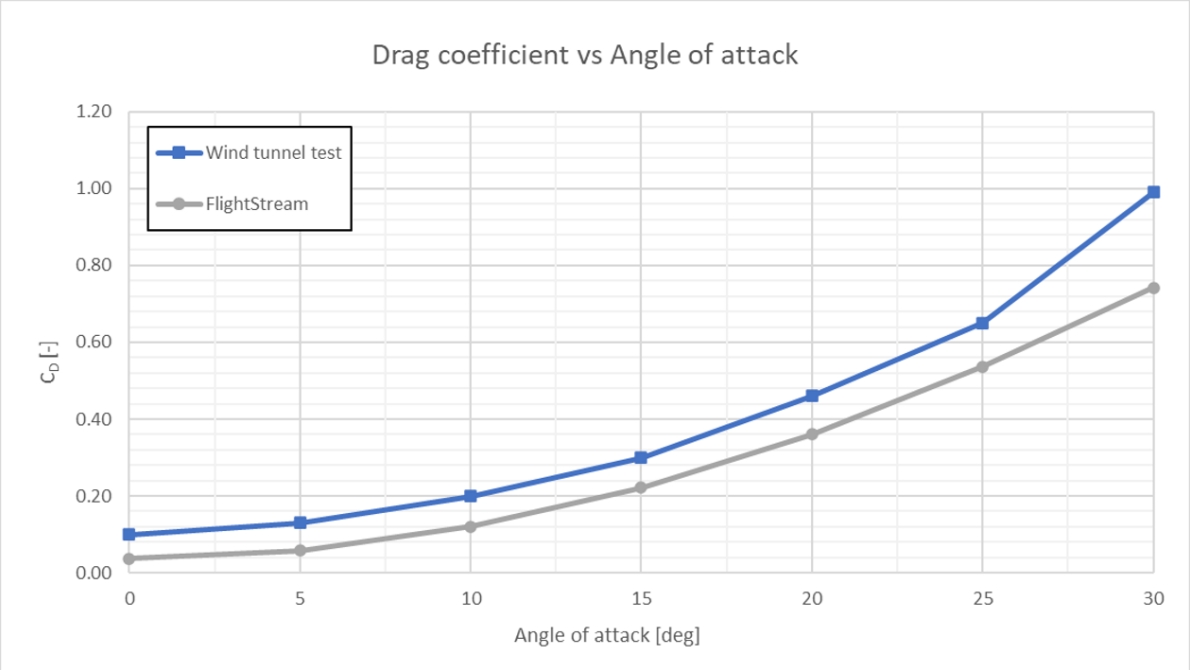

Figure 4.5: Comparison lift coefficient NASA wind tunnel test vs FlightStream, propeller excluded

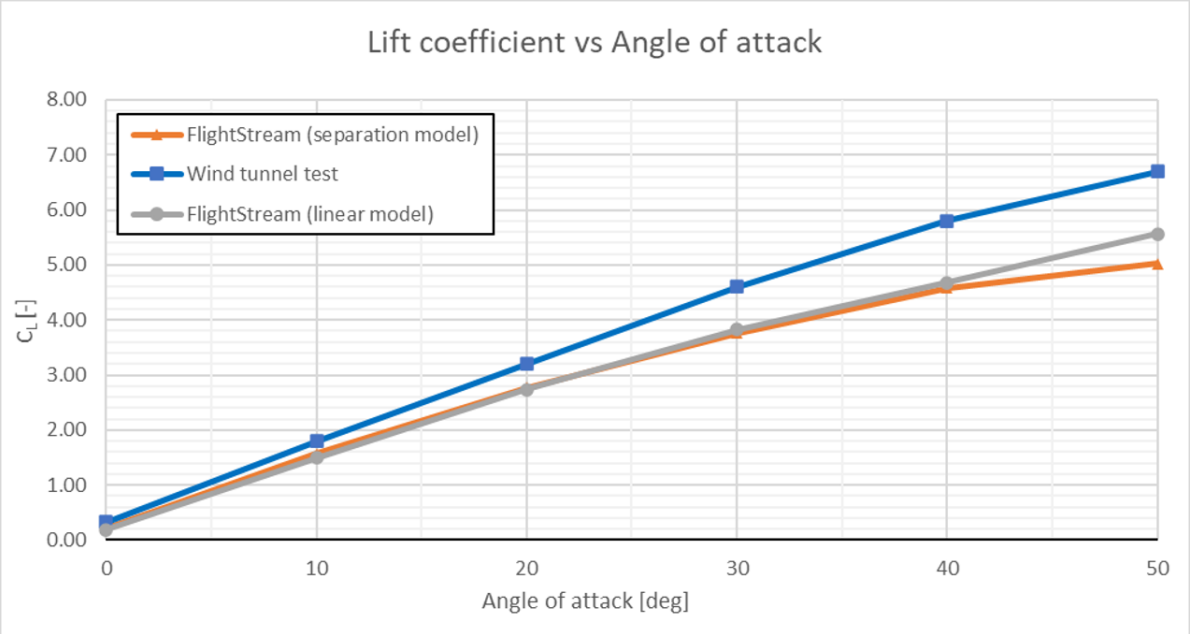

Figure 4.6: Comparison lift coefficient NASA wind tunnel test vs FlightStream, vane at 0 deg, Tc = 1.88

FlightStream can be seen in Figure 4.8 and for the drag coefficient in Figure 4.9. The thrust coefficient for this analysis was equal to 1.8.

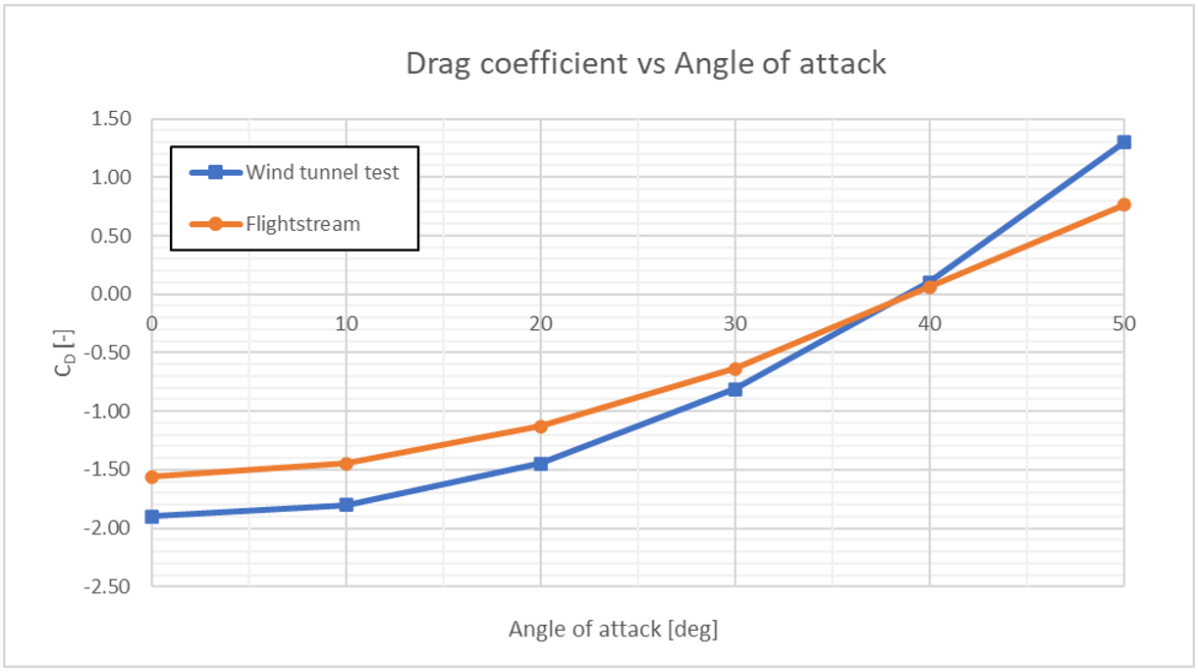

Figure 4.7: Comparison lift coefficient NASA wind tunnel test vs FlightStream, vane at 0 deg, Tc = 1.88

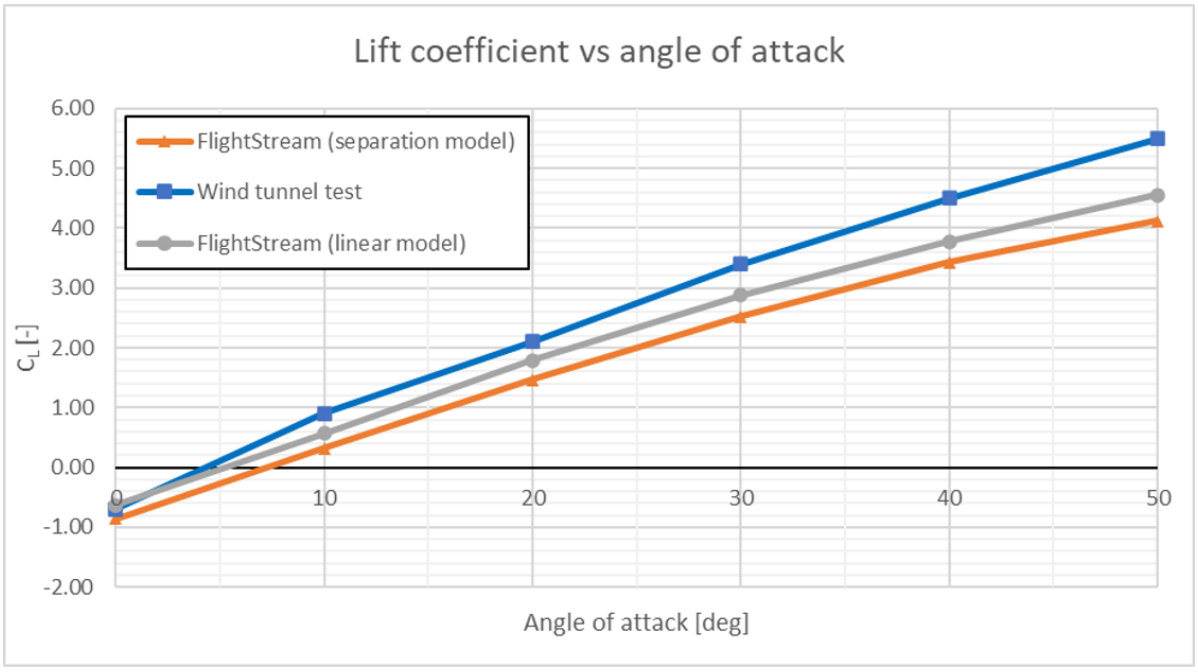

Figure 4.8: Comparison lift coefficient NASA wind tunnel test vs FlightStream, vane at -17 deg, Tc = 1.8

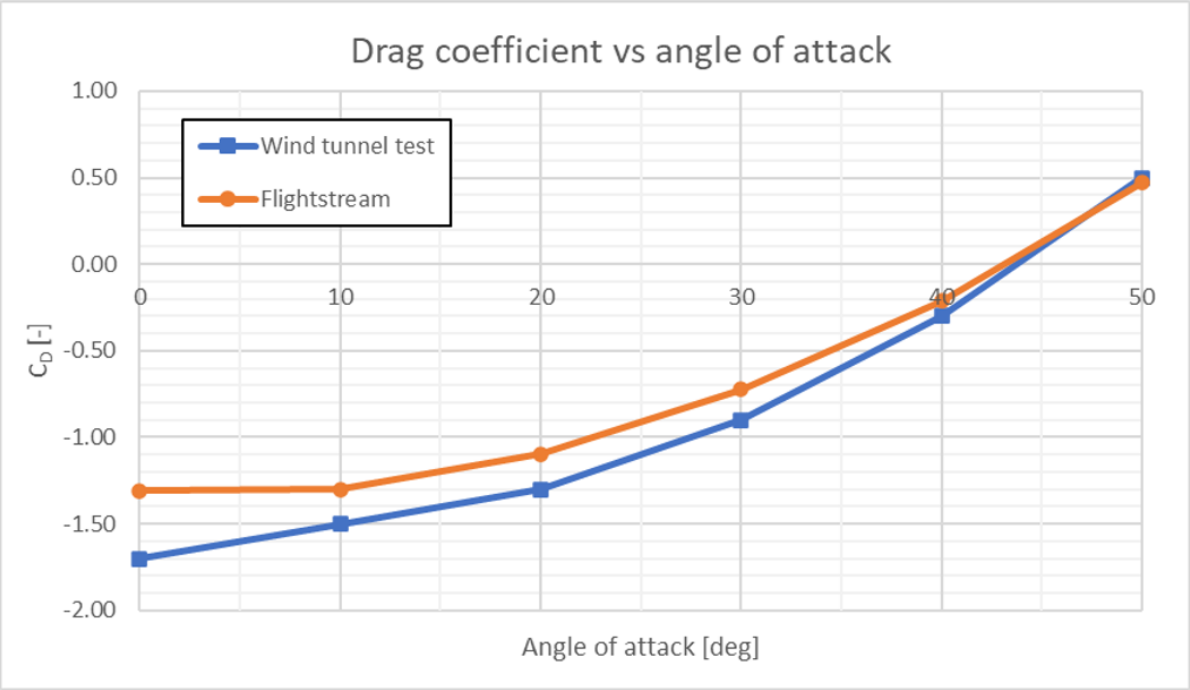

Figure 4.9: Comparison lift coefficient NASA wind tunnel test vs FlightStream, vane at -17 deg, Tc = 1.8

4.4. Analytical methods

Since FlightStream did not produce accurate results for the drag coefficient and underestimated the lift coefficient under powered conditions. Other methods have been identified to compare the results with FlightStream. These methods are analytically derived and are praised in literature. The first analytical method assessed is developed by Weissinger. Werle[54], who conducted a review on the various analytical methods available, found that: "It was found that Weissinger's approximation provides a consistent and accurate representation of the exact lifting-line computational solutions for a very wide range of aspect ratios A. None of the other approximate models were found to do as well". Harinarain[10] as mentioned in Chapter 2 also used the Weissinger method.

Using Weissingers approximate model, the lift coefficient can be calculated using Equation (4.1). Where ξ_W is given by Equation (4.2) and $\lambda = \frac{1}{AR}$. Furthermore, the aspect ratio (AR) of the duct is defined as $\frac{D_{duct}}{c_{duct}}$. The drag coefficient is then calculated using Equation (4.3). The results for the lift coefficient vs angle of attack can be seen in Figure 4.10. From this figure, it can be seen that Weissingers model cannot match the lift curve of the wind-tunnel test. The lift curve slope has a lower gradient and hence deviates throughout the whole angle of attack range. The results for the drag coefficient can be seen in Figure 4.11. Similarly, it is not able to match the curve of the wind-tunnel test. However, it produces similar results as Flightstream and also estimates better at the higher angles of attack. Please note that these results are for the unpowered condition. Furthermore, Weissingers approximate model is developed assuming a simple ring wing, so the vanes and struts have to be included separately using a different model.

Another analytical method which is developed more recently is the method of Maqsood and Go[28]. They introduced a further developed model, where the performance of the annular wing was estimated using the leading-edge suction analogy. With this concept, the total lift is calculated by taking the sum of the potential-flow lift, which is calculated using Equation (4.4) and the lift associated with the leading edge and side edge vortices, which is calculated using Equation (4.5). This allows for a parameterization of the overall lift into pressure-induced contributions and vortex-induced contributions. Equation (4.6) is used to calculate the drag coefficient. The constants in these equations are determined using empirical techniques by Maqsood and Go[28].

$$C_{L,duct} = \frac{\pi}{2}\xi_W 2\pi\alpha \tag{4.1}$$

$$\xi_W = \frac{1}{1+\lambda(\pi/2)+\lambda\arctan(1.2\lambda)} \tag{4.2}$$

$$C_D = C_{D_0} + \frac{C_L}{\pi ARe} \tag{4.3}$$

$$C_{L_p} = 2.812 \cdot AR \cdot sin\alpha \cdot cos^2\alpha \tag{4.4}$$

$$C_{L_v} = \pi \cdot cos\alpha \cdot sin^2\alpha \tag{4.5}$$

$$C_D = C_{D_0} + 0.15(AR)^{-1.237} C_L^2 \tag{4.6}$$

From Figure 4.10, it can be seen that the model of Maqsood is better at predicting the lift curve slope compared to the method of Weissinger. However, it is still not able to match the curve of the wind-tunnel test as well as FlightStream does. The drag coefficient vs angle of attack graph can be seen in Figure 4.11. From this figure, it can be seen that the model of Maqsood is not able to predict the drag coefficient as well as the other models. At small angles of attack it is able to match the curve of Weissinger and FlightStream with a small deviation, however at larger angles of attack the curves increasingly deviate from each other. This means that the empirical constants which are determined by Maqsood and Go[28] are not designed for these larger angles of attack.

To allow a better comparison, the lift coefficient and drag coefficient of the vane and struts have been extracted from the FlightStream analyses and added to the coefficients obtained from Weissinger and Maqsood. The new lift coefficients curves can be seen in Figure 4.12. From this graph, it can be seen that the lift curve

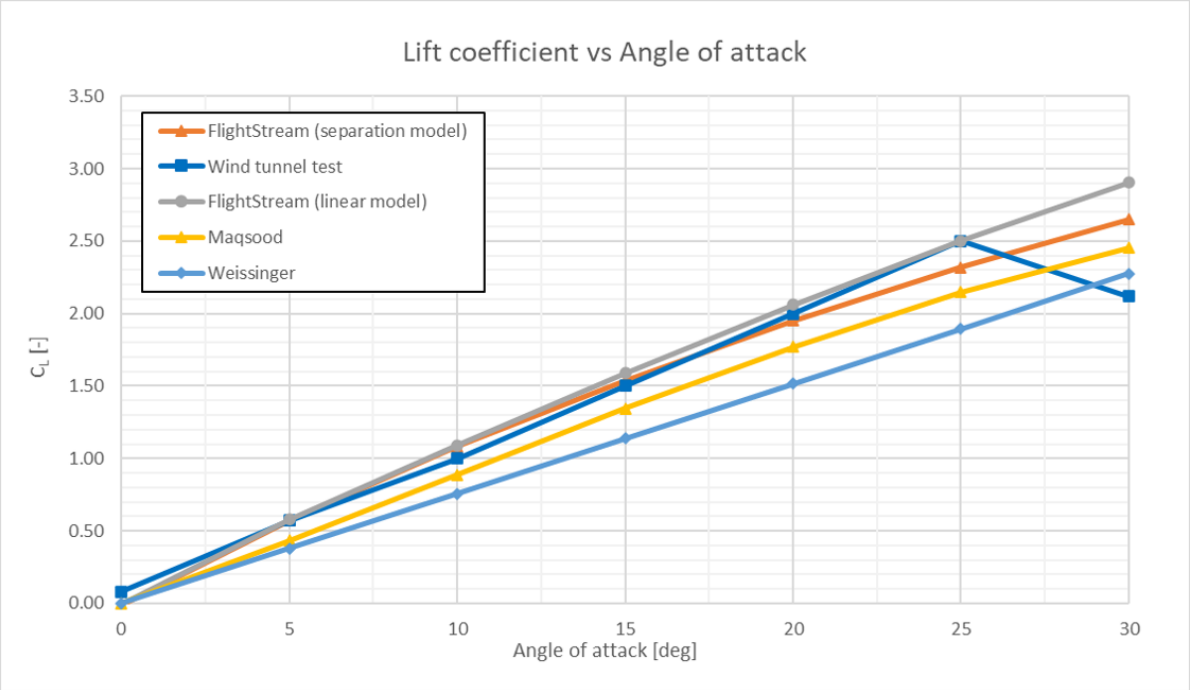

Figure 4.10: Comparison lift coefficient NASA wind tunnel test vs FlightStream and analytical methods

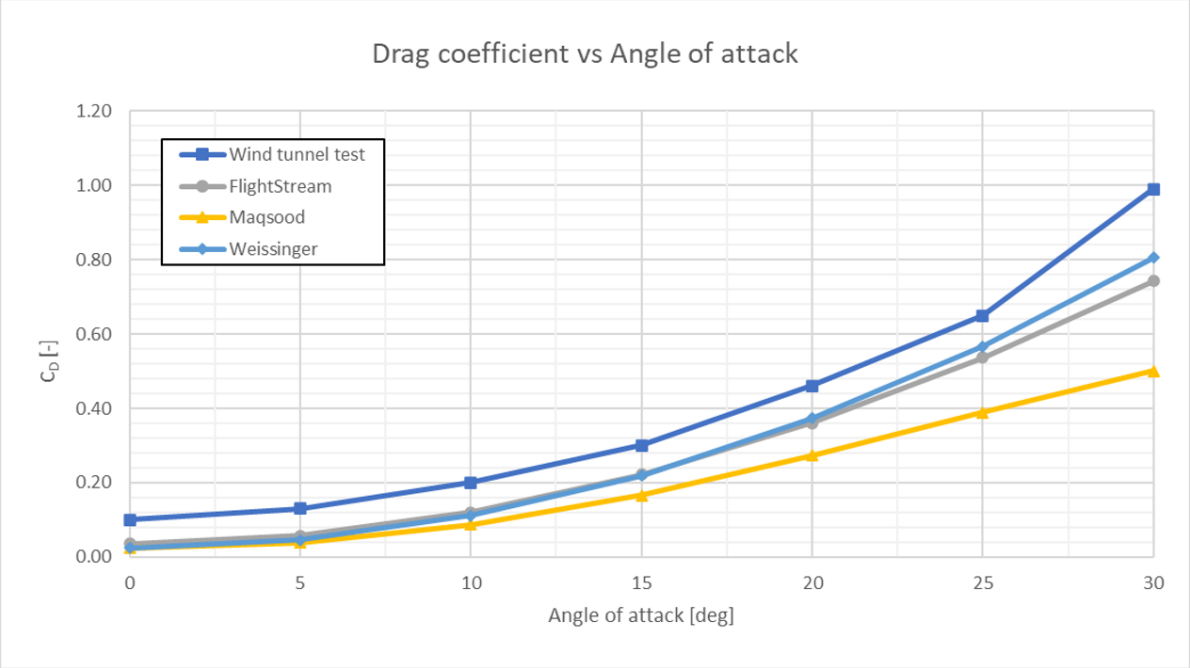

Figure 4.11: Comparison lift coefficient NASA wind tunnel test vs FlightStream and analytical methods

slope of Weissinger is now comparable to the FlightStream linear model and following the curve of the wind-tunnel test closely. The model of Maqsood has a slightly higher lift curve slope compared to the wind-tunnel test and is overestimating the lift coefficient at the higher angles of attack. The new drag coefficient curves can be seen in Figure 4.13. With the corrections applied, the Weissinger model curve is predicting the drag coefficient better than FlightStream at the higher angles of attack. The model of Maqsood is now able to match the drag coefficient curve of FlightStream. This indicates that the model of Weissinger is able to approximate the lift and drag coefficients of the ring wing well.

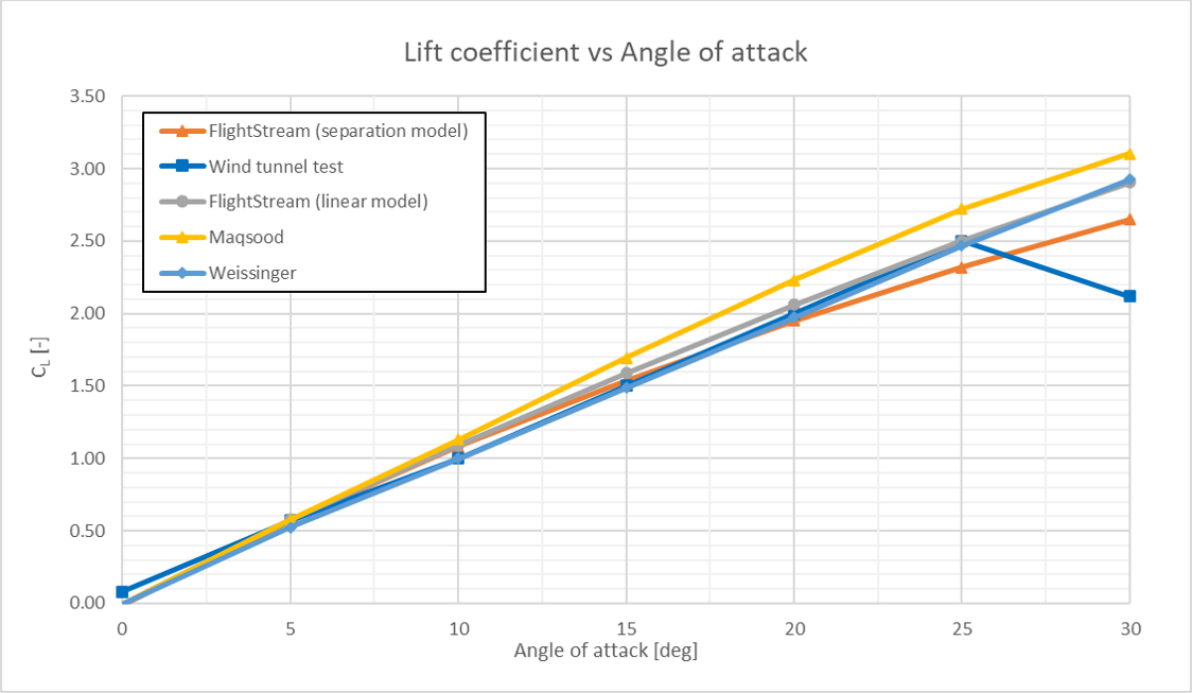

Figure 4.12: Comparison lift coefficient NASA wind tunnel test vs FlightStream and analytical methods [corrected]

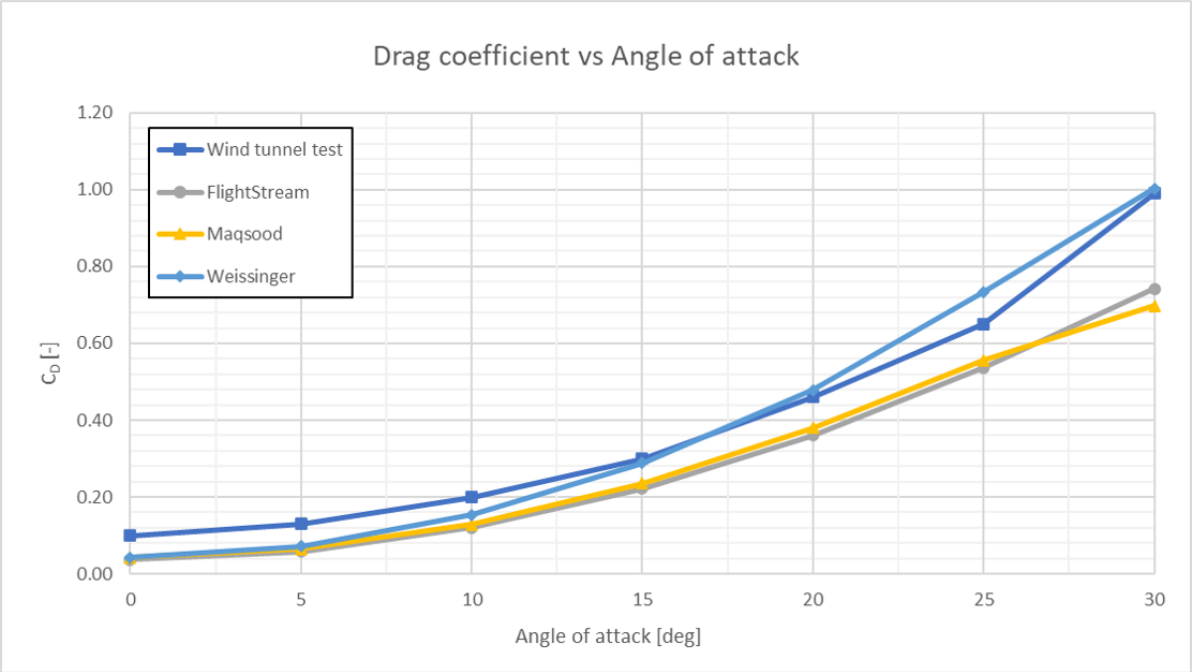

Figure 4.13: Comparison lift coefficient NASA wind tunnel test vs FlightStream and analytical methods [corrected]

4.5. Conclusion

With this in mind, the decision was made to proceed with FlightStream, even though the drag coefficient is underpredicted. The model of Weissinger does allow for a better drag coefficient prediction. However, this means a good estimation method has to be obtained for the struts and vanes. Furthermore, in FlightStream it is possible to model the complete aircraft and obtain the influence of the wing and fuselage on the propulsive stabiliser. FlightStream also enables the user to obtain the results of each component of the aircraft separately, in order to analyse how much influence a certain part has on the whole aircraft. Of course, higher fidelity

models such as CFD can also be used for a better estimation. However, for the purpose of this research, the higher fidelity models are out of scope.

5
Results

In this chapter the results of the analyses are presented. First, in Section 5.1 the analysis method is described and the results for the single duct analyses are presented. In Section 5.2 the results of the FlightStream analyses for the complete aircraft are presented, with the differences between the installed and uninstalled duct. The results for the possible propulsive stabiliser positions for various wing positions are presented in Section 5.3.

5.1. FlightStream duct analysis

As mentioned in the previous chapter, FlightStream has been used as the aerodynamic analysis tool. The propulsive stabiliser consists of 2 ducts with pylons, where each duct has a vertical and horizontal vane and a centrebody. In this section the lift, drag and moment coefficient results are presented for a single duct with vanes and centrebody, the propeller is modelled as an actuator disk. FlightStream utilises the Conway actuator disk model in the analysis with uniform loading. In the volume behind the actuator disk, the calculated slipstream velocities are superimposed on the flow field[55]. The influence of the complete aircraft on the propulsive stabiliser is also analysed and the results are presented in the next section. Furthermore, for this analysis the duct pylon which connects the duct to the fuselage is also not modelled. Since the pylon disrupts the results when comparing the effect of the duct size on the lift, drag and moment coefficient.

The duct is first modelled in OpenVSP, the initial meshing is done through the tessellation control in OpenVSP. Then, using the CompGeom tool in OpenVSP, a triangulated surface mesh is created which is watertight. This is then exported as a TRI file into FlightStream, after which the trailling edges and wake termination nodes have to be marked. With this done, the actuator disk can be inserted in the duct and the thrust required is inputted. The graphs shown in this section have been run at take-off thrust. The analysis is run with the settings as can be seen in Table 5.1, from the validation study, which is presented in Chapter 4, these settings have been found to provide the best solution.

The analysis is run from an angle of attack of $-20°$ to $20°$, with steps of $2°$. Six different sizes have been configured, ranging from 1.5m in diameter to 4m in diameter. The 1.71m chord and centrebody with a length of 2.43m an diameter of 0.83m has been kept constant for all the duct sizes. These dimensions have been extracted from the final design in the research performed by Stavreva[21], where the duct has a diameter of 3.5m. This is used as the baseline for this research and will be denoted as "initial" in the upcoming graphs. A visualisation of the analysis performed on the initial duct can be seen in Figure 5.1. Lastly, as reference area to determine the coefficients, the wing surface area which is equal to $65.76m^2$ is used. This has been done in order to allow for a fair comparison between the different duct sizes, but to also see how much the duct forces influences the complete aircraft.

5.1.1. Lift coefficient

The result of the lift coefficient vs angle of attack can be seen in Figure 5.2. From this figure, it can be observed that increasing the duct size results in a higher lift coefficient. Furthermore, it has been observed that the same amount of negative lift is produced at a negative angle of attack compared to positive lift at the same

Solver settings	
Lift model	Vorticity
Drag model	Vorticity
Moment model	Linear pressure
Boundary layer	Turbulent
Viscous model	Momentum integral
Flow seperation	True

Table 5.1: Solver settings FlightStream validation study

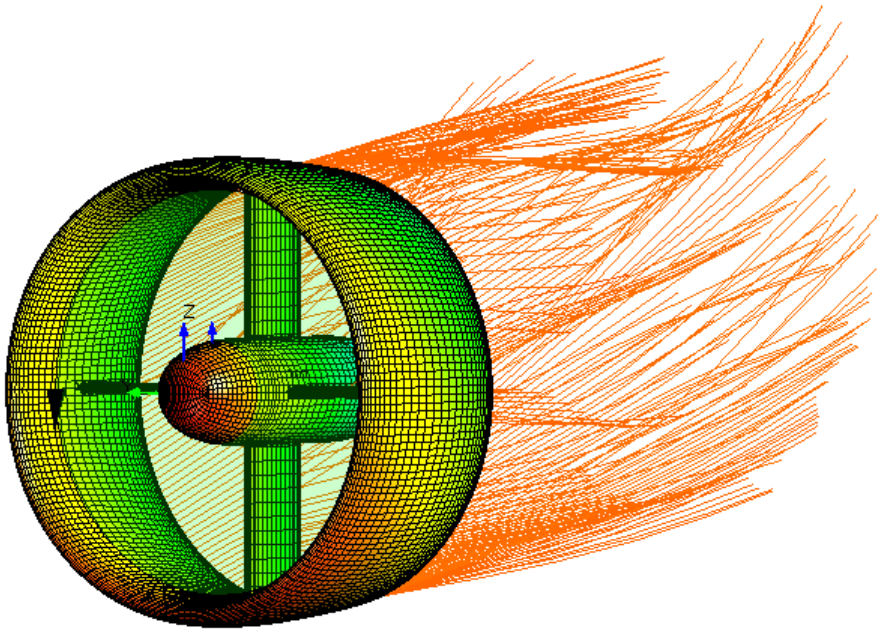

Figure 5.1: FlightStream analysis visualisation

positive angle of attack. This is due to the uncambered NACA0012 airfoil used on the duct.

5.1.2. Drag coefficient

The results of the drag coefficient vs angle of attack can be seen in Figure 5.3. From this figure, it can be seen that at smaller angles of attack +/- 10°, the smaller duct sizes have the largest drag coefficient. This can be seen more clearly in Figure 5.4. This is due to the control vanes inside the duct, where the control vane drag is more dominant than the duct drag at smaller angles of attack. The control vanes inside the larger ducts have a higher aspect ratio compared to the control vanes inside the smaller ducts, since the chord is kept constant. These higher aspect ratio vanes are more efficient and hence have a lower drag coefficient. The opposite occurs at larger angles of attack, where the duct drag becomes more dominant and the larger duct sizes have the largest drag coefficient.

5.1.3. Moment coefficient

The moment coefficient vs angle of attack graph can be seen in Figure 5.5. From this figure, it can be observed that at negative angles of attack, positive moment is obtained. The quarter chord of the duct is used as moment reference point and positive moment indicates counterclockwise rotation. At positive angles of attack, a negative moment is obtained. Furthermore, it can be observed that the moment coefficient extremes increase with duct size. Lastly, the result of the 1.5m duct size is questionable, due to the highly oscillatory behaviour. This is due the centrebody which becomes more dominant than the duct.

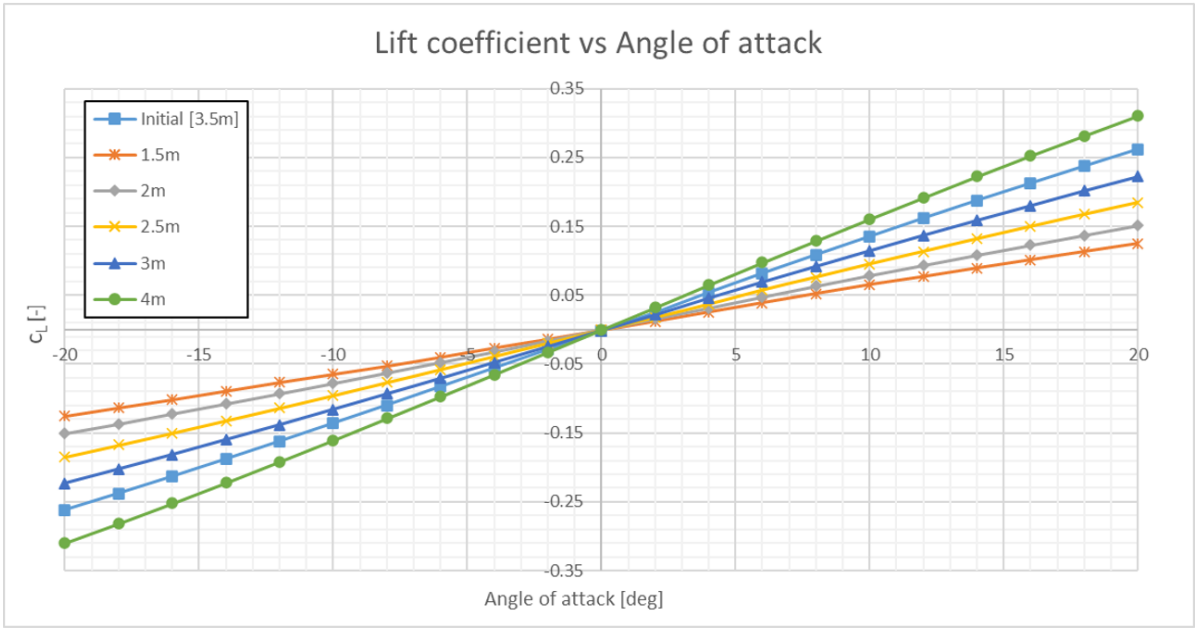

Figure 5.2: Lift coefficient vs Angle of attack for various duct sizes

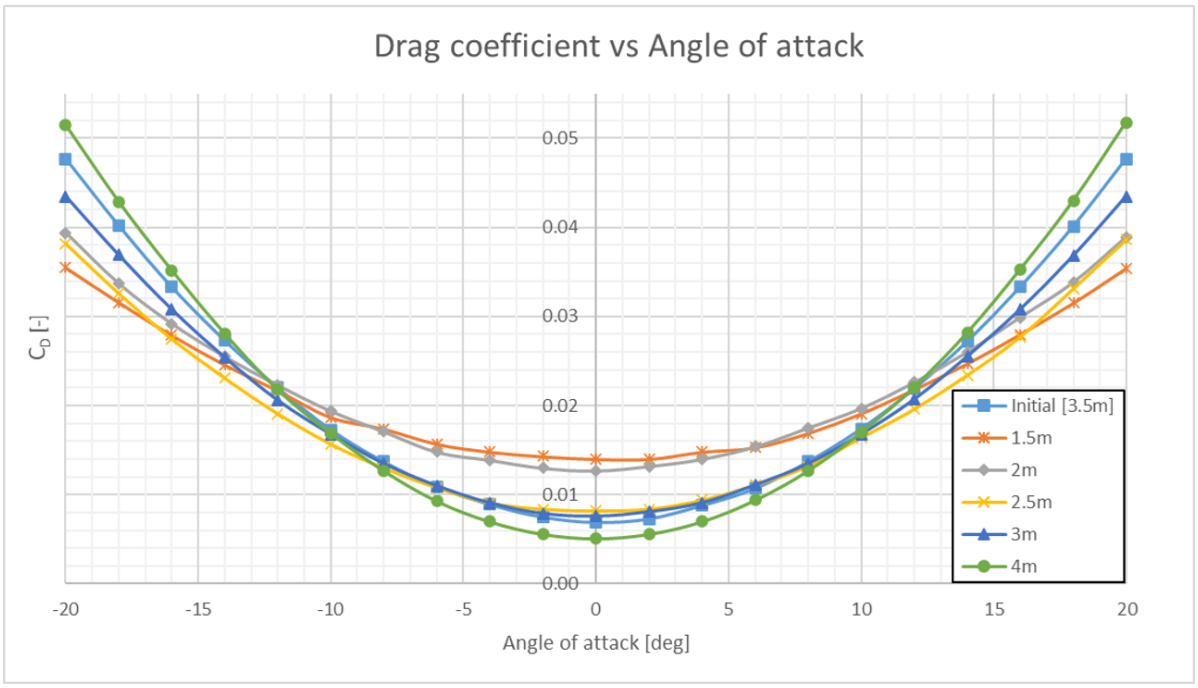

Figure 5.3: Drag coefficient vs Angle of attack for various duct sizes

5.1.4. Control vane excluded

To understand how much the control vanes influences the lift, drag and moment coefficient. The analysis of the duct with duct diameter of 3.4m with take-off thrust is performed again, with the control vanes removed. From Figure 5.6, it can be observed that the control vanes do not influence the lift coefficient. Only at the larger angles of attack, a small difference can be observed. This is due to the vertical control vanes that do not produce lift and the horizontal control vanes which cancel each others lift out. Since the wake of the propeller induces positive lift on one control vane and negative lift on the other, causing a net effect of no lift. This means that the control vanes have a marginal effect on the total lift coefficient.

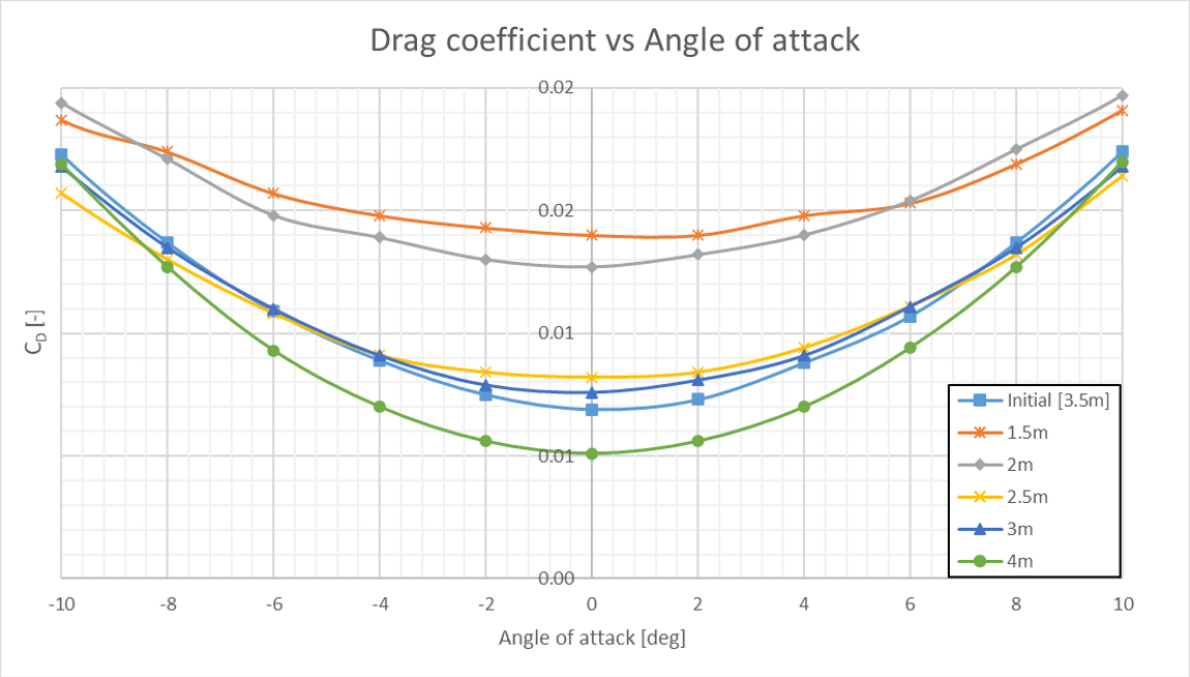

Figure 5.4: Drag coefficient vs Angle of attack for various duct sizes zoomed in

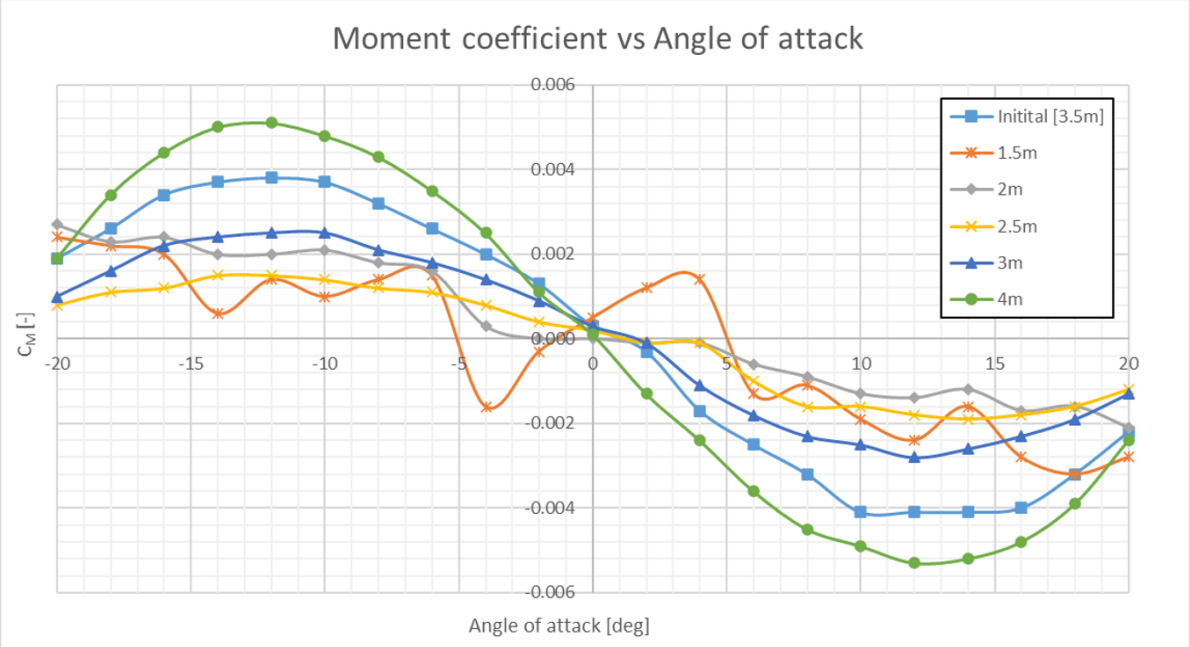

Figure 5.5: Moment coefficient vs Angle of attack for various duct sizes

The difference for the drag coefficient is much more noticeable, as can be seen in Figure 5.7. As expected, the duct without control vanes have a lower drag coefficient. Although the control vanes cancels each others lift, the lift is produced at the control vanes which also results in lift induced drag. Apart from lift induced drag, skin friction drag also has an effect on the difference. The difference between the drag coefficient stays roughly constant throughout the whole angle of attack range and is between 0.004-0.005.

The largest difference can be observed for the moment coefficient as can be seen in Figure 5.8. It can be seen that the duct with control vanes produce a much larger pitching moment coefficient than the duct with-

out control vanes. This is due to the position of the control vanes, since these are located behind the quarter chord point of the duct, the point which is used as reference for the moment calculation. Hence, providing a larger restoring pitching moment coefficient.

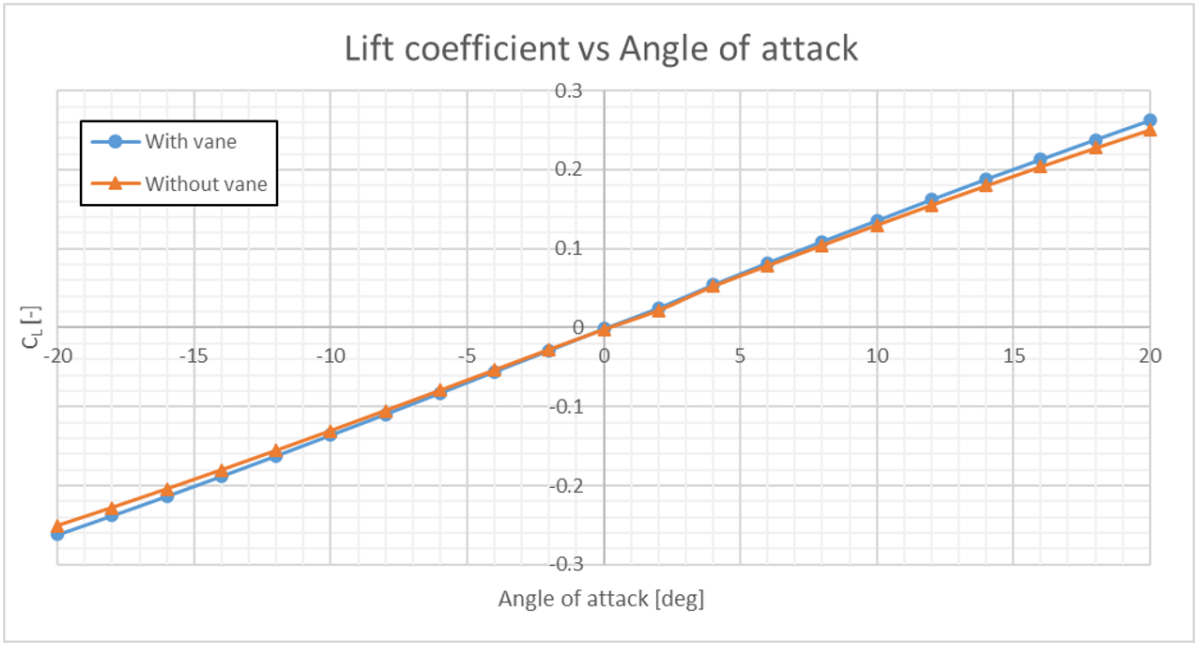

Figure 5.6: Influence control vanes on Lift coefficient vs Angle of attack

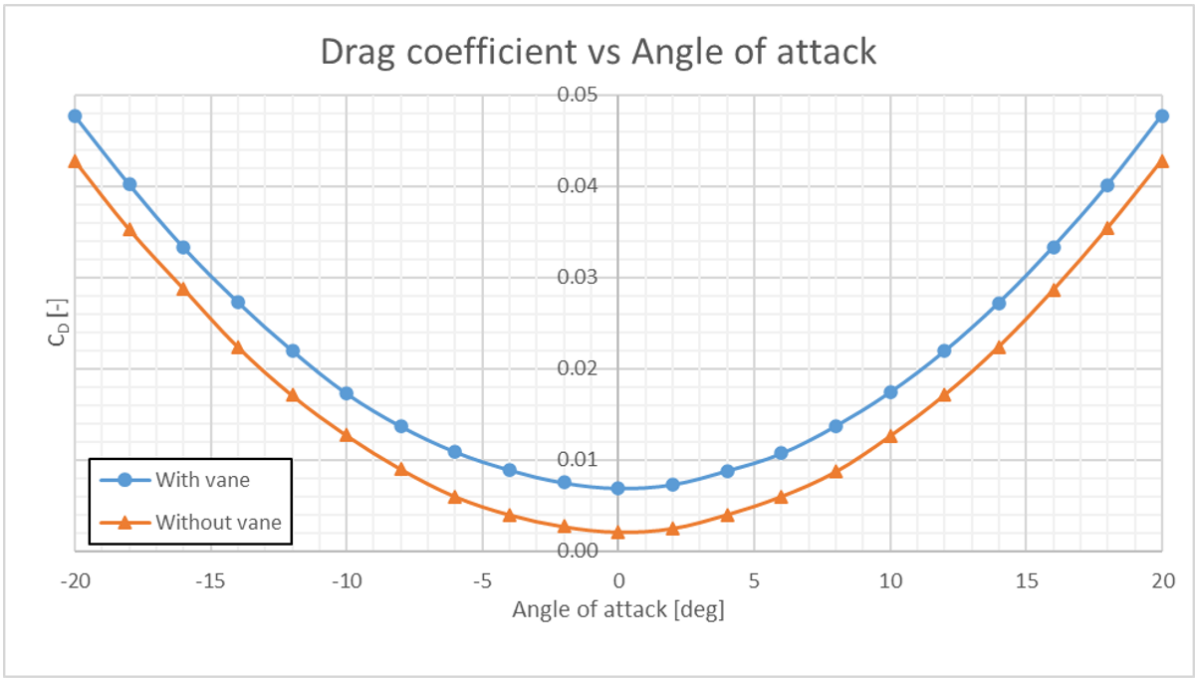

Figure 5.7: Influence control vanes on Drag coefficient vs Angle of attack

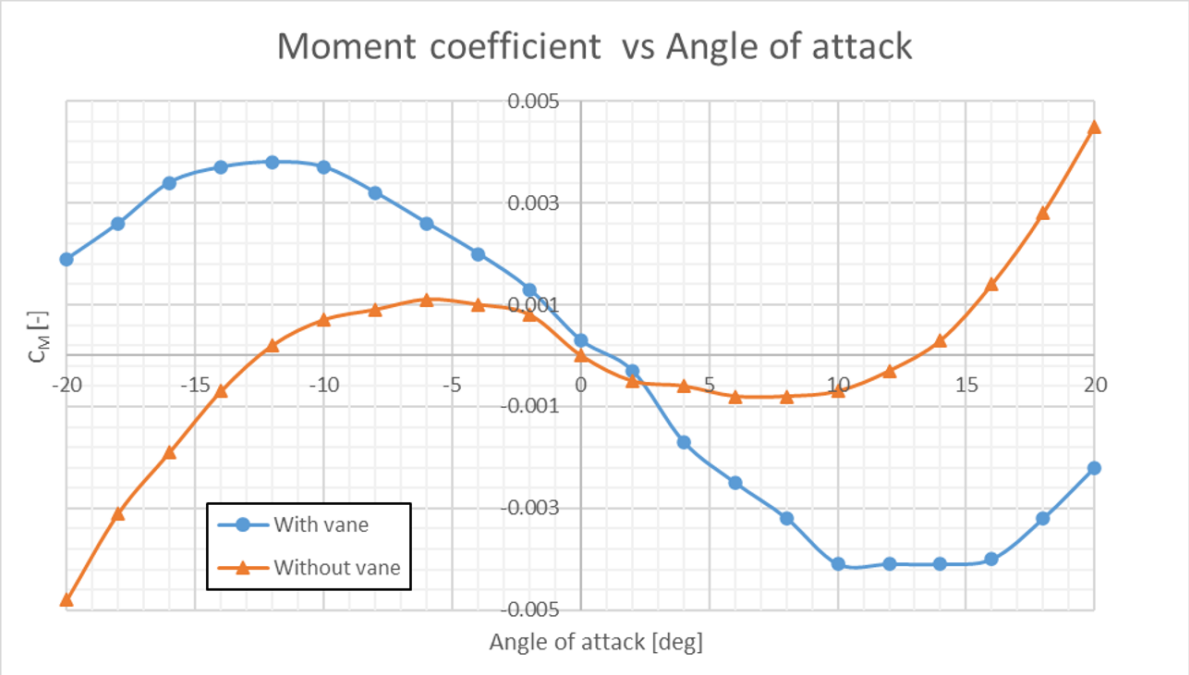

Figure 5.8: Influence control vanes on Moment coefficient vs Angle of attack

5.2. FlightStream complete aircraft analysis

In order to understand how the wake of the aircraft influences the performance of the duct, the complete aircraft is modelled in OpenVSP and exported into FlightStream using the same method as described in the previous section. FlightStream allows the user to analyse the components individually, so the complete aircraft is run and the individual forces of each component is extracted to analyse in depth. The parameters used to design the the aircraft are obtained from the final design of the research performed by Stavreva[21]. The aircraft side and front view can be seen in Figure 5.9. The analysis in FlightStream has been run at take-off thrust from an angle of attack of $-10°$ to $20°$, with steps of $2°$.

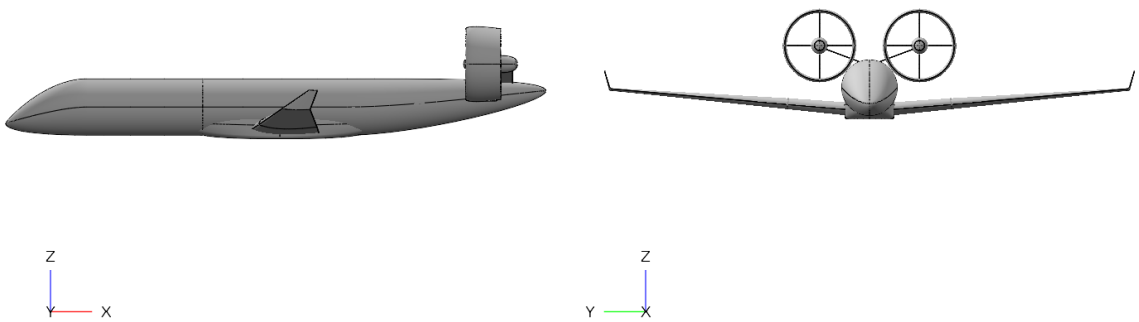

(a) Side view

(b) front view

Figure 5.9: Complete aircraft modelled

5.2.1. Comparison duct with and without aircraft wake

The difference for the lift coefficient can be seen in Figure 5.10. FFrom this figure it can be observed that the duct installed produces less lift compared to the duct uninstalled. This is as expected, since the fuselage as well as the wing downwash causes the ducts to experience a smaller angle of attack and hence less lift is created. This influence is approximately 4 degrees, since the installed duct produces 0 lift at 4 degrees angle of attack, while for the uninstalled duct this occurs at 0 degrees angle of attack. Furthermore, at negative angles of attack, the influence of the aircraft amplifies the negative angle and hence more negative lift is created for the installed duct. This has also an effect on the drag coefficient and can be seen in Figure 5.11, where there is a horizontal shift. Since more negative lift is created at negative angles of attack, this results into more induced drag. Therefore, the drag coefficient of the installed duct is larger at negative angles of attack. However, at positive angles of attack the influence of the aircraft induces a smaller angle of attack, so less lift is created and hence less induced drag. Hence a smaller drag coefficient for the installed duct compared to the uninstalled duct.

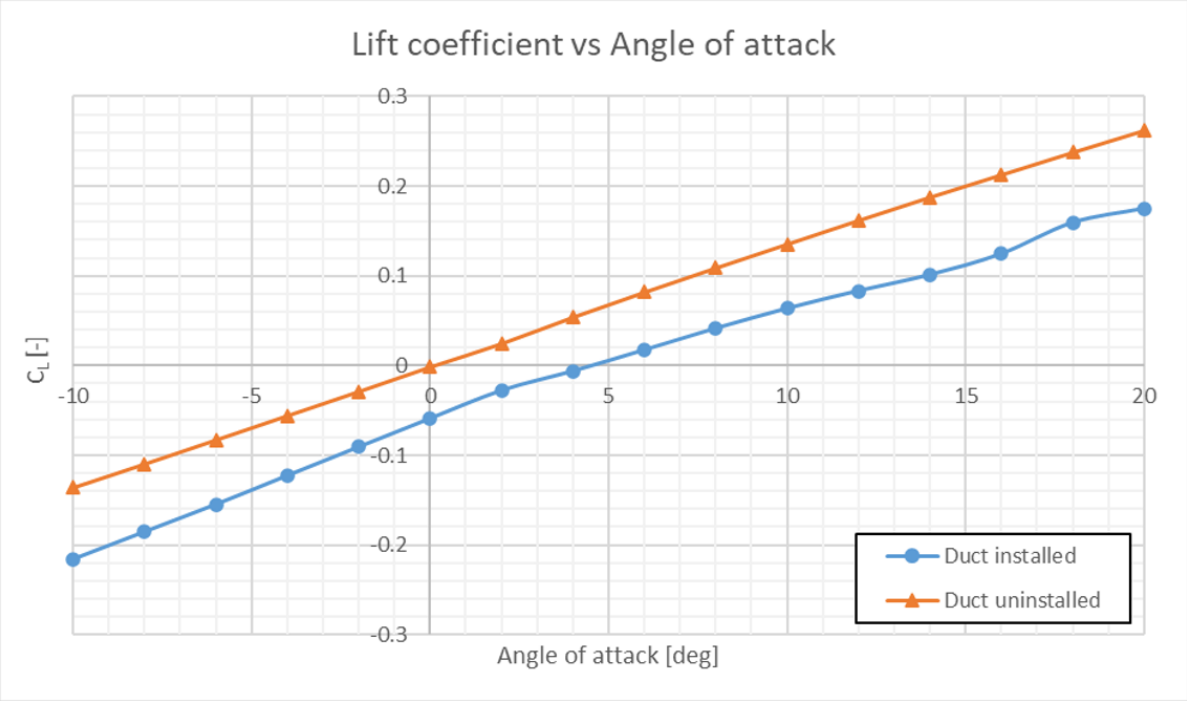

Figure 5.10: Influence aircraft wake on duct Lift coefficient vs Angle of attack

5.2.2. Individual components aircraft

The lift coefficient vs angle of attack curve for each of the components of the aircraft can be seen in Figure 5.12. Please note that for all the individual components, the wing area is used as reference for the lift coefficient. From this figure, it can be seen that the main contributor to the total lift coefficient is the wing, since this is the largest lifting surface. The other components are all close to zero, with the duct providing the second largest lift coefficient, followed by the duct pylon and the control vanes.

In Figure 5.13 the drag coefficient vs angle of attack curve for each component can be seen. Similar to the lift coefficient, the wing is the dominant contributor to the total drag coefficient due to the lift induced drag that is generated. From this figure, it can also be observed that the duct pylon is a large drag producer. From FlightStream data, this is mostly due to the zero-lift drag coefficient, which is dominant compared to the other components. The duct pylon curve however shows non-linear behaviour, which could be due to part of the duct pylon which is behind the propeller wake. The duct itself has a relatively small drag coefficient and this is followed by the control vanes and fuselage, which are all close to zero. Lastly, it can also be observed that for the negative angles of attack the difference in drag coefficient between the components is smaller than the positive angles of attack. Since, less lift is created at the negative angles of attack, so also less lift-induced drag.

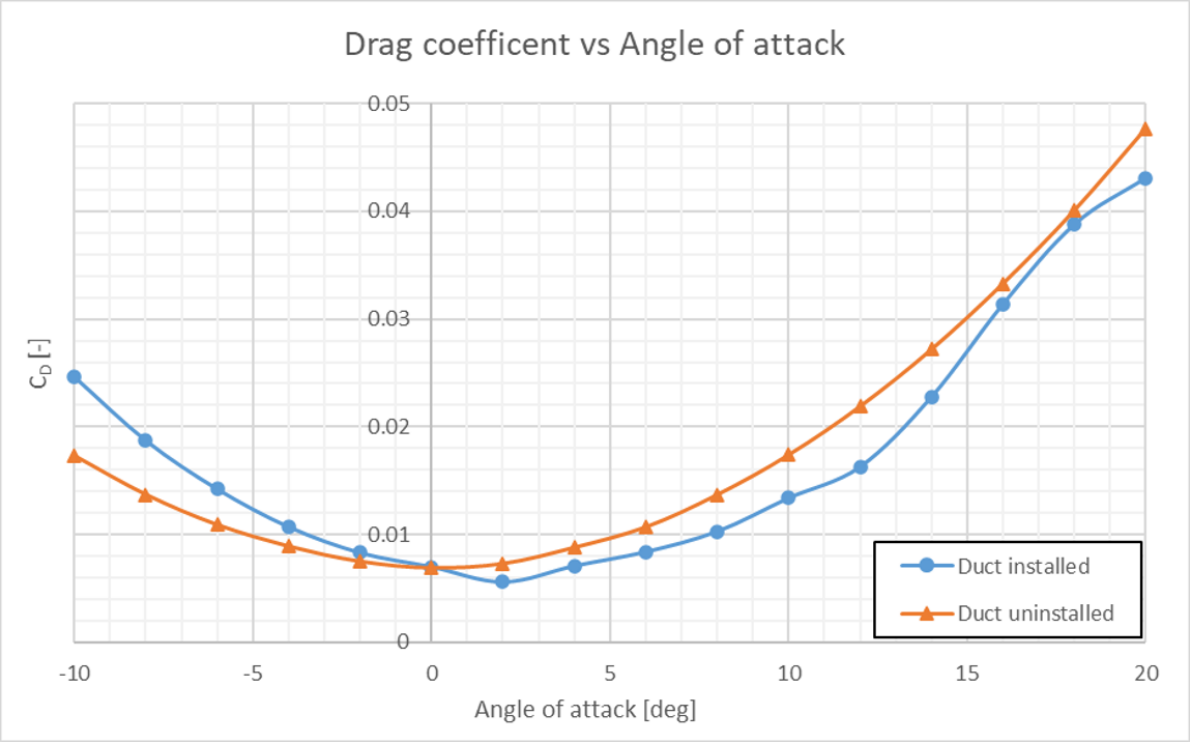

Figure 5.11: Influence aircraft wake on duct Drag coefficient vs Angle of attack

The moment coefficient vs angle of attack for the different components can be seen in Figure 5.14. Overall, the aircraft in this configuration is stable. This can be seen due to negative slope, so $\frac{dC_M}{d\alpha} < 0$. Breaking this down into individual components, it can be seen that as expected the fuselage has a destabilising effect. Whereas the wing and duct provide a stabilising pitching moment. The pitching moment coefficient of the duct pylon and control vanes remain relatively constant throughout the whole angle of attack range.

5.3. Possible propulsive stabiliser positions

With the forces that the duct is able to provide known, the Matlab program as described in Section 3.4 is run to obtain results on possible propulsive stabiliser positions for 4 different wing positions. The control & stability requirement is assessed for take-off, descent and cruise. Since no combination of propulsive stabiliser/wing position could satisfy take-off, descent and cruise requirements simultaneously, the data is presented separately for all cases. Table 5.5 present the data for the wing location at 44.4% fuselage length, as was also used in the research of Stavreva[21]. The first row stands for the propulsive stabiliser CG position, this is shifted from 90% fuselage length to 60% fuselage length with steps of 5%. The first column stands for the propulsive stabiliser duct size that is assessed. This gives a combination of wing location, duct size and propulsive stabiliser position. For each of the combination this is assessed for take-off (TO), descent (DE) and cruise (CR) configuration, as indicated in the table. A number is presented that indicates which duct installation angle is able to provide sufficient force for control and stability. If the neutral point stability is not satisfied, this is denoted with "NP" and if the force provided by the duct is not sufficient for stability and control, this is denoted with "TF". Table 5.6 presents the data for the wing at 47.5% fuselage length. The results for the wing at 50% fuselage length can be seen in Table 5.7. Lastly, the results for the wing at 52% fuselage length can be seen in Table 5.8.

From these analyses it has been observed that some combination of wing location, duct size and propulsive stabiliser position do satisfy the control & stability requirements. However this would mean the propulsive stabiliser installation angle has to be adjusted to this. Furthermore, it can be observed that positioning the propulsive stabiliser more to the front, results in less available combinations to satisfy the requirements. This is as expected, since the duct is not able to generate the increased force due to the smaller distance between

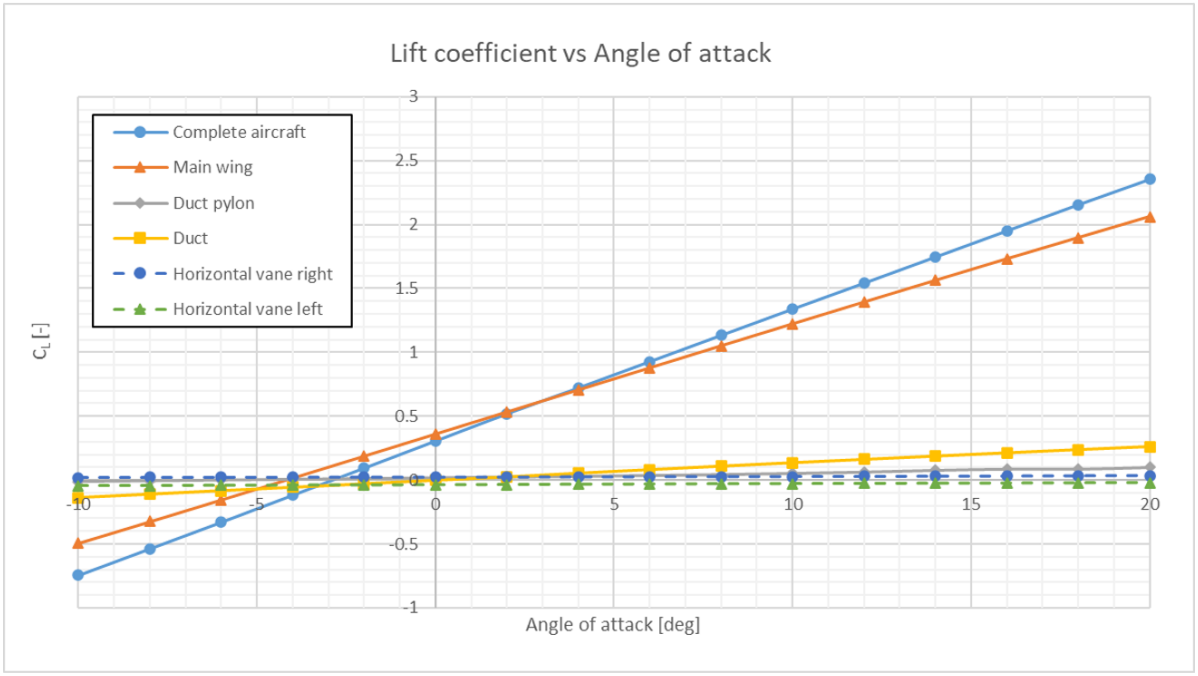

Figure 5.12: Lift coefficient vs angle of attack per component complete aircraft

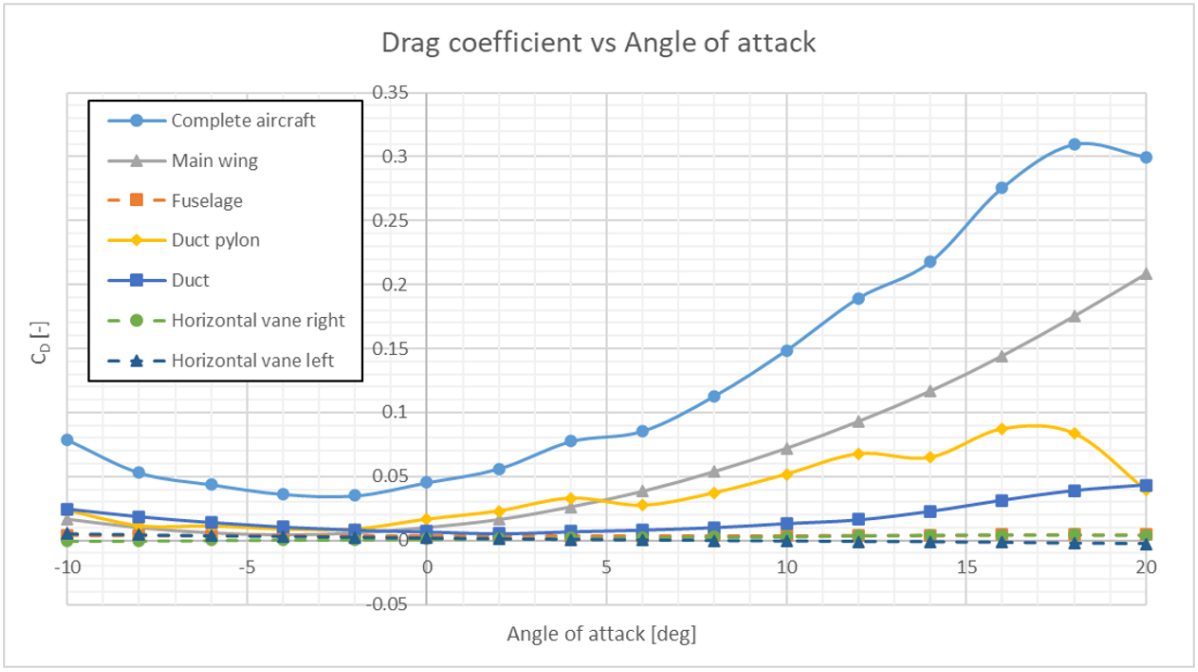

Figure 5.13: Drag coefficient vs angle of attack per component complete aircraft

propulsive stabiliser CG and aircraft CG (tail arm). Comparing the results of the different wing positions, it can also be observed that the further aft the wing is placed, the less forward the propulsive stabiliser can be positioned compared to the more forward wing positions. One could also argue based on these results that it would be better to position the wing slightly rearwards at 47.5% fuselage length instead of the initial wing position of 44.4%. Since this allows for more combinations looking at the descent requirement at aft duct positions. This is due to $x_{cg} - x_{ac}$ which becomes smaller when moving the wing aft, hence reducing the moment arm of the wing lift and thereby reducing the lift required by the duct.

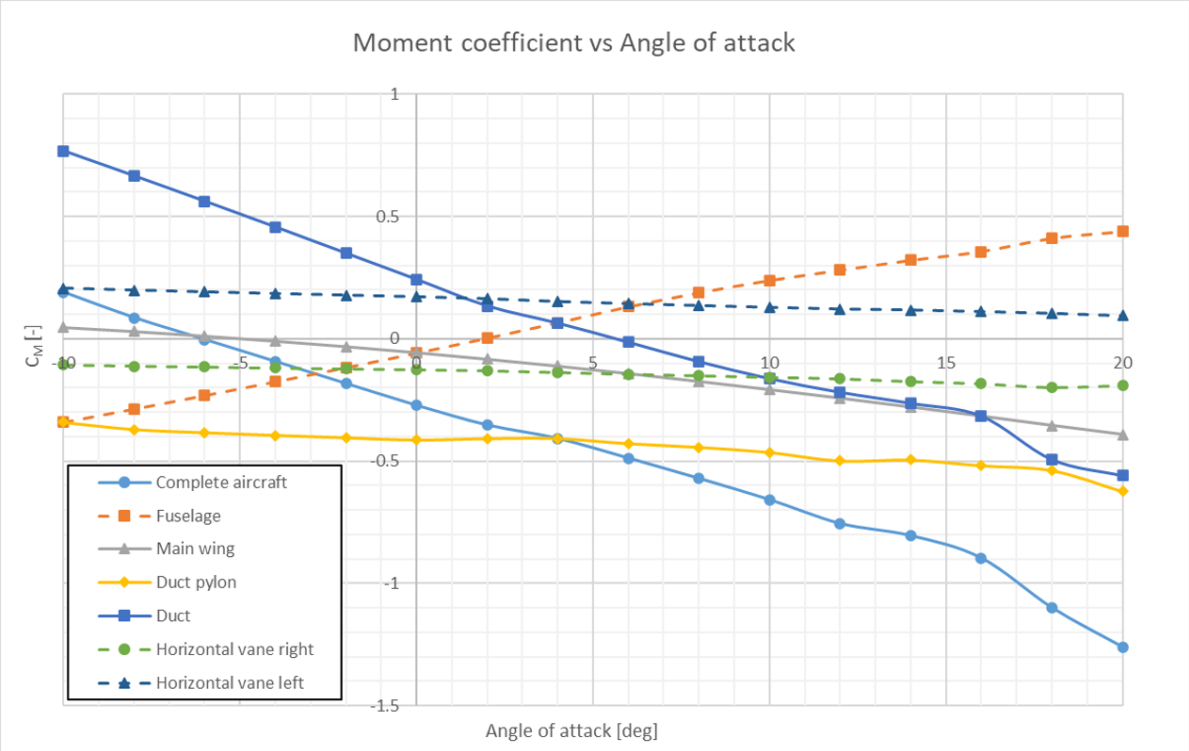

Figure 5.14: Moment coefficient vs angle of attack per component complete aircraft

The wing is not placed further aft than 52% fuselage length, since this is out of bounds for the ESDU method and hence no aerodynamic centre location will be obtained. Furthermore, the wing is also not placed further in front of 44.4% fuselage length, since this resulted in no available propulsive stabiliser positions, as the tail force is not sufficient.

To understand what this means in terms of cruise performance, 3 cases have been run in FlightStream, where the full aircraft model is used and the propulsive empennage is adjusted with the installation angle according to the table. In all 3 cases the wing is positioned at 44.4% fuselage length (L_f), which means Table 5.5 is used. The first case analysed is with the propulsive empennage at 90% L_f and with a 3.5m duct. This can be seen as the base case. In the second analysis the propulsive empennage is move forward to 80% L_f, this resulted in a drag reduction of -1.02%. In the third case the propulsive empennage is placed at 90% L_f, similar to the base case, however the duct diameter is reduced to 3m. This resulted in a drag reduction of -21.59% compared to the base case. This is also summarised in Table 5.2.

Table 5.2: Comparison cruise analysis

Case	**Total drag [N]**	**Difference w.r.t. base**
1: 3.5m, 90% L_f, 4deg	19004.82	0.0%
2: 3.5m, 80% L_f, 4deg	18810.87	-1.02%
3: 3m, 90% L_f, 6deg	14902.52	-21.59%

The drag of the various components are analysed more in depth, to understand where this large difference between the 3.5m duct and 3m duct originates. The values for each component is tabulated and can be seen in Table 5.3. The induced drag (Di) and zero-lift drag (D0) values can be seen for the four main components of the aircraft, all values are in Newton. The other components such as the control vanes are left out since these had a marginal difference. From this comparison it can be seen that the largest difference in drag is due to the zero-lift drag of the duct and duct pylon. A reduction in zero-lift drag is expected for the smaller duct

and duct pylon, since these components are smaller and hence less surface area. However, a reduction of this magnitude was not expected. There is a small increase in the lift induced drag of the 3m duct, since the 3m duct is at a higher installation angle compared to the 3.5m duct. Furthermore, a difference between the zero-lift drag of the fuselage can be observed, which was not expected. Since in both cases the fuselage dimensions remained the same. This could indicate that FlightStream has difficulties predicting zero-lift drag for this aircraft configuration and further research on this is required. FlightStream utilises a momentum integral model to calculate the viscous forces. A Coles near wall velocity profile is applied to the available boundary layer to calculate viscous drag forces.[56] A new model developed by Olsen[57] is also applied to the skin friction equation, which includes surface roughness height. This allows for the surface roughness effects to be included in the boundary layer transition and flow separation and viscous drag calculation.[58].

Table 5.3: Drag component analyses [powered conditions] (values in Newton)

	3.5m duct		**3m duct**		**Difference**	
Component	Di	D0	Di	D0	Di	D0
Fuselage	0	2186	0	1439	0	-747
Main wing	2311	1839	2814	1860	+502	+21
Duct	784	4901	1099	3827	+314	-1704
Duct pylon	746	5796	697	2514	-49	-3282

To understand how much these differences are influenced by the propeller. The analysis has been performed again with the same configuration, however in unpowered condition. The results can be seen in Table 5.4. From this table it can be observed that the largest difference again comes from the zero-lift drag of the duct and duct pylon. While the difference in duct drag is similar to the powered analysis. The difference in duct pylon zero-lift drag is smaller than in the powered analysis. The difference in induced drag of the duct pylon has now increased in unpowered conditions, where the 3m duct pylon has more induced drag compared to the 3.5m duct pylon. The opposite happens for the induced drag of the duct, where the difference becomes small. The fuselage and main wing show similar behaviour to the powered analysis.

Table 5.4: Drag component analyses [powered conditions] (values in Newton)

	3.5m duct		**3m duct**		**Difference**	
Component	Di	D0	Di	D0	Di	D0
Fuselage	0	2231	0	1445	0	-785
Main wing	2310	1865	2806	1863	+496	-2
Duct	817	4254	804	2283	-13	-1970
Duct pylon	761	5936	1161	4111	+400	-1825

Lastly, in order to understand the how much the CG excursion is for the propulsive stabiliser at the rear of the aircraft compared to the CG excursion of the propulsive stabiliser positioned more to the front, a loading diagram is created. The loading diagram is created for the propulsive stabiliser positioned at 95% fuselage length (L_f) and 70% L_f and can be seen in Figure 5.15. From this figure, it can be seen that there is a large shift forward of approximately 0.21MAC in CG range of the propulsive stabiliser at 70% L_f at Operating Empty Weight. At Maximum Take-off Weight, this difference is 0.13MAC. This is as expected since the propulsive stabiliser is positioned more to the front. It can also be observed that the propulsive stabiliser at 95% L_f has a larger CG excursion of 0.29MAC compared to 0.24MAC for the propulsive stabiliser at 70% L_f. Furthermore, the influence of wing position on CG range has also been analysed. The comparison between the aircraft wing at 44.4% L_f and 47.5% L_f can be seen in Figure 5.16. From this figure, a rearward shift of the loading diagram can be seen of approximately 0.23m. The difference in CG excursion stays approximately the same, with the wing at 47.5% L_f having a 0.06m larger CG excursion.

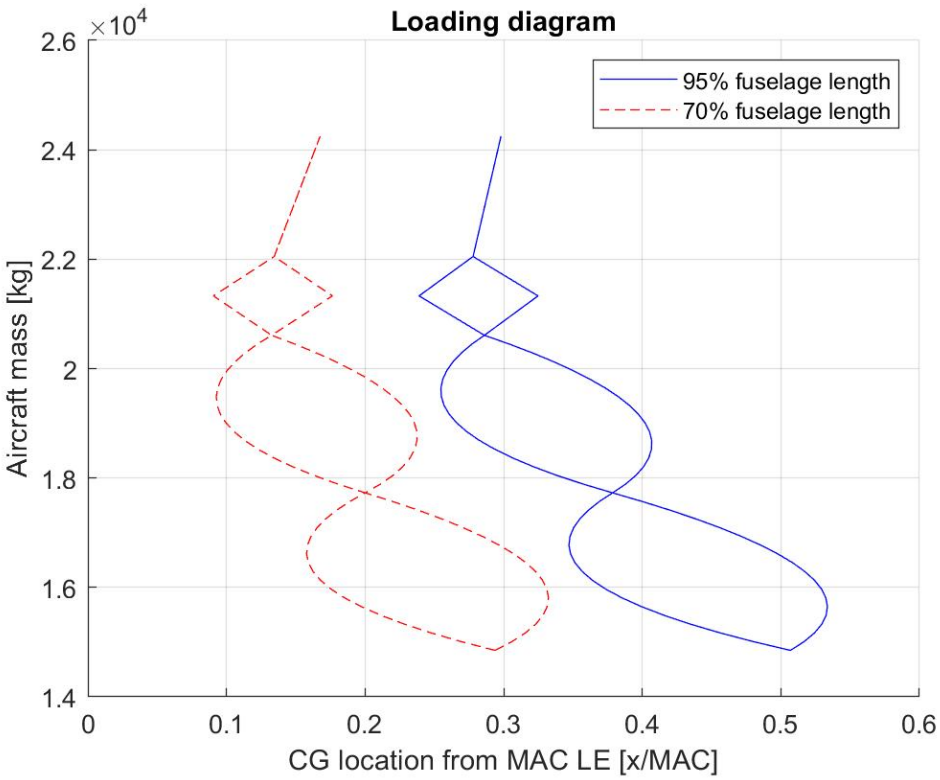

Figure 5.15: Comparison loading diagram for two propulsive stabiliser positions

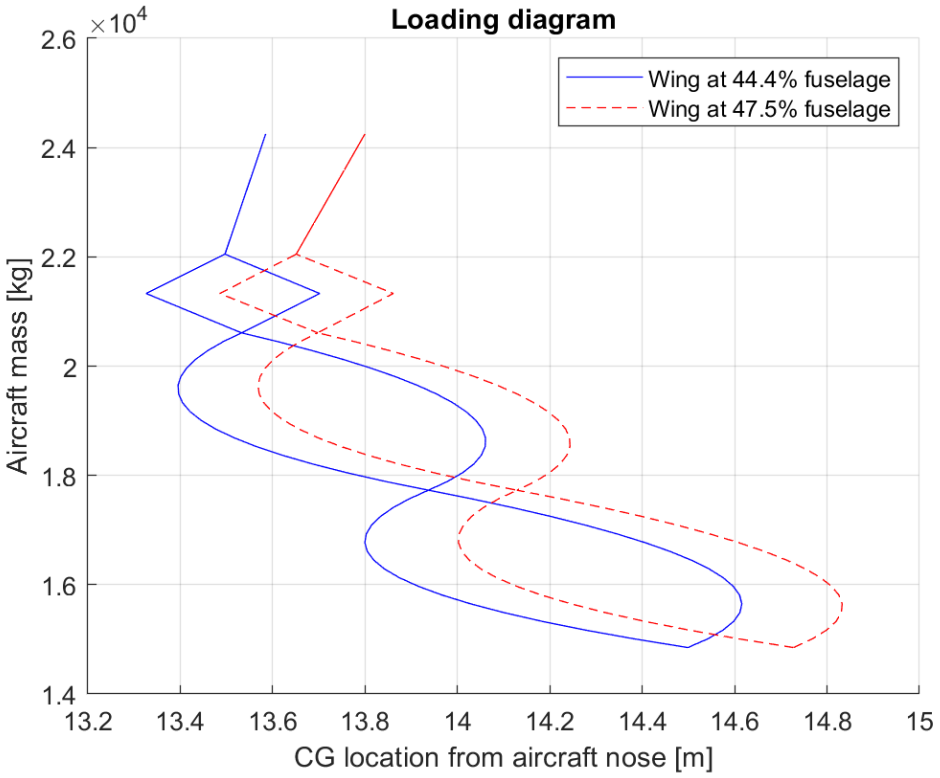

Figure 5.16: Comparison loading diagram for two wing positions

5.4. Conclusion

From these analyses it can be concluded that for descent requirements it could be more beneficial to position the wing at 47.5% fuselage length. Furthermore, positioning the propulsive stabiliser more to the front results in less available combinations to satisfy the requirements. Furthermore, from analysing 3 cases in cruise, a significant drag reduction is achieved by using a smaller duct at higher angle of attack, compared to a larger duct at lower angle of attack. However, there are certain effects in the prediction of the zero-lift drag which are not as anticipated and hence further research is required on this. Using the same duct size and angle of attack but positioning it more to the front resulted in minimal drag reduction. Lastly, positioning the propulsive stabiliser more forward results in a forward shift of CG range and a smaller CG excursion. Positioning the wing rearward by 2.5% L_f has a marginal difference in CG excursion and shifts the CG range backward by approximately 0.23m.

Table 5.5: Possible duct installation angle for wing location 44.4% L_f

CG / Duct	**95%** L_f			**90%** L_f			**85%** L_f			**80%** L_f			**75%** L_f			**70%** L_f			**65%** L_f			**60%** L_f		
	TO	DE	CR	TO	DE	CR	TO	DE	CR	TO	DE	CR	TO	DE	CR	TO	DE	CR	TO	DE	CR	TO	DE	CR
1.5m	4	NP	NP	2	NP	NP	-4	NP	NP	-8	NP	NP	-16	NP	NP	TF	NP	NP	TF	NP	NP	TF	NP	NP
2m	4	NP	NP	2	NP	NP	-4	NP	NP	-8	NP	NP	-12	NP	NP	-20	NP	NP	TF	NP	NP	TF	NP	NP
2.5m	4	NP	NP	2	NP	NP	-4	NP	NP	-8	NP	NP	-12	NP	NP	-18	14	NP	TF	12	NP	TF	TF	-6
3m	2	TF	6	6	TF	6	-4	TF	4	-6	TF	4	-10	16	4	-16	10	2	TF	10	0	TF	TF	-4
3.5m	2	TF	4	8	20	4	-2	18	4	-6	16	4	-8	12	2	-14	8	2	-20	10	-2	TF	TF	-4
4m	2	16	4	8	16	4	-2	14	4	-4	12	4	-8	10	4	-12	6	2	-18	10	2	TF	TF	-2

Table 5.6: Possible duct installation angle for wing location 47.5% L_f

CG / Duct	**95%** L_f			**90%** L_f			**85%** L_f			**80%** L_f			**75%** L_f			**70%** L_f			**65%** L_f			**60%** L_f		
	TO	DE	CR	TO	DE	CR	TO	DE	CR	TO	DE	CR	TO	DE	CR	TO	DE	CR	TO	DE	CR	TO	DE	CR
1.5m	-6	NP	NP	-10	NP	NP	-14	NP	NP	-20	NP	NP	TF	NP	NP	TF	NP	NP	TF	NP	NP	TF	TF	TF
2m	-6	NP	NP	-8	NP	NP	-12	NP	NP	-18	NP	NP	TF	-16	NP	TF	TF	-6	TF	TF	-12	TF	TF	-18
2.5m	-4	20	4	-8	14	4	-12	8	2	-16	6	2	TF	-12	-2	TF	TF	-6	TF	TF	-10	TF	TF	-18
3m	-4	14	4	-6	10	2	-10	6	2	-14	6	2	-18	-8	-2	TF	-18	-4	TF	TF	-8	TF	TF	-14
3.5m	-4	12	2	-6	8	2	-8	6	2	-12	4	-2	-16	-6	-2	TF	-14	-4	TF	TF	-6	TF	TF	-12
4m	-4	8	2	-6	6	2	-8	4	2	-10	0	2	-14	-6	-2	-20	-12	-2	TF	TF	-4	TF	TF	-8

Table 5.7: Possible duct installation angle for wing location 50% L_f

CG / Duct	**95%** L_f			**90%** L_f			**85%** L_f			**80%** L_f			**75%** L_f			**70%** L_f			**65%** L_f			**60%** L_f		
	TO	DE	CR	TO	DE	CR	TO	DE	CR	TO	DE	CR	TO	DE	CR	TO	DE	CR	TO	DE	CR	TO	DE	CR
1.5m	-14	NP	NP	-18	NP	NP	TF	NP	NP	TF	NP	NP	TF	TF	-18	TF	TF	TF	TF	TF	TF	TF	TF	TF
2m	-12	6	2	-16	-4	2	-20	-16	-4	TF	TF	-6	TF	TF	-10	TF	TF	-16	TF	TF	TF	TF	TF	TF
2.5m	-10	4	2	-14	-4	-2	-18	-12	-2	TF	TF	-4	TF	TF	-8	TF	TF	-12	TF	TF	-18	TF	TF	TF
3m	-8	4	2	-12	-2	-2	-14	-8	-2	-20	-16	-4	TF	TF	-6	TF	TF	-8	TF	TF	-12	TF	TF	TF
3.5m	-8	4	2	-10	-2	-2	-12	-6	-2	-16	-12	-4	TF	-20	-4	TF	TF	-8	TF	TF	-10	TF	TF	-18
4m	-6	2	2	-8	-2	-2	-12	-6	-2	-14	-10	-2	-20	-16	-4	TF	TF	-6	TF	TF	-8	TF	TF	-14

Table 5.8: Possible duct installation angle for wing location 52% L_f

CG / Duct	**95%** L_f			**90%** L_f			**85%** L_f			**80%** L_f			**75%** L_f			**70%** L_f			**65%** L_f			**60%** L_f		
	TO	DE	CR	TO	DE	CR	TO	DE	CR	TO	DE	CR	TO	DE	CR	TO	DE	CR	TO	DE	CR	TO	DE	CR
1.5m	-18	NP	NP	TF	TF	-8	TF	TF	-12	TF	TF	-18	TF	TF	TF	TF	TF	TF	TF	TF	TF	TF	TF	TF
2m	-16	-12	-2	-20	TF	-4	TF	TF	-8	TF	TF	-10	TF	TF	-16	TF	TF	TF	TF	TF	TF	TF	TF	TF
2.5m	-14	-8	-2	-18	-16	-4	TF	TF	-6	TF	TF	-8	TF	TF	-12	TF	TF	-16	TF	TF	TF	TF	TF	TF
3m	-12	-6	-2	-14	-12	-2	-18	-20	-4	TF	TF	-6	TF	TF	-8	TF	TF	-12	TF	TF	-18	TF	TF	TF
3.5m	-10	-6	-2	-12	-10	-2	-16	-16	-4	-20	TF	-6	TF	TF	-6	TF	TF	-10	TF	TF	-14	TF	TF	TF
4m	-10	-4	-2	-12	-8	-2	-14	-12	-2	-18	-18	-4	TF	TF	-6	TF	TF	-8	TF	TF	-12	TF	TF	-18

6

Conclusions & Recommendations

This report presented the research with the objective to study the positioning of the ducted fan propulsive stabiliser. Considering its impact on stability and control by development of a method to predict aerodynamic/stability & control derivatives for variable position and duct/fan size.

The Delft University Unconventional Configuration (DUUC) aircraft entails two ducted fan propulsive stabilisers at the rear of the aircraft. These stabilisers consist of two control vanes mounted downstream of the duct. From previous research on the DUUC, where the propulsive stabiliser was in a fixed, aft-fuselage position with a fixed duct aspect ratio. It has been observed that the rear center of gravity (CG) position and large shift in CG due to the propulsive stabiliser poses a number of challenges.

In order to study the positioning of the propulsive stabiliser. A new method is developed which utilises an ESDU method, AVL and FlightStream. The method of ESDU is used to determine the position of the aerodynamic center of the wing-fuselage combination. With AVL the lift, drag and moment of the wing-fuselage is obtained. FlightStream is used to determine the aerodynamic characteristics of the ducted propeller. Flightstream is a surface-vorticity solver which is more stable, more robust and has a lower sensitivity to surface perturbations, when compared to potential-flow solver which are pressure-based.

From FlightStream ducted propeller validation analysis it has been observed that the vorticity solver is able to produce accurate lift coefficient results in unpowered conditions compared to analytical methods such as Weissinger and Maqsood. However, it is not able to predict stall. It should be noted that Weissinger and Maqsood do produce accurate results if the effects of the vanes and struts are added separately, with Weissinger producing the best results. The drag coefficient is underpredicted by FlightStream throughout the whole angle of attack range, where Weissinger again produces better results when the influence of the vanes and struts are added. In powered conditions the lift coefficient is also underpredicted, with a small difference in the vorticity and pressure model. This underprediction is approximately 17%, which indicates that in the analyses to determine the required duct size, the duct size is overestimated. The drag coefficient is also underpredicted in the powered conditions. The decision was made to proceed with FlightStream, even though the drag coefficient is underpredicted and analytical methods can produce accurate results, since with FlightStream it is possible to model the complete aircraft and obtain the influence of the wing and fuselage on the propulsive stabiliser. FlightStream also enables the user to obtain the results of each component of the aircraft separately, in order to analyse how much influence a certain part has on the whole aircraft.

From the analyses of various duct sizes it has been observed that the larger the duct size the higher the lift coefficient, using the wing area as the surface area for all the analyses. The opposite is true for the drag coefficient, where the drag is larger for smaller duct sizes at low angles of attack. This is due to the control vanes inside the duct, where the control vane drag is more dominant than the duct drag at smaller angles of attack. The control vanes inside the larger ducts have a higher aspect ratio compared to the control vanes inside the smaller ducts, since the chord is kept constant. These higher aspect ratio vanes are more efficient and hence have a lower drag coefficient. At angle of attack above 10°, the larger duct sizes produce the most drag, since the duct drag becomes more dominant. Furthermore, a clear effect could be observed in the lift coefficient

due to the wing and fuselage effects when comparing the installed and uninstalled duct.

Utilising a novel method combining an ESDU method, AVL and FlightStream, it has been observed that there are configuration of wing position, propulsive stabiliser position and duct size feasible, to guarantee a stable and controllable aircraft. However, this would mean that the duct installation angle has to be adjusted accordingly for cruise, take-off and descent. From these analyses it has been observed that for descent requirements it could be more beneficial to position the wing at 47.5% fuselage length, since this allowed for more feasible combinations. Furthermore, positioning the propulsive stabiliser more to the front results in less available combinations to satisfy the requirements. This was as expected, since the tail arm reduced. With a smaller tail arm, a larger lift is required by the ducts which were not feasible at a certain point. From analysing 3 cases in cruise, a significant drag reduction is achieved by using a smaller duct at higher installation angle, compared to a larger duct at lower installation angle. However, there are certain effects in the prediction of the zero-lift drag which are not as anticipated and hence further research is required on this. Furthermore, it has been observed that using the same duct size and installation angle however positioning it more to the front of the aircraft resulted in minimal drag reduction. Lastly, positioning the propulsive stabiliser at 70% fuselage length compared to 90% fuselage length results in a forward shift of approximately 0.13MAC to 0.21MAC of CG range and a 0.06MAC smaller CG excursion.

It is recommended for further research to validate the zero-lift drag calculation on the aircraft. Since the zero-lift drag results produced by FlightStream were not as anticipated. FlightStream fulfilled the purpose to analyse various configurations relatively quick with high fidelity. This allowed the user to obtain an overview of various plausible aircraft configurations. It is recommended now to analyse certain configurations with in detail with CFD for example and validate these results against FlightStream. Furthermore, it is recommended to include the effects of the duct weight on the calculations. Since for these analyses the 3.5m duct weight is used for all the analyses, while in reality this changes for the various duct sizes and hence have an effect on the aircraft centre of gravity position. The larger duct size compared to the base model will put the CG more aft and hence the tail arm is smaller, which means the duct lift is underestimated. The opposite is true for the smaller duct sizes, where the duct lift is overestimated. Lastly, the analyses performed in these research were based on the static longitudinal stability characteristics of the aircraft. It is recommended for further research to also investigate the lateral and directional stability characteristics as well as the the dynamic stability characteristics.

Bibliography

[1] EASA, EEA, and EUROCONTROL. *European Aviation Environmental Report 2019*, volume 40. 2019.

[2] C. Varriale, K. Hameeteman, M. Voskuijl, and L. Veldhuis. A thrust-elevator interaction criterion for aircraft optimal longitudinal control. 2019. doi: 10.2514/6.2019-3001.

[3] F.M. de Piolenc and G.E. Wright. *Ducted Fan Design*. CreateSpace Independent Publishing Platform, 2nd edition, 2001.

[4] A.G. Rao. Lecture-4: Engine design trends. Lecture notes, 2018. AE4238 Aero Engine Technology.

[5] 11.5 Trends in thermal and propulsive efficiency. `http://web.mit.edu/16.unified/www/FALL/thermodynamics/notes/node84.html`, retrieved: 26-11-2020.

[6] Cfm56-5b pip: the engine of choice for the a320ceo family. `https://www.safran-aircraft-engines.com/commercial-engines/single-aisle-commercial-jets/leap/leap-1a`, retrieved: 26-11-2020.

[7] Leap-1a: chosen to power the airbus a320neo. `https://www.safran-aircraft-engines.com/commercial-engines/single-aisle-commercial-jets/leap/leap-1a`, retrieved: 26-11-2020.

[8] Airbus a320 aircraft characteristics - airport and maintenance planning. `https://www.airbus.com/content/dam/corporate-topics/publications/backgrounders/techdata/aircraft_characteristics/Airbus-Commercial-Aircraft-AC-A320-Feb18.pdf`, retrieved: 26-11-2020.

[9] J.Weissinger. On the aerodynamics of ring wings, 1. the pressure distribution on a thin, almost axially symmetric wing in subsonic flow. *Technical Report*, 1957. David Taylor Model Basin.

[10] V.N. Harinarain. *Aerodynamic Performance Study on a Ducted Propeller System for Propulsion and Control & Stability Applications*. Master Thesis, 2017.

[11] M.H.Sadraey. *Aircraft Design: A Systems Engineering Approach*. John Wiley & Sons, 2012.

[12] M. Drela and H. Youngren. Axisymmetric analysis and design of ducted rotors. `http://web.mit.edu/drela/Public/web/dfdc/DFDCtheory12-31.pdf`, 2005.

[13] K.J. Grunwald an dK.W.Goodson. Aerodynamic loads on an isolated shrouded-propeller configuration for angles of attack from -10 deg to 110 deg. Technical report, Langley Research Center, 1962.

[14] J.A. Mulder, W.H.J.J. van Staveren, J.C. van der Vaart, E. de Weerdt, C.C. de Visser, A.C. in 't Veld, and E. Mooij. *Lecture Notes AE3202 Flight Dynamics*. 10 March 2013.

[15] E. Torenbeek. *Synthesis of Subsonic Airplane Design*. Springer, 1982.

[16] N.H.M. van den Dungen. *Synthesis of an Aircraft Featuring a Ducted Fan Propulsive Empennage*. Master Thesis, 2017.

[17] K.J.M. Hameeteman. *Unconventional Propulsive Empennage - Future or Fiction? Stability & Control Analysis and the Effect of Scaling of the DUUC*. Master Thesis, 2017.

[18] P. Wu. A physics-based approach to assess critical load cases for landing gears within aircraft conceptual design. 2019. doi: https://doi.org/10.4233/uuid:193f6664-0f19-488f-af6a-21b17ba75be0.

[19] J. Roskam. *Airplane Design pt. 6: Determination of Stability Control and Performance Characteristics*. Roskam Aviation and Engineering, 1985.

[20] Anon. *Military Standard - Flying Qualities of Piloted Aircraft*. Department of Defense, mil-std-1797a edition, 1990.

[21] M.N. Stavreva. *Structural Sizing Method for Propulsive Empennage System.* Master Thesis, 2020.

[22] R. Vos and M. Hoogreef. System-level assessment of tail-mounted propellers for regional aircraft. *31st Congress of the International Council of the Aeronautical Science*, 2018.

[23] Q.R.Wald. The aerodynamics of propellers. *Progress in Aerospace Sciences*, pages 42(2),85–128, 2006.

[24] F. Hitchens. *Propeller Aerodynamics: The History, Aerodynamics and Operation of Aircraft.* Auk Academic, 1st edition, 2015.

[25] Ger. J.J. Ruijgrok. *Elements of Airplane Performance.* VSSD, 2nd edition, 2009.

[26] B. Lil, H. Lul, and S.Deng. Validation of an actuator disk model for numerical simulation of propeller. *Part G: Journal of Aerospace Engineering*, 229(8):pp. 1454–1463, 2014. Proceedings of the Institution of Mechanical Engineers.

[27] E. Torenbeek and H. Wittenberg. *Flight Physics : Essentials of Aeronautical Disciplines and Technology, with Historical Notes.* Springer, 2009.

[28] A. Maqsood and T.H. Go. Aerodynamic estimation of annular wings based on leading-edge suction analogy. *AIAA JOURNAL*, Vol. 51(No. 2), 2013.

[29] H. S. Ribner. The ring airfoil in nonaxial flow. *Journal of Aeronautical Sciences*, Vol. 14(No. 9):pp. 529–530, 1947.

[30] H. S. Fletcher. Experimental investigation of lift, drag and pitching moment of five annular airfoils. *National Advisory Committee for Aeronautics*, 1957. NACA TN 4117.

[31] L. W. Traub. Experimental investigation of annular wing aerodynamics. *Journal of Aircraft*, Vol. 46(No. 3):pp. 988–996, 2009.

[32] M. Anderson, K. Lehmkuehler, D. Ho, K.C. Wong, and P. Hendrick. Propeller location optimisation for annular wing design. *International Micro Air Vehicle Conference and Flight Competition*, 2013.

[33] L. W. Traub. Preliminary investigation of the effects of stagger on an annular wing. *Journal of Aircraft*, Vol. 54(No. 6), 2017.

[34] A. Sacks and J. Burnell. Ducted propellers - a critical review of the state of the art. Technical report, Advanced Research Division of Hiller Aircraft Corporation, 1959.

[35] D.M.Black, H.S. Wainauski, and C.Rohrbach. Shrouded propellers - a comprehensive performance study. *AIAA 5th Annual Meeting and Technical Display*, 1968.

[36] W. Zhang, N. Fan, Z. Wang, and Y. Wu. Modeling and aerodynamic analysis of a ducted-fan micro aerial vehicle. *Proceedings of International Conference on Modelling, Identification & Control*, pages p. 768–73, 2012.

[37] L.P. Parlett. Aerodynamic characteristics of a small-scale shrouded propeller at angles of attack from 0○ to 90○. Technical report, NACA, 1955.

[38] W. Graf, J. Fleming, , and W. Ng. Improving ducted fan uav aerodynamics in forward flight. *AIAA Aerospace Sciences Meeting and Exhibit*, 2008.

[39] S. Yilmaz, D. Erdem, and M. Kavsaoglu. Effects of duct shape on a ducted propeller performance. *51st AIAA Aerospace Sciences Meeting including the New Horizons Forum and Aerospace Exposition*, 2013.

[40] P.F. Yaggy and G.W. Goodson. Aerodynamics of a tilting ducted fan configuration. Technical report, NASA, 1961.

[41] U.S. Navy's All Hands magazine, October 1959.

[42] A.I. Abrego and R.W. Bulaga. Performance study of a ducted fan system. *AHS Aerodynamics, Aeroacoustic ...*, 2002.

[43] K.W. Mort and B. Gamse. A wind-tunnel investigation of a 7-foot- diameter ducted propeller. Technical report, NASA, 1967.

[44] M. drela and h. youngren. `http://web.mit.edu/drela/Public/web/avl/avl_doc.txt`, retrieved: 19-05-2021.

[45] R.W. Gilbey. Aerodynamic centre of wing-fuselage combinations. Technical report, ESDU 76015, 2013.

[46] R.W. Gilbey and P.D. Chappell. Lift-curve slope and aerodynamic centre position of wings in inviscid subsonic flow. Technical report, ESDU 70011, 2012.

[47] T.J.E. Schouten. *Assessment of Conceptual High-Capacity Regional Turbopropeller Aircraft*. Master Thesis, 2018.

[48] A. Filippone. *Advanced Aircraft Flight Performance*. Cambridge University Press, volume 34 of cambridge aerospace series edition, December 2012.

[49] B. Sandoz, V. Ahuja, and R.J. Harfield. Longitudinal aerodynamic characteristics of a v/stol tilt-wing four-propeller transport model using a surface vorticity flow solver. *AIAA Aerospace Sciences Meeting, 2018*, 2018. doi: 10.2514/6.2018-2070.

[50] S. Johnson, D. van Dommelen, V. Ahuja, and R. Harfield. Investigation of the static longitudinal characteristics of a full-scale light single-engine airplane using a surface vorticity solver. *AIAA Aerospace Sciences Meeting, 2018*, 2018. doi: 10.2514/6.2018-1259.

[51] P.B. Sargent and W.A.J. Anemaat. Benchmarking a robust panel code for ducted fan vtol aircraft design. *2018 Applied Aerodynamics Conference*, 2018.

[52] R. Hartfield. Cad-based workflows. VSP workshop, 2017.

[53] Research in Flight. Flightstream 11.4. release notes, .

[54] M.J. Werle. Aerodynamic loads and moments on axisymmetric ring-wing ducts. *AIAA JOURNAL*, pages Vol. 52, No. 10, 2014.

[55] Xiaofan Fei. Evaluation of a commercial surface vorticity flow solver for the modeling of propeller-wing interaction. *NASA Langley Research Center*, 2019.

[56] Research in Flight. Flightstream 2020.1. release notes, .

[57] A. S. Olsen, N. R. Garcia, and C. Bak. Improved roughness model for turbulent flow in 2d viscid-inviscid panel methods. *Journal of Wind Energy*, 2019.

[58] Research in Flight. Flightstream 2020.2. release notes, .